DEVELOPMENT OF SUSTAINABLE AND DEGRADABLE THERMOSETS AND ELASTOMERS

A Dissertation

Presented to

the Faculty of the Department of Chemical & Biomolecular Engineering

University of Houston

In Partial Fulfillment

of the Requirements for the Degree

Doctor of Philosophy

in Chemical Engineering

by

Guozhen Yang

August 2016

DEVELOPMENT OF SUSTAINABLE AND DEGRADABLE
THERMOSETS AND ELASTOMERS

_____
Guozhen Yang

Approved:

_____
Chair of the Committee
Megan L. Robertson, Assistant Professor,
Chemical & Biomolecular Engineering

Committee Members:

_____
Gila Stein, Associate Professor,
Chemical & Biomolecular Engineering

_____
Jeffrey D. Rimer, Associate Professor
Chemical & Biomolecular Engineering

_____
Debora Rodrigues, Associate Professor
Civil and Environmental Engineering

_____
Mina Dawood, Associate Professor
Civil and Environmental Engineering

_____
Suresh K. Khator, Associate Dean,
Cullen College of Engineering

_____
Michael P. Harold, Professor and Chair,
Chemical & Biomolecular Engineering

Acknowledgement

I would like to express my sincerest gratitude to my advisor, Prof. Megan L. Robertson, who offered me the opportunity to the world of polymer researches. She always encouraged me to think and learn from both success and failure. I am very impressed by her integrity, knowledge, intelligence and diligence. I am grateful for her guidance, enthusiasm, and ongoing encouragement over my Ph.D. program.

I truly appreciate my committee members Professor Gila Stein, Professor Jeffrey D. Rimer, Professor Debora Rodrigues and Professor Mina Dawood for their time and effort on my dissertation and defense. Additionally, I am also grateful for the helpful suggestions from Professor Raymond Flumerfelt and Professor Manolis Doxastakis in my qualifier exam, and from Dr. Stein and Dr. Rimer in my proposal defense.

I wish to thank our collaborators: Professor Karen L. Wooley, and Samantha L. Kristufek, Lauren A. Link, and Khoi Van from Texas A&M University for their effort and helpful discussion in thiol-ene synthesis and 2D NMR analysis. I want to thank Professor Haleh Ardebili, and Mejdi Kammoun for access and training to dynamic mechanical analysis, and Professor Ramanan Krishnamoorti, Brian Rohde, and Daehak Kim for their assistance in experiments of FTIR and TGA. I would also like to offer my deep thanks to Dr. Charles Anderson for his time and dedication to the 2D-NMR measurements and analysis in the University of Houston, Department of Chemistry Nuclear Magnetic Resonance Facility. I also want to thank Professor Anil K. Bhowmick from the Indian Institute of Technology Kharagpur for the helpful discussions about thiol-ene results. I am also grateful for the helpful discussions regarding primary loop formation in networks from Professor Bradley D. Olsen and Rui Wang in Massachusetts Institute of Technology.

I also want to acknowledge the Texas Space Grant Consortium, the National Science Foundation, Norman Hackerman Advanced Research Program and University of Houston start-up funds for support of this research project, and Huntsman, Arkema and Dow Chemicals for providing materials samples for this work.

I would like to thank all present and former members in Dr. Robertson's lab for their support and friendship over the years: Avantika Singh, Shu Wang, Brian J. Rohde, Vivek Yadav, Wenyue Ding, Tyler Cooksey, Jialin Qiu, Hiruy Tesefay, and Rawan Almallahi. Especially, many thanks are given to Brian J. Rohde and Hiruy Tesefay, who directly participated in my researches on epoxy resins. I also feel lucky to have my friends in chemical engineering department: Jinsu Kim, Shuai Qian, Wei Dai, Lei Liu, Yang Zheng, Kai He, Daehak Kim. I will cherish our friendship.

Finally, I would like to express my dearest thanks to my family who encouraged and supported me in pursing my goal. I thank my parents, Xuehai Yang and Wanzhen She, my sister Huachun Yang, my parents-in-law, Yaozhong Shen, and Qiuhong Xi, as they have always been there for me. I also express my deepest thanks to my wife, Yan Shen and my daughter, Scarlet.

DEVELOPMENT OF SUSTAINABLE AND DEGRADABLE THERMOSETS AND ELASTOMERS

An Abstract

of

A Dissertation

Presented to

the Faculty of the Department of Chemical & Biomolecular Engineering

University of Houston

In Partial Fulfillment

of the Requirements for the Degree

Doctor of Philosophy

in Chemical Engineering

by

Guozhen Yang

August 2016

Abstract

The development of renewable energy and material sources is of utmost importance due to the finite supply of petroleum and environmental implications of petroleum processing. In this study, epoxy thermosets and thiol-ene elastomers were synthesized from bio-derived materials – phenolic acids and soybean oil.

Elastomeric polymer films derived from thiol-ene chemistry are attracting an increasing commercial interest, due to their ease of preparation and superior physical properties. Plant-sourced phenolic acids offer the presence of multiple hydroxyl and carboxyl groups leads to ease of functionalization. In this study, thiol-ene networks were synthesized through the photoinitiated reaction between allylated plant-based phenolic acids (salicylic acid, 3-hydroxybenzoic acid, 4-hydroxybenzoic acid, gentisic acid and gallic acid) and a multifunctional thiol. Allylation of the phenolic acids proceeded to high conversion and yield, and high conversion of both thiol and allyl functional groups was observed in the thiol-ene network formation. The phenolic acids produced networks with high degrees of homogeneity and few defects, as evidenced by narrow glass transitions and consistency of their tensile behavior with the ideal elastomer model at low-to-moderate strains. This work developed fundamental relationships between the molecular structure of the phenolic acids and the physical properties of the resulting networks.

Epoxy thermosets are widely applied in coatings, adhesives, automotive components, wind turbine blades and other applications, due to their superior chemical, electrical and heat resistance, adhesion and mechanical properties. However, these are crosslinked polymers within which all molecules are connected by covalent bonds, making it difficult to recycle them after their useful lifetime. In this study, epoxidized soybean oil

and epoxidized phenolic acid were employed to develop epoxy resins with degradability and high strength. Epoxy thermosets were synthesized containing epoxidized soybean oil and traditional petroleum-derived epoxy resin components (diglycidyl ether of bisphenol A [DGEBA] and methylene dianiline). Significant differences were observed in the hydrolytic degradation characteristics of the polymers in basic solutions. However, the flexible aliphatic chain of soybean oils decreased the glass transition temperature of the epoxy resins. As biorenewable monomers, plant-derived phenolic acids contain rigid aromatic rings which were expected to provide mechanical strength to the epoxy resins. Epoxidized phenolic acid were utilized to synthesize epoxy thermosets with an anhydride curing agent. The resulting epoxy resins exhibited thermal and mechanical behavior to traditional DGEBA-based epoxy resins.

Table of Contents

List of Figures

List of Tables

List of Schemes

Chapter 1 Introduction

As petroleum is a finite resource and processing of petroleum oils leads to environmental emissions, current efforts in academia and industry promote the utilization of renewable resources for the derivation of polymers.[1, 2] Diverse classes of biomass provide sustainable sources for polymers production. Many studies focus on the application of agriculture coproducts in polymers because of their abundance and low price, including nonfood sources of celluloses, lignin and natural rubber, and food sources of starches, sugar and vegetable oils.[3] There are also a diversity of literature studies on utilizing components derived from plants for polymers with high performance, such as quercetin,[4] rosin,[5-8] vanillin,[9] and phenolic acids.[10] The feedstocks are chemically modified to monomers with specific chemical structures and functional groups for incorporation into polymers. In order to replace commercial petroleum-derived monomers, important factors include designing polymers with comparable physical properties, maintaining low price and wide availability of the feedstock, and utilizing a manufacture procedure that is similar to established processes.

Biodegradation of polymers after their intended use is attracting more attention recently due to concerns about the accumulation of polymers in the environment.[11, 12] The polymers disposed in landfills slowly leak toxins, and in some cases reside in oceans, jeopardizing marine species.[13] In general, crosslinked polymers such as thermosets and elastomers present a particular challenge, as they cannot be recycled at the end of their useful lifetime. The crosslinked network (Figure 1.1) of conventional thermosetting polymers contributes to its long-term use, excellent mechanical properties, but also resistance to degradation after its useful life.[14] Presently, options for re-use of the material

include grinding up into small particulates to make fillers, or incineration. Introducing degradable cleavable points throughout the network is an attractive option for improving the (bio)degradability of a thermosetting material. Some studies have reported the use of the ester group[15, 16] and the urethane group[17, 18] in degradation of crosslinked polymers. However, degradability may conflict with durability and longevity of the materials. As a result, disposable goods have attracted more attention for the development of biodegradable materials, which can be composted after one-time use. Nonetheless, for durable goods, it is highly attractive to study the stability at a mild condition and the (bio)degradation at an extreme condition in the development of biodegradable polymers.

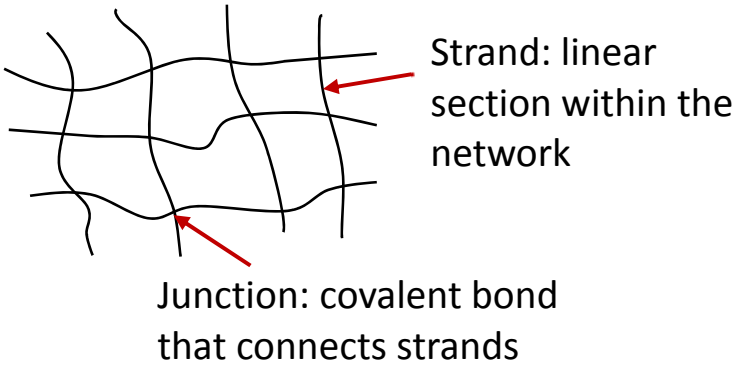

Figure 1.1: Structure of crosslinked network

In this study, we aimed to develop crosslinked polymers from biomass sources (shown in Figure 1.2). We modified bio-based molecules to monomers and synthesized the resulting crosslinked polymers, focusing on two classes of materials: thiol-ene elastomers and epoxy thermosets derived from plant-based phenolic acids. Additionally, we explored the development of epoxy resins from soybean oil which undergo hydrolytic degradation, providing a route to (bio)degradable thermoset polymers.

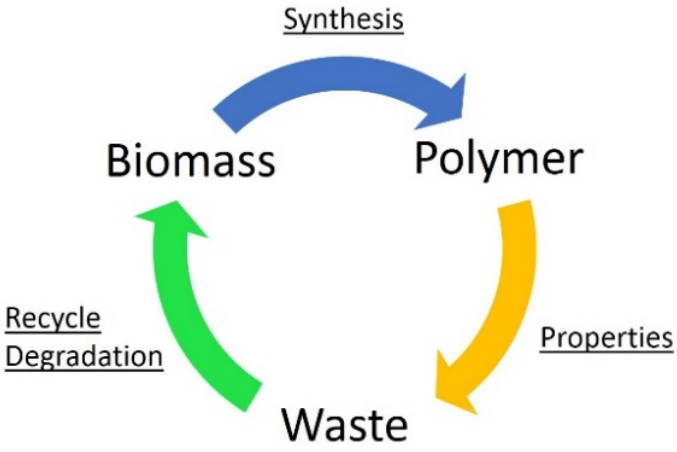

Figure 1.2**:** Life cycle of polymers derived from biomass

1.1 Thiol-Ene Elastomers

Thiol-ene elastomers, which are traditionally derived from petrochemical-based thiol- and ene-containing monomers, are attractive materials for coatings and adhesives,[19] due to their ease of fabrication, low shrinkage and stress,[20] and high degree of network homogeneity[19, 21-23] relative to other elastomeric materials. The thiol-ene chemistry employed to synthesize these elastomeric films has many advantageous features including high conversion and yield, rapid reaction rates, solvent-free conditions, lack of water and oxygen sensitivity, lack of byproducts, and ability to impart spatial and temporal control over the reaction (in the case of photoinitiation).[19, 21]

A diverse array of ene- and thiol-bearing molecules have been investigated for the preparation of thiol-ene networks,[19, 21, 22] though they are predominantly derived from petroleum-sources. Biorenewable molecules are attractive replacements for the components of thiol-ene elastomers as mild reaction conditions are employed, and the ability to conduct solvent-free syntheses enhances their environmental benefit. Relatively few studies have reported the derivation of thiol-ene elastomeric films using biorenewable

components; some notable examples include the use of vegetable oils and their fatty acids,[24-28] carbohydrates,[29, 30] terpenes,[31] and other plant-derived molecules.[32, 33] Black *et al.* functionalized caster oil with acrylate, allyl and vinyl ether groups and observed that aging within one week increased the degree of crosslinking and enhance physical performance; however, the long fatty acid chains within the vegetable oil produced a low crosslinking density, which decreased the storage modulus of resulting thiol-ene elastomer.[25] Furthermore, the use of acrylate monomers resulted in homopolymerization in addition to the thiol-ene curing.[25] Additionally, sucrose was allylated[29, 30] and quinic acid was acrylated[32] to prepare thiol-ene elastomers. Sucrose and quinic acid contain rigid aromatic rings, which may potentially increase the strength and glass transition of the elastomer, but also contain many hydroxyl and carboxylic acid groups. It was necessary to develop a more complex synthetic procedure to protect some of the functional groups before functionalization, in order to obtain a difunctional or trifunctional monomer. Exploring biobased monomers for thiol-ene applications, with rigid chemical structures and varying functionality that do not require complex multistep synthetic procedures to prepare, is an open challenge.

1.2 Epoxy Thermosets

Epoxy resins are widely applied in composite, coating, adhesive, automotive, and other applications, due to their superior chemical, electrical and heat resistance, adhesion, and mechanical properties.[34] Nowadays epoxy resins also play an important role in wind power, a renewable energy source and attractive alternative to fossil fuel.[35] Traditional epoxy resins are derived from petroleum, which produces harmful environmental impacts when processed. Additionally, there are potential health impacts from residual monomers

and additives in polymers and traditional epoxy resins are derived from bisphenol A, a chemical that has received much attention due to negative health consequences.[36] Therefore, it is a worthwhile goal to fabricate sustainable epoxy resins from renewable, non-toxic feedstocks.

Prior studies have investigated sustainable replacements for traditional epoxy resins components. Sustainable small molecules have been utilized in epoxy resins, such as vegetable oils, [37-60] sugars,[61, 62] rosin,[7, 8, 63] and quercetin.[4] The vegetable oil-containing epoxy resins exhibit a higher fracture toughness and impact strength, with a corresponding decrease in the glass transition temperature, due to a decrease in the crosslink density and increase in chain flexibility.[37-45, 48, 50, 51] Isosorbide, a glucose-derived molecule, has attracted recent attention due to its rigid structure and the presence of hydroxyl groups which are amendable to conversion to the epoxide groups required for the epoxy resin synthesis. Though isosorbide-based epoxy resins have desirable attributes,[61, 62, 64-67] they also exhibit significant water-uptake relative to conventional epoxy resins.[62, 64] Natural polymers applied in epoxy resins includes cellulose,[68] lignin,[69 70] and natural rubber.[71, 72] Cellulose, a polysaccharide, is an abundant biosource for polymer preparation, including grass, wood and straw. Varma et. al modified cellulosic fibers by attaching pendant primary amine groups to form a curing agent for epoxy resins;[68] however, the studies focused on filler applications of cellulose fibers within the epoxy resin matrix. [73-77] Nowadays, the diglycidyl ether of bisphenol A (DGEBA) is one of the most common commercial epoxy monomers for epoxy resins, which is petroleum-derived and of high mechanical strength, but brittle. Current research on bio-based epoxy resins is focused on developing an

alternative to DGEBA with comparable strength, modulus, and glass transition, as well as improved toughness.

1.3 Plant-Derived Phenolic Acids as Feedstocks for Thermosets and Elastomers

Phenolic acids are plant metabolites widely distributed in nature.[78-81] They are often found in plant byproducts including the skins and seeds of fruits and vegetables.[78-81] Phenolic acids offer many advantages as biorenewable monomers: their rigid aromatic rings are expected to provide mechanical strength to the resulting polymers and the presence of multiple hydroxyl groups and carboxyl groups leads to ease of functionalization. Through the choice of phenolic acid, the number and relative placement of hydroxyl and carboxyl groups can be varied, which is expected to be a convenient method of tuning the physical properties of the resulting polymers. Though no known studies have used phenolic acids for the preparation of thiol-ene networks, a few prior studies have developed epoxy resins from phenolic acid-based feedstocks. Aouf *et al.* epoxidized gallic acid (containing four functional groups) and cured the epoxidized monomer with isophorone diamine to form an epoxy resin.[10, 82] A few other studies focused on enhancing mechanical properties of gallic acid-based epoxy resins by incorporating graphene components.[83-85] Fourcade *et al.* synthesized a multi-epoxide monomer from a polyol and 4-hydroxybenzoic acid.[86] Additionally, salicylic acid was utilized to accelerate amine-epoxide reactions used to cure epoxy resins,[87] and to improve the traditional epoxy resins as a modifier.[78, 88-90]

1.4 Vegetable Oils as Feedstocks for Epoxy Resins

Vegetable oils have a triglyceride structure (Figure 1.3), containing various fatty acids, such as stearic acid, palmitic acid, oleic acid, linoleic acid, linolenic acid and

ricinoleic acid.[91] Epoxidized vegetable oil (EVO) is a derivative of vegetable oil obtained by converting the carbon-carbon double bonds on the fatty acid chain to an epoxide group. Common EVOs include epoxidized soybean oil (ESO), epoxidized linseed oil (ELO), epoxidized castor oil (ECO), and epoxidized palm oil.

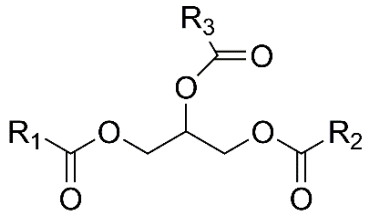

Figure 1.3: Chemical structure of a triglyceride. R1, R2, R3, are fatty acids

In general, epoxy resins derived from EVOs exhibit lower glass transition temperatures and better flexibility.[92] Previous research has indicated that even a small amount of the oil present in an epoxy resin can make the network more flexible.[93,55] Many studies in the literature have focused on using vegetable oils as a substitute for traditional epoxy resin components. Espinoza-Perez *et al.* compared various curing agents in EVO/ epoxy phenol novolac system.[49] Superior to other curing agents, bis(p-aminocyclohexyl) methane (PACM) composites showed only a slight reduction in the flexural modulus, when compared with PACM neat resins with 0% EVO.[49] Tan and Chow found that the high concentration of catalyst 2-ethyl-4-methylimidazole increased the reaction conversion and crosslink densities of the thermally cured ESO.[94] The DGEBA/ECO/N-benzylpyrazinium hexafluoroantimonate system exhibited maximum cure activation energy and initial decomposed temperature at 10 wt % ECO content.[95] Both the impact strength and the fracture toughness were improved by blending ESO or ELO into an epoxy resin containing diglycidyl ether of bisphenol F/ methyltetrahydrophthalic anhydride.[96] The adhesive lap shear strength and the impact strength of the DGEBA/ESO blend was significantly

improved by the addition of ESO.[97] Altuna *et al.* indicated 40% ESO epoxy resins had the maximum impact strength and showed phase separation, as evidenced by scanning electron microscopy (SEM).[51] However, it is also reported that the addition of ESO into epoxy resins decreased the glass transition, modulus and strength.[93, 95, 98]

1.5 Degradable Thermoset Polymers

The inherent ester groups on the triglyceride molecule have the potential to increase the degradability of epoxy resins. EVO is a triglyceride derivative with epoxide groups, which can participate into epoxy curing reaction. Hita *et al.* studied lipids degraded in soil and monitored their hydrolysis and oxidation.[15] Shogren *et al.* examined the biodegradability through respirometry of various thermoset polymers prepared from EVOs.[16] The ester linkage is also thermally cleavable. A series of epoxies with primary, secondary and tertiary esters were thermally degraded and it was observed that the polymers containing tertiary esters decomposed at lower temperatures than primary and secondary esters.[99]

There are other strategies for the development of degradable crosslinked polymers. The urethane group is also a cleavable functional group. Poly(ester-urethane)s (PEUs) degraded at a significant rate under soil burial condition, and hydrolytic degradation rate of PEUs was large in in 3% and 10% NaOH solutions at 37 ◦C with 20% weight loss in two days.[18] Literature by Li *et al.* indicates the polymer cured by the diepoxides with carbamate group started to decompose at lower temperature, between 200–300°C as compared with 350°C for the cured sample of the commercial cycloaliphatic epoxide.[100] Permanganate oxidation of the double bonds and cleavage of tertiary carbamate by strong acids can degraded the network.[101] Buchwalter *et al.* introduced either acetal or ketal group

into the epoxy structure. These cured epoxy resins containing acetal/ketal linkage could be cleaved into small molecules by immersing the epoxies into hot acid solution.[17] The high photosensitivity of polyethers on exposure to UV has been shown to result from the oxidizability of carbon atoms in the α position to the oxygen atoms.[102] Tesoro and Sastri reported conventional epoxy resins cured with aromatic diamines containing disulfide linkages; by pulverizing the cured epoxies to powders and treating these powders with reagents to convert the disulfide linkages into thiols, the cured epoxies could be recycled.[103,104]

1.6 Objectives of the thesis

The specific aims of this research are as follows:

1. Investigate Structure-Property Relationships of Sustainable Thiol-ene Networks derived from Phenolic Acids.

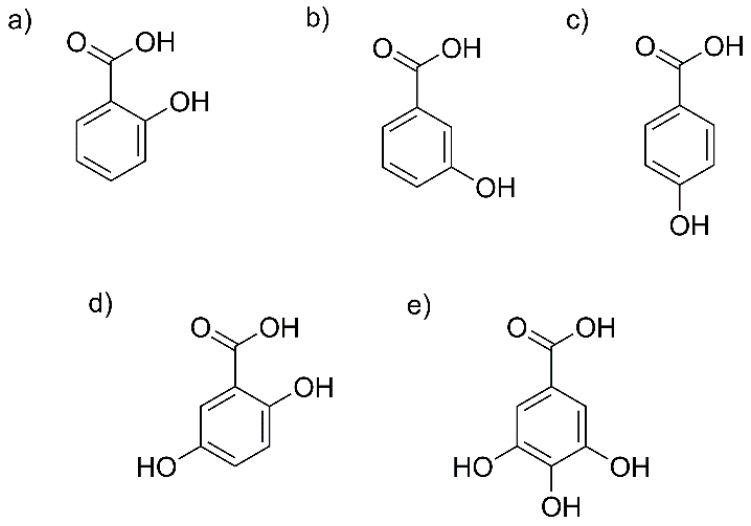

Figure 1.4: Chemical structures of phenolic acids used in this study: a) salicylic acid (SA), b) 3-hydroxybenzoic acid (3HBA), c) 4-hydroxybenzoic acid (4HBA), d) gentisic acid (GenA), e) gallic acid (GalA).

Five allylated phenolic acids (Figure 1.4) were investigated as components of thiol-ene networks: difunctional molecules with varying placement of functional groups (*ortho*,

meta, and *para*) and molecules with varying number of functional groups (ranging from 2-4). The thermal, mechanical, and structural properties of the thiol-ene networks were investigated. This work developed fundamental relationships between the functionality of the phenolic acids (number and placement of functional groups) and the physical properties of the resulting networks.

2. Develop Sustainable Epoxy Resins with Hydrolytic Degradability from Soybean Oil.

The hydrolytic degradation of polymers of varying soybean oil content was explored using accelerated degradation in a basic medium. The degradability of epoxy resins containing diglycidyl ether of bisphenol A (DGEBA), epoxidized soybean oil (ESO), and a multifunctional amine, methylene dianiline (MDA), was probed through measuring the sample mass over time in a sodium hydroxide solution. Additionally, the curing reaction was monitored through differential scanning calorimetry (DSC). The glass transition temperature and thermal degradation properties were also characterized through DSC and thermogravimetric analysis.

3. Develop Epoxy Resins with High Mechanical Performance from Bio-derived Phenolic Acids.

Difunctional epoxidized phenolic acids were explored as replacements for DGEBA in epoxy resins, as their rigid aromatic rings were anticipated to produce polymers of high modulus and glass transition, similar to DGEBA-based epoxy resins. The functional groups (one hydroxyl group and one carboxyl group) were readily converted to epoxide groups. Difunctional molecules (as opposed to epoxidized phenolic acids with greater functionality[10]) were selected to mimic the functionality of the traditional DGEBA monomer. This study explored the synthesis, thermal and mechanical properties of epoxy

resins derived from two difunctional phenolic acids: salicylic acid (SA) and 4-hydroxybenzoic acid (4HBA). The physical properties of these biorenewable epoxy resins were benchmarked to that of a conventional DGEBA-based epoxy resin.

1.7 Overview of this thesis

In the following chapters, the dissertation is organized as outlined below:

Chapter 2 describes the experimental methods used in this study. Detailed information on chemicals used, synthesis procedures and characterization techniques are included. The results of monomer modification (allylation and epoxidation) and polymer synthesis (thiol-ene click reaction and epoxy curing reaction) are discussed.

Chapter 3 discusses the effect of functional group placement on thiol-ene networks from monohydroxybenzoic acids, each containing one carboxylic acid and one hydroxyl group: salicylic acid (*ortho*-HBA or SA), 3-hydroxybenzoic acid (*meta*-HBA or 3HBA) and 4-hydroxybenzoic acid (*para*-HBA or 4HBA).

Chapter 4 discusses the effect of functional group number on thiol-ene networks from phenolic acids: the monohydroxybenzoic acids shown above (containing two functional groups), gentisic acid (GenA, with three functional groups), and gallic acid (GalA, with four functional groups).

Chapter 5 presents the hydrolytic degradation of epoxy resins derived from soybean oil which contain degradable ester groups. The curing agent is 4,4'-methylenedianiline (MDA), in which the functional groups are not degradable.

Chapter 6 investigates the thermal and mechanical properties of sustainable epoxy resins derived from SA and 4HBA. They are compared with a commercial epoxy resin, synthesized ying bisphenol A diglycidyl ether (DGEBA).

Chapter 7 provides a summary and conclusions of this research. An outlook of the challenges and future work is also discussed.

Chapter 2 Experimental Methods

2.1 Modification of Phenolic Acids

In this study, phenolic acids were modified in a two-step procedure prior to polymerization. Scheme 2.1 shows the general scheme for allylation followed by epoxidzation (SA is provided as an example). In the first step, hydroxyl and carboxyl groups on the phenolic acid are converted to allyl groups. The allylated phenolic acids were used to synthesize thiol-ene elastomers (Chapters 3 4). The allyl groups were then converted to epoxide groups, for the synthesis of epoxy resins (Chapter 6).

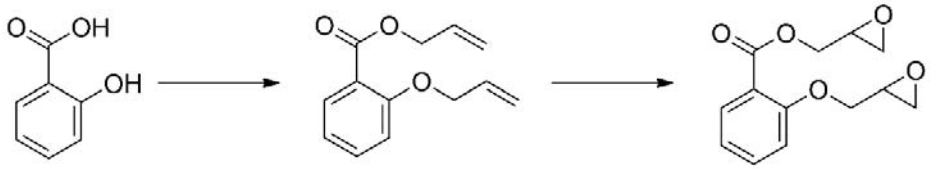

Scheme 2.1 Modification of salicylic acid

2.1.1 Synthesis of Allylated Phenolic Acids

Allylation of the phenolic acids was conducted following literature procedures.[10, 105] Phenolic acid (10 g) was dissolved into 340 mL N,N-dimethylformamide (DMF, BDH, ≥99.8%, ACS reagent) in a 1000 mL glass round bottom flask equipped with a rubber septum and a magnetic stirring bar. The temperature was maintained at 0 °C using an ice bath. Potassium carbonate (K_2CO_3, ≥99.0%, ACS reagent) was added to the flask (the molar ratio of K_2CO_3 to phenolic acid was 2.20 to 1.00 (for SA, 3HBA and 4HBA), 3.30 to 1.00 (for GenA), and 4.40 to 1.00 (for GalA)). After 3 min of stirring, allyl bromide (97%) was added dropwise with a syringe (the molar ratio of allyl bromide to phenolic acid was 2.20 to 1.00 (for SA, 3HBA and 4HBA), 3.30 to 1.00 (for GenA), and 4.40 to 1.00 (for GalA). The solution was stirred at room temperature for 48 h. Next, 340 mL distilled water was added into the solution. The solution was mixed with an equivalent volume of ethyl

acetate (BDH, ≥99.5%, ACS grade) and a separatory funnel was used to recover the ethyl acetate phase which contained the product. The remaining aqueous phase was extracted two additional times with ethyl acetate (the volume of ethyl acetate was equal to the aqueous phase volume in each extraction). The organic phase containing the allylated phenolic acid was washed with an equivalent volume of saturated brine and purified through drying with magnesium sulfate (BDH, ≥99.0%, anhydrous reagent grade) followed by distillation using a rotary evaporator to remove ethyl acetate. DMF was removed from the allylated phenolic acid through drying in a vacuum oven at 50 °C, until the NMR peaks associated with DMF (7.96 ppm, 2.94 ppm, 2.78 ppm) were not observed.

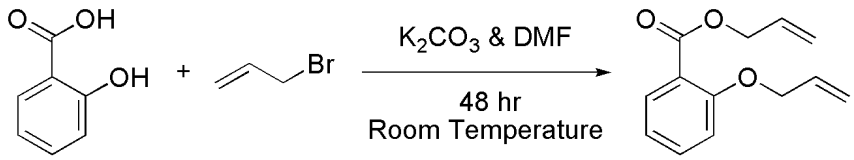

Scheme 2.2 Allylation of SA

The ^{1}H NMR spectrum of allylated SA is shown in Figure 2.1.[106, 107] No peaks are detected at 13.93 (carboxyl group in SA) and 11.27 (hydroxyl group in SA) ppm, indicating the disappearance of the hydroxyl and carboxyl groups. The peaks located in the region of 4-6 ppm correspond to the allyl groups in the allylated SA. The ratio of the peak area associated with the CH_2-O protons on the allyl group (4.58-4.69 ppm) to the peak area associated with the aromatic protons (6.80-7.90 ppm) should theoretically be 2:4 if there is complete conversion of the carboxyl and hydroxyl groups to allyl groups. Using the data shown in, this ratio is 4.04:4.00, which is very close to the theoretical prediction. The reaction conversion was calculated to be 99.5%, using the integrals of peaks associated with aromatic protons. Allylated SA was isolated in an 84% yield. The 4-hydroxybenzoic

acid (4HBA), gentisic acid (GenA) and gallic acid (GalA) were allylated following the same procedures. The ratio of the peak area associated with the CH_2-O protons on the allyl group to the peak area associated with the aromatic protons is very close to the theoretical prediction from complete conversion. These results are summarized in Table 2.1.

Table 2.1: ^{1}H NMR Characterization of Phenolic Acid Allylation

Phenolic acid	Conversion[a]	Peak area of CH_2O on allyl group : peak area of aromatic protons[b]	Yield
SA	99.5%	4.04:4.00 (4:4)	84%
3HBA	99.4%	4.12:4.00 (4:4)	77%
4HBA	99.6%	4.00:4.00 (4:4)	88%
GenA	97.5%	6.06:3.00 (6:3)	78%
GalA	100%	8.10:2.00 (8:2)	80%

[a]Within error of ^{1}H NMR measurement
[b]Theoretical ratio is given in parentheses

Allyl (2-allyloxy)benzoate (referred to as "allylated SA" in this manuscript): ^{1}H NMR (400 MHz, DMSO-d_6, ppm): δ 7.65 (dd, J = 7.7, 1.8 Hz, 1H), 7.50 (ddd, J = 8.5, 7.4, 1.8 Hz, 1H), 7.12 (dd, J = 8.5, 0.6 Hz, 1H), 7.00 (ddd, J = 7.7, 7.4, 0.6 Hz, 1H), 6.04-5.93 (m, 2H), 5.44 (ddt, J = 17.3, 1.9, 1.9 Hz, 1H), 5.37 (ddt, J = 17.2, 1.7, 1.7 Hz, 1H), 5.24-5.20 (m, 2H), 4.72 (ddd, J = 5.3, 1.7, 1.3 Hz, 2H), 4.61 (ddd, J = 4.7, 1.9, 1.3 Hz, 2H). ^{13}C NMR (100 MHz; DMSO-d_6): δ 165.4, 157.1, 133.6, 133.2, 132.7, 130.8, 120.3, 120.2, 117.7, 117.0, 113.8, 68.6, 64.9. FTIR (ATR) 3083, 3017, 2987, 2936, 2877, 1728, 1648, 1601, 1582, 1489, 1340, 1424, 1411, 1377, 1360, 1301, 1245, 1165, 1133, 1102, 1073, 996, 930, 854, 755, 706, 670, 654 cm^{-1}.

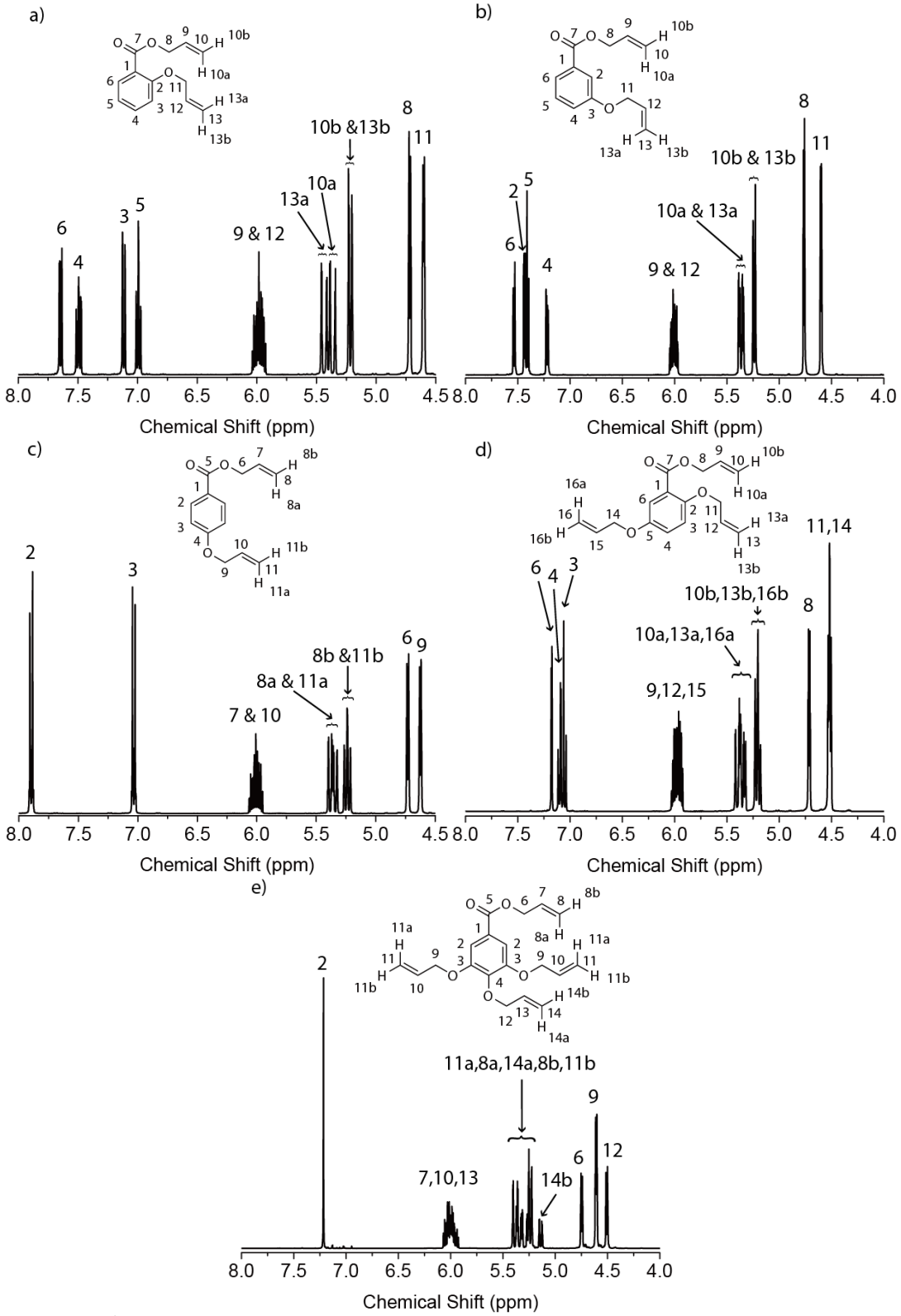

Figure 2.1: ^{1}H NMR data obtained from a) allylated SA, b) allylated 3HBA, c) allylated 4HBA, d) allylated GenA, e) allylated GalA.

Allyl 3-allyloxybenzoate (referred to as "allylated 3HBA" in this manuscript): ^{1}H NMR (400 MHz, DMSO-d_6, ppm): δ 7.54 (ddd, *J* =7.79, 1.37, 1.37 Hz, 1H), 7.44 (dd, *J* = 2.75, 1.83 Hz, 1H), 7.42 (dd, *J* = 7.79, 7.79 Hz, 1H), 7.23 (ddd, *J* = 8.24, 2.75, 0.92 Hz, 1H), 6.06-5.96 (m, 2H), 5.40-5.34 (m, 2H), 5.24 (ddt, *J* = 10.53, 1.37, 1.37 Hz, 2H), 4.77 (ddd, *J* = 5.50, 1.37, 1.37 Hz, 2H), 4.61 (ddd, *J* = 5.04, 1.37, 1.37 Hz, 2H). ^{13}C NMR (100 MHz; DMSO-d_6, ppm): δ 165.7, 158.8, 133.9, 133.1, 131.4, 130.6, 122.1, 120.6, 118.5, 118.1, 115.2, 68.9, 65.7. FTIR (ATR) 3082, 2943, 2877, 1720, 1649, 1599, 1585, 1487, 1443, 1424, 1361, 1319, 1291, 1272, 1213, 1158, 1107, 1078, 1027, 993, 983, 928, 875, 809, 754, 682, 640 cm^{-1}.

Allyl (4-allyloxy)benzoate (referred to as "allylated 4HBA" in this manuscript): ^{1}H NMR (400 MHz, DMSO-d_6): δ 7.93 (d, *J* = 9.0 Hz, 2H), 7.07 (d, *J* = 9.0 Hz, 2H), 6.10-5.98 (m, 2H), 5.44-5.35 (m, 2H), 5.30-5.24 (m, 2H), 4.76 (ddd, *J* = 5.3, 1.5, 1.5 Hz, 2H), 4.66 (ddd, *J* = 5.2, 1.5, 1.5 Hz, 2H). ^{13}C NMR (100 MHz, DMSO-d_6): δ 165.0, 162.2, 133.1, 132.9, 131.3, 121.9, 118.0, 117.7, 114.7, 68.5, 64.8. FTIR (ATR) 3086, 3050, 2989, 2941, 2873, 1714, 1649, 1605, 1581, 1509, 1455, 1421, 1361, 1313, 1268, 1251, 1169, 1102, 1011, 995, 929, 847, 769, 697, 668, 633 cm^{-1}.

Allyl 2,5-bis(allyloxy)benzoate (referred to as "allylated GenA" in this manuscript): ^{1}H NMR (400 MHz, DMSO-d_6, ppm): δ 7.18 (d, *J* = 2.93 Hz, 1H), 7.10 (dd, *J* = 8.79, 2.93 Hz, 1H), 7.05 (d, *J* = 8.79 Hz, 1H), 6.03-5.92 (m, 3H), 5.43-5.32 (m, 3H), 5.23-5.17 (m, 3H), 4.71 (ddd, *J* = 5.37, 1.47, 1.47 Hz, 2H), 4.54-4.50 (m, 4H). ^{13}C NMR (100 MHz; DMSO-d_6, ppm): δ 165.7, 152.1, 151.8, 134.2, 134.0, 133.1, 121.5, 120.3, 118.3, 118.0, 117.4, 116.8, 116.3, 70.0, 69.3, 65.5. FTIR (ATR) 3084, 3020, 2987, 2946,

2880, 1729, 1705, 1648, 1612, 1581, 1559, 1497, 1455, 1421, 1360, 1281, 1237, 1201, 1156, 1105, 1066, 1025, 996, 926, 892, 810, 780 cm^{-1}.

Allyl 3,4,5-tris(allyloxy)benzoate (referred to as "allylated GalA" in this manuscript): ^{1}H NMR (400 MHz, DMSO-d_6, ppm): δ 7.21 (s, 2H), 6.07-5.93 (m, 4H), 5.41-5.22 (m, 7H), 5.14 (ddt, *J* = 10.5, 1.47, 1.47 Hz, 1H), 4.75 (ddd, *J* = 5.37, 1.47, 1.47 Hz, 2H), 4.61 (ddd, *J* = 4.88, 1.47, 1.47 Hz, 4H), 4.51 (ddd, *J* = 5.86, 1.47, 1.47 Hz, 2H). ^{13}C NMR (100 MHz, DMSO-d_6, ppm): δ 165.4, 152.4, 141.6, 134.9, 134.0, 133.2, 125.1, 118.4, 118.0, 117.8, 108.4, 73.7, 69.9, 65.7. FTIR (ATR) 3080, 3021, 2985, 2945, 2871, 1716, 1648, 1586, 1498, 1455, 1422, 1375, 1362, 1328, 1290, 1264, 1236, 1204, 1130, 1109, 986, 926, 863, 812, 764 cm^{-1}

3-hydroxybenzoic acid: ^{1}H NMR (400 MHz, DMSO-d_6, ppm): δ 12.74 (broad s, 1H), 9.75 (broad s, 1H), 7.33 (d, *J* = 7.56 Hz, 1H), 7.29 (s, 1H), 7.24 (t, *J* = 7.56 Hz, 1H), 6.95 (d, *J* = 7.56 Hz, 1H). ^{13}C NMR (100 MHz; DMSO-d_6, ppm): δ 167.9, 157.9, 132.6, 130.1, 120.5, 120.4, 116.3.

Gentisic acid: ^{1}H NMR (400 MHz, DMSO-d_6, ppm): δ 13.75 (broad s, 1H), 10.65 (broad s, 1H), 9.13 (s, 1H), 7.11 (d, *J* = 2.93 Hz, 1H), 6.92 (dd, *J* = 8.79, 2.93 Hz, 1H), 6.75 (d, *J* = 8.79 Hz, 1H). ^{13}C NMR (100 MHz; DMSO-d_6, ppm): δ 172.3, 154.6, 149.9, 124.3, 118.3, 115.0, 113.1.

Gallic acid (GalA): ^{1}H NMR (400 MHz, DMSO-d_6, ppm): δ 12.22 (s, 1H), 9.17 (s, 2H), 8.82 (s, 1H), 6.88 (s, 2H). ^{13}C NMR (100 MHz; DMSO-d_6, ppm): δ 168.0, 145.9, 138.5, 120.9, 109.2.

2.1.2 Epoxidization of Allylated Phenolic Acids

The epoxidation of allylated phenolic acid (SA and 4HBA) was conducted following literature procedures for conversion of the allyl groups to epoxide groups.[10] Allylated phenolic acid (5.00 g, 22.9 mmol) was dissolved into 500 mL chloroform in a 1000 mL glass round bottom flask equipped with a rubber septum and a magnetic stirring bar. mCPBA (31.6 g, 183 mmol) was added to the flask (molar ratio of mCPBA to allylated phenolic acid was 8.00 to 1.00). The solution was stirred at 40 °C for 24 h. Next, the solution was washed with an equivalent volume of a 10% (wt/v) Na_2SO_3 aqueous solution and recovered using a separatory funnel. The organic phase was then washed with an equivalent volume of a saturated $NaHCO_3$ aqueous solution, and recovered using a separatory funnel. Finally, the organic phase was washed with an equivalent volume of distilled water, and recovered using a separatory funnel. The chloroform was then removed from the product using a rotary evaporator. The epoxidized salicylic acid (ESA) product was purified by silica gel chromatography using petroleum ethers/ethyl acetate (80/20), while the epoxidized 4-hydroxybenzoic acid (E4HBA) product was purified by silica gel chromatography using petroleum ethers/chloroform (80/20). The organic solvent was removed using a rotary evaporator and the product was dried in a vacuum oven at 50 °C overnight.

The ^{1}H NMR spectrum of ESA is shown in Figure 2.2a. No peaks are detected at 4.81 – 4.61 (OCH_2 in allyl group), 6.10 – 5.98 (-CH= in allyl group) and 5.53 – 5.25 ($=CH_2$ in allyl group) ppm, indicating the disappearance of the allyl groups. The peaks located in the region of 4.7-2.7 ppm correspond to the glycidyl groups in the ESA. The ratio of the peak area associated with the CH_2-O protons on the glycidyl group (4.65-4.05 ppm) to the

peak area associated with the aromatic protons (7.89-6.95 ppm) should theoretically be 4:4 if there is complete conversion of the carboxyl and hydroxyl groups to allyl groups. Using the data shown in Figure 2.2a, this ratio is 4.00:4.00, which is very close to the theoretical prediction. ESA was isolated in a 70% yield. The allylated 4-hydroxybenzoic acid (4HBA) was epoxidized following the same procedures. The allylated 4HBA was isolated in a 48% yield. These results are summarized in Table 2.2.

Epoxidized salicylic acid (referred to as "ESA" in this manuscript): ^{1}H NMR (400 MHz, chloroform-d, ppm): δ 7.85 (dd, *J* = 7.79, 0.92 Hz, 1H), 7.47 (ddd, *J* = 7.79, 7.79, 1.83 Hz, 1H), 7.01 (ddd, *J* = 7.79, 7.79, 0.92 Hz, 1H), 6.98 (d, *J* = 8.24 Hz, 1H), 4.62 (ddd, *J* = 12.36, 3.21, 3.21 Hz, 1H), 4.33 (dd, *J* = 11.22, 3.21 Hz, 1H), 4.20-4.13 (m, 1H), 4.08 (dd, *J* = 11.22, 5.04 Hz, 1H), 3.43-3.39 (m, 1H), 3.36-3.32 (m, 1H), 2.95-2.88 (m, 3H), 2.77-2.74 (m, 1H). ^{13}C NMR (100 MHz; chloroform-d, ppm): δ 165.8, 158.3, 133.9, 132.1, 121.0, 120.2, 113.9, 69.4, 65.4, 65.2, 50.2, 49.6, 44.8. FTIR (ATR) 1724, 1601, 1583, 1491, 1450, 1382, 1344, 1301, 1245, 1167, 1132, 1085, 1074, 1049, 1023, 972, 909, 844, 756, 703, 662, 644, 634, 624, 607 cm^{-1}.

Epoxidized 4-hydroxybenzoic acid (referred to as "E4HBA" in this manuscript): ^{1}H NMR (400 MHz, chloroform-d, ppm): δ 8.02 (d, *J* = 9.16 Hz, 2H), 6.94 (d, *J* = 9.16 Hz, 2H), 4.63 (dd, *J* = 12.60, 2.86 Hz, 1H), 4.30 (dd, *J* = 11.17, 2.86 Hz, 1H), 4.13 (dd, *J* = 12.03, 6.3 Hz, 1H), 3.99 (dd, *J* = 11.17, 6.30 Hz, 1H), 3.39-3.36 (m, 1H), 3.35-3.31 (m, 1H), 2.93 (dd, *J* = 4.58, 4.58 Hz, 1H), 2.89 (dd, *J* = 4.58, 4.58 Hz, 1H), 2.77 (dd, *J* = 5.15, 2.86 Hz, 1H), 2.72 (dd, *J* = 5.15, 2.86 Hz, 1H). ^{13}C NMR (100 MHz; chloroform-d, ppm): δ 166.0, 162.5, 131.9, 122.7, 114.3, 68.9, 65.3, 50.0, 49.7, 44.8, 44.7. FTIR (ATR) 1703,

1606, 1582, 1511, 1483, 1451, 1423, 1344, 1304, 1273, 1258, 1173, 1138, 1112, 1104, 1077, 1033, 991, 971, 914, 906, 882, 864, 843, 811, 767, 693, 669, 649, 633, 611 cm^{-1}.

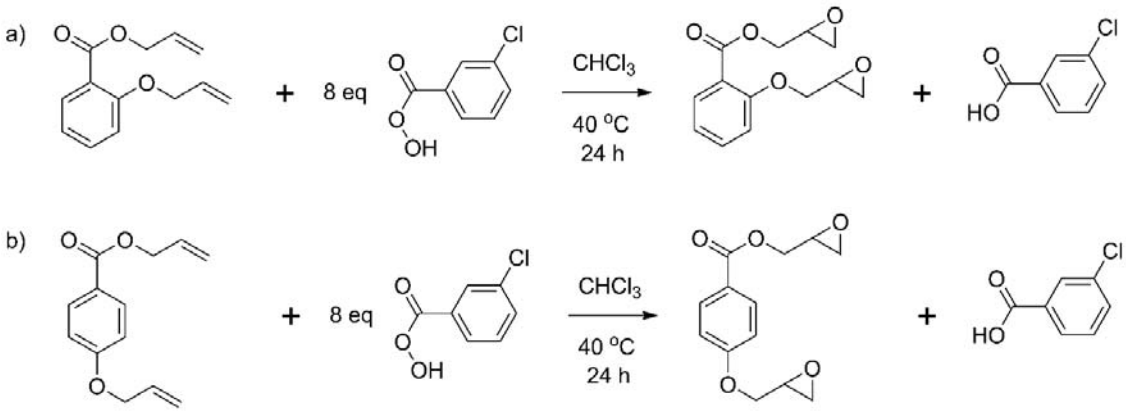

Scheme 2.3: Epoxidization of allylated a) salicylic acid and b) 4-hydroxybenzoic acid.

Table 2.2: ^{1}H NMR Characterization of Phenolic Acid Epoxidation

phenolic acid	peak area of CH_2O on glycidyl group : peak area of aromatic protons[a]	% yield
SA	4.12:4.00 (4:4)	70%
4HBA	4.09:4.00 (4:4)	48%

[a]Theoretical ratio is given in parentheses

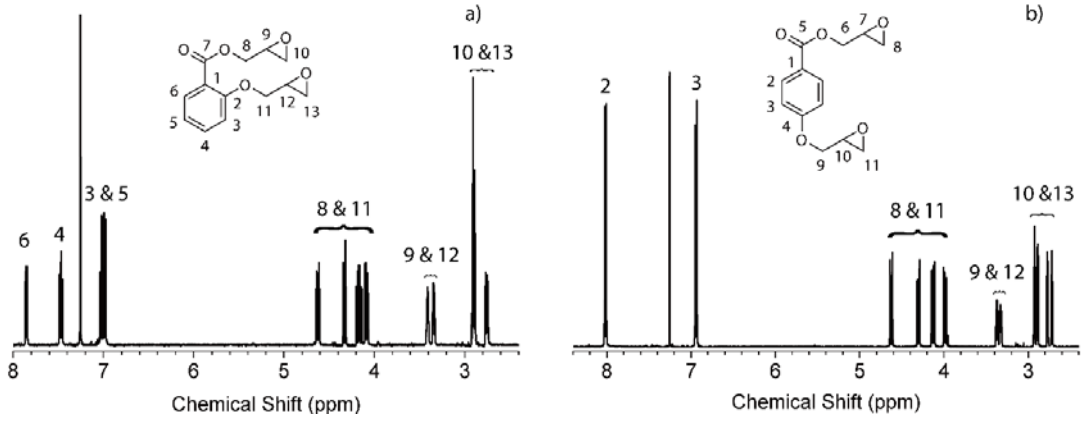

Figure 2.2: ^{1}H NMR data obtained from a) epoxidized SA, b) epoxidized 4HBA.

2.2 Synthesis of Thiol-Ene Networks

Thiol-ene chemistry[21, 108] follows the well-established step-growth radical mechanism (Scheme 2.4). Allyl ethers generally exhibit high reactivity in the thiol-ene

reaction,[19] and thiol-allyl ether systems exhibit high propagation rates relative to rates of chain transfer.[109] This offers a versatile platform for polymer synthesis due to its lack of sensitivity to water and oxygen, high conversion and yield, lack of byproducts, rapid reaction rates, solvent-free conditions, and ability to impart spatial and temporal control over the reaction (in the case of photoinitiation).[19, 21] The resulting films offer advantages of low shrinkage and stress,[20] and high degree of network homogeneity[19, 21-23] relative to other elastomeric materials.

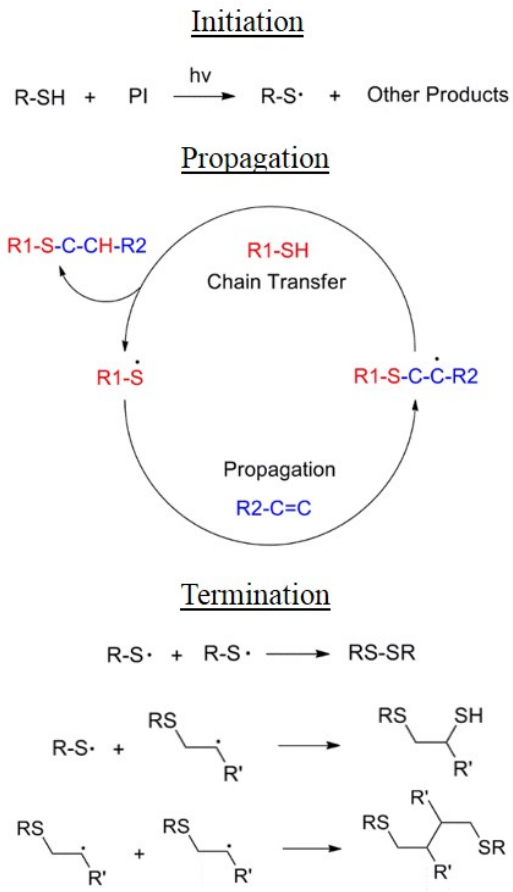

Scheme 2.4: General thiol–ene photopolymerization process

The UV curing of thiol-ene networks (Scheme 2.5) followed procedures similar to those reported in ref. [32]. The allylated phenolic acid was mixed with pentaerythritol tetrakis(3-mercaptopropionate) (PETMP, >95%) (stoichiometry based on equal molar

functional groups) and 1 wt% of the photo-initiator 2,2-dimethoxy-2-phenylacetophenone (DMPA, 99%) at room temperature in a 20 mL vial (using magnetic stirring), which was covered by aluminum foil. The mixture was placed in the following sample holders appropriate for each characterization experiment: a) between two glass slides with a 0.4 mm glass spacer for TGA, DSC, DMA and ATR-FTIR, b) between two NaCl windows (32 mm diameter, 3 mm thick) with a 0.05 mm Teflon spacer for transmission-mode FTIR, and c) in a Teflon dogbone-shaped mold following ASTM D638 (bar type 5, thickness 0.4 mm) for tensile testing. The sample was exposed under continuous 365 nm UV light (4 watt, Spectroline ENF-240C) for 15 min and transferred to a convection oven at 150 °C for a specified period of time, summarized in Table 2.3. The photoinitiated thiol-ene reaction between the allylated phenolic acids and the tetra-functional thiol PETMP (Scheme 2.5), which was monitored through FTIR.

FTIR spectra obtained upon UV curing of the allylated phenolic acids with the multifunctional thiol PETMP are shown in Figure 2.3. In all spectra, conversion of the thiol was monitored through disappearance of the peak located at 2570 cm^{-1} (S–H stretching), quantified in Tables S1-S5, while network formation was observed through an increase in the intensity of the peak located at 2950 cm^{-1} (alkane C-H stretching). Conversion of allyl groups on the allylated phenolic acids was monitored by decreases in the following peak intensities over time: 932 and 996 cm^{-1} (olefinic =C-H bending), 1647 cm^{-1} (C=C stretching), and 3080 cm^{-1} (olefinic =C-H stretching). We could not determine whether the peaks associated with the allyl groups disappeared completely, as they were all located in the vicinity of neighboring peaks (Figure 2.3). The peak located at 932 cm^{-1} may also include contributions from C-O stretching of ester groups present in both the phenolic acids

and PETMP.[110, 111] As increasing the UV exposure time beyond 15 min did not result in any appreciable differences in the FTIR spectra or conversion (Tables S1-S5), 15 min was chosen as the UV exposure time for all allylated phenolic acids (Table 2.3). The relative number and placement of allyl groups did not significantly impact the photoinitiated thiol-ene reaction between the allylated phenolic acids and PETMP.

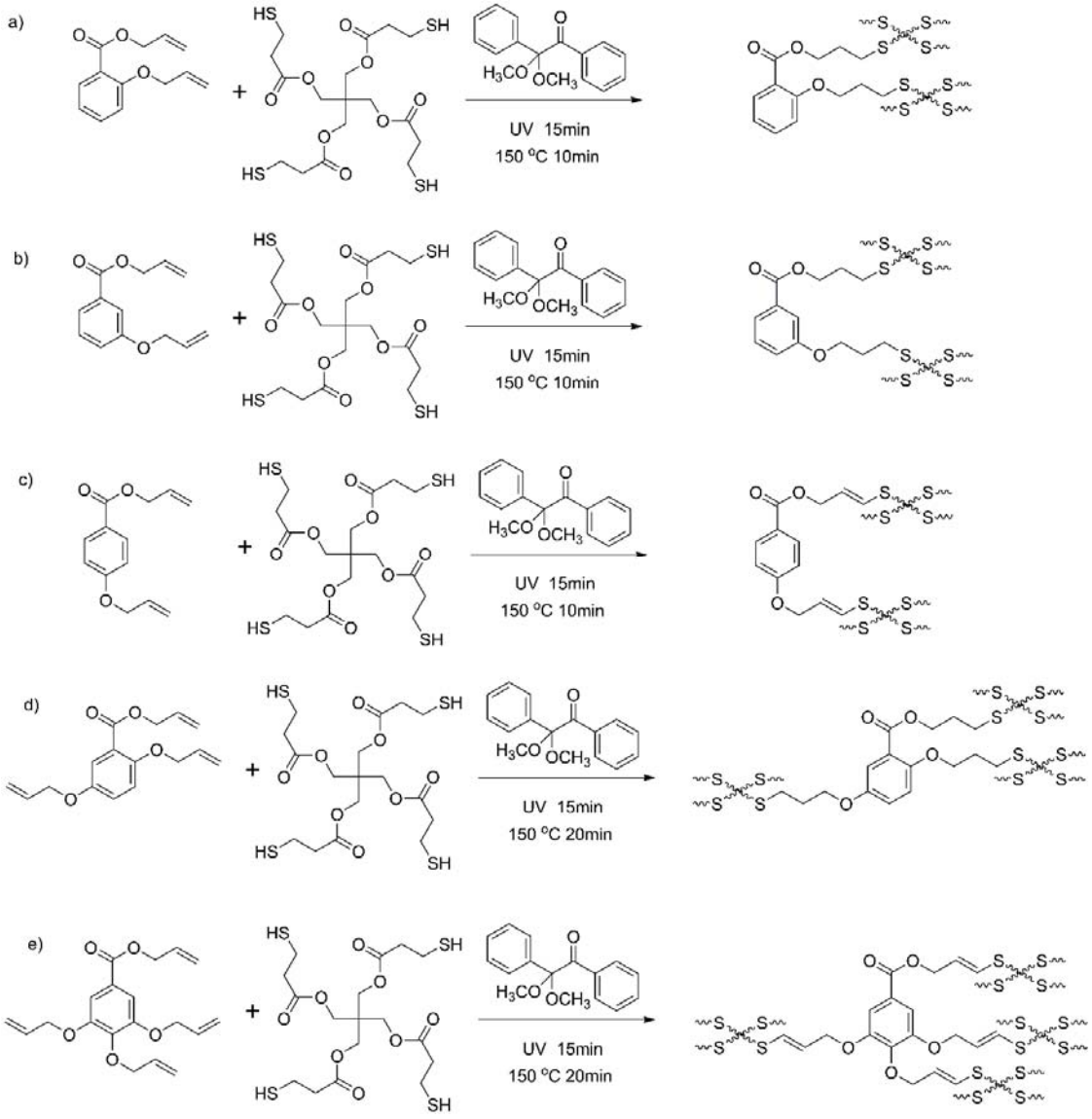

Scheme 2.5: Photoinitated thiol-ene reaction between the tetra-functional thiol PETMP and a) allylated SA, b) allylated 3HBA, c) allylated 4HBA, d) allylated GenA and e) allylated GalA.

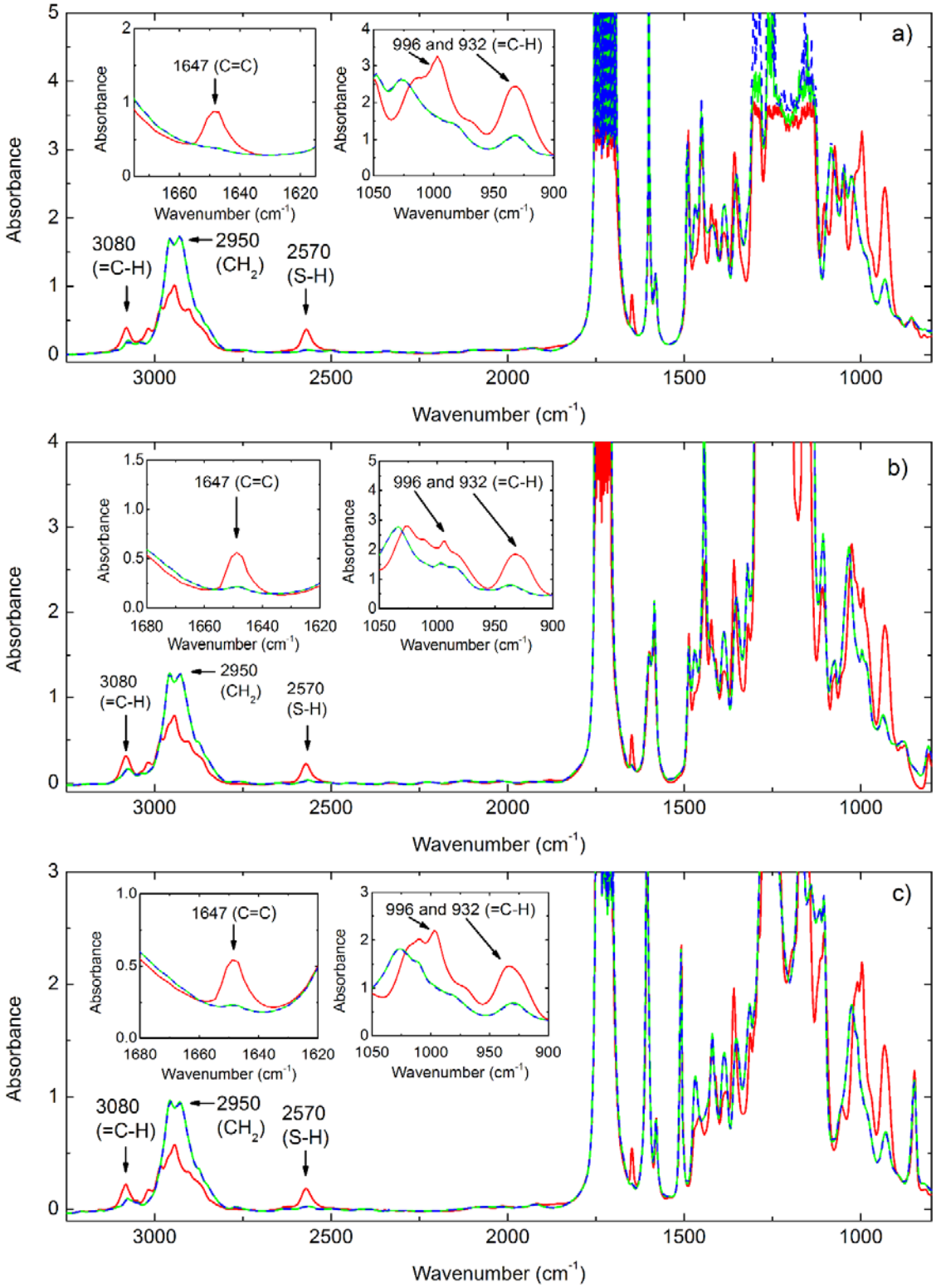

Figure 2.3: FTIR data obtained from a mixture of PETMP, photoinitiator, and a) allylated SA b) 3HBA,and c) 4HBA: before curing (red solid), after 15 min of UV exposure (green solid), and after 30 min of UV exposure (blue dashed).

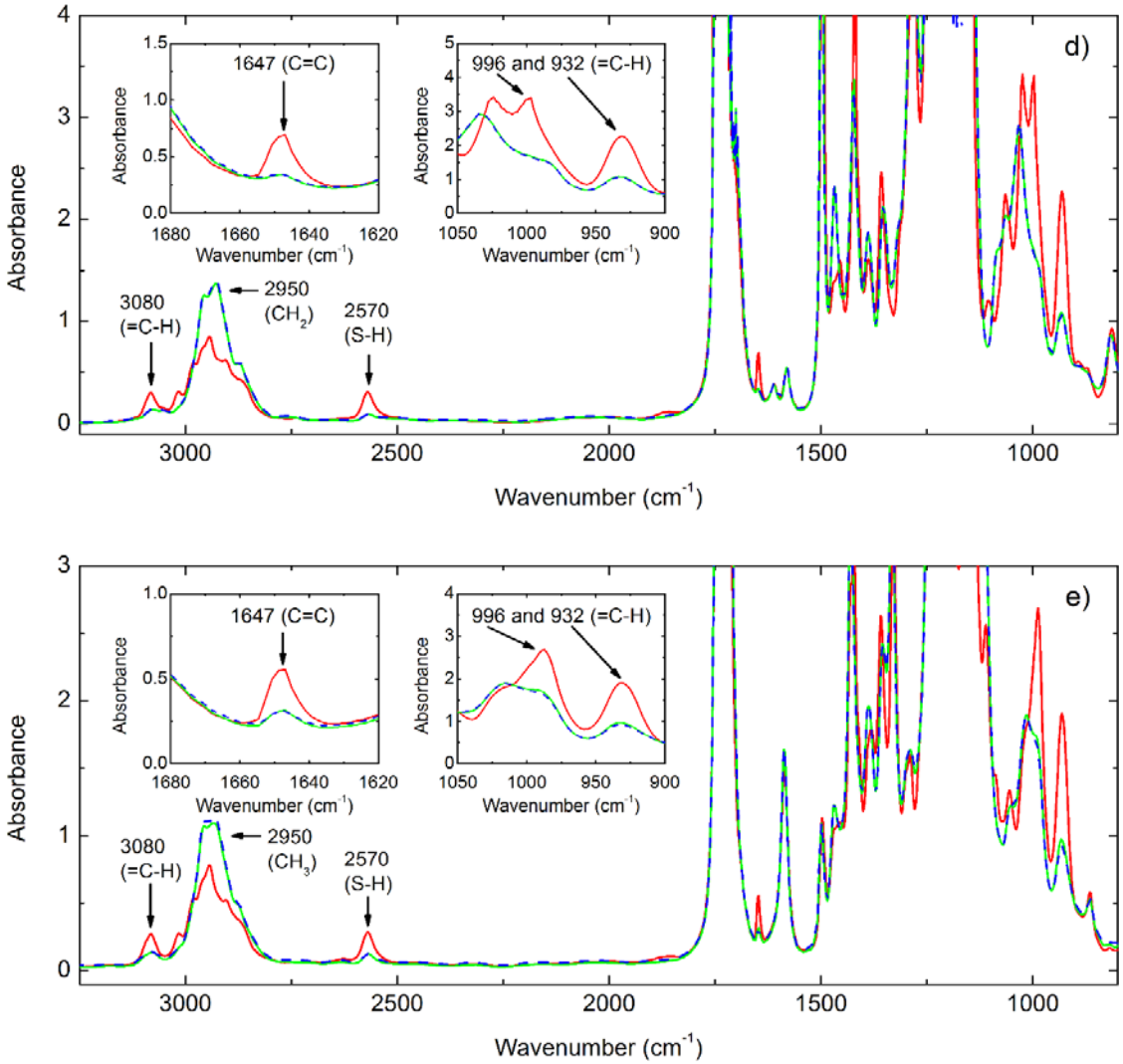

Figure 2.3: FTIR data obtained from a mixture of PETMP, photoinitiator, and d) allylated GenA and e) GalA: before curing (red solid), after 15 min of UV exposure (green solid), and after 30 min of UV exposure (blue dashed).

FTIR and differential scanning calorimetry (DSC) were employed to identify the isothermal annealing time for the thiol-ene networks following UV exposure, to achieve the highest possible conversion of functional groups. Thiol-ene networks were prepared through 15 min of exposure to UV followed by isothermal curing in a convection oven at 150 °C (the reaction conversion increased after the 150 °C post-cure, detailed in Tables S1-S5). In Figure 2.4 and Figure 2.5, the maximum absorbance of various FTIR peaks and glass transition temperature (T_g) are plotted as functions of the isothermal annealing time.

For the networks derived from difunctional phenolic acids (SA, 3HBA, and 4HBA), the conversion and T_g did not change upon increasing the isothermal annealing time beyond 10 min, and therefore an isothermal annealing time of 10 min was chosen. In the case of networks derived from multifunctional phenolic acids (GenA and GalA), a slightly longer isothermal annealing time of 20 min was chosen (to ensure the maximum possible conversion of functional groups, which did not change for annealing times beyond 20 min). The UV and isothermal curing protocols are summarized in Table 2.3.

Network synthesized from allylated SA: FTIR (ATR) 2953, 2929, 1732, 1600, 1582, 1491, 1467, 1452, 1420, 1388, 1352, 1302, 1244, 1166, 1135, 1085, 1047, 1028, 931, 757, 704, 663 cm^{-1}.

Network synthesized from allylated 3HBA: FTIR (ATR): 2922, 2852, 1737, 1716, 1600, 1584, 1488, 1469, 1443, 1387, 1352, 1320, 1275, 1225, 1140, 1106, 1074, 1033, 997, 937, 886, 808, 756, 683 cm^{-1}.

Network synthesized from allylated 4HBA: FTIR (ATR) 2954, 2921, 1736, 1710, 1605, 1580, 1510, 1468, 1421, 1385, 1353, 1316, 1273, 1251, 1168, 1140, 1105, 1028, 928, 849, 770, 697, 644 cm^{-1}.

Network synthesized from allylated GenA: FTIR (ATR): 2917, 2849, 1736, 1609, 1580, 1541, 1498, 1467, 1423, 1388, 1353, 1284, 1239, 1202, 1144, 1031, 930, 817, 784, 766, 746 cm^{-1}.

Network synthesized from allylated GalA: FTIR (ATR): 2916, 2849, 1737, 1647, 1586, 1499, 1469, 1429, 1387, 1355, 1332, 1288, 1207, 1145, 1114, 1052, 1015, 931, 871, 843, 766 cm^{-1}.

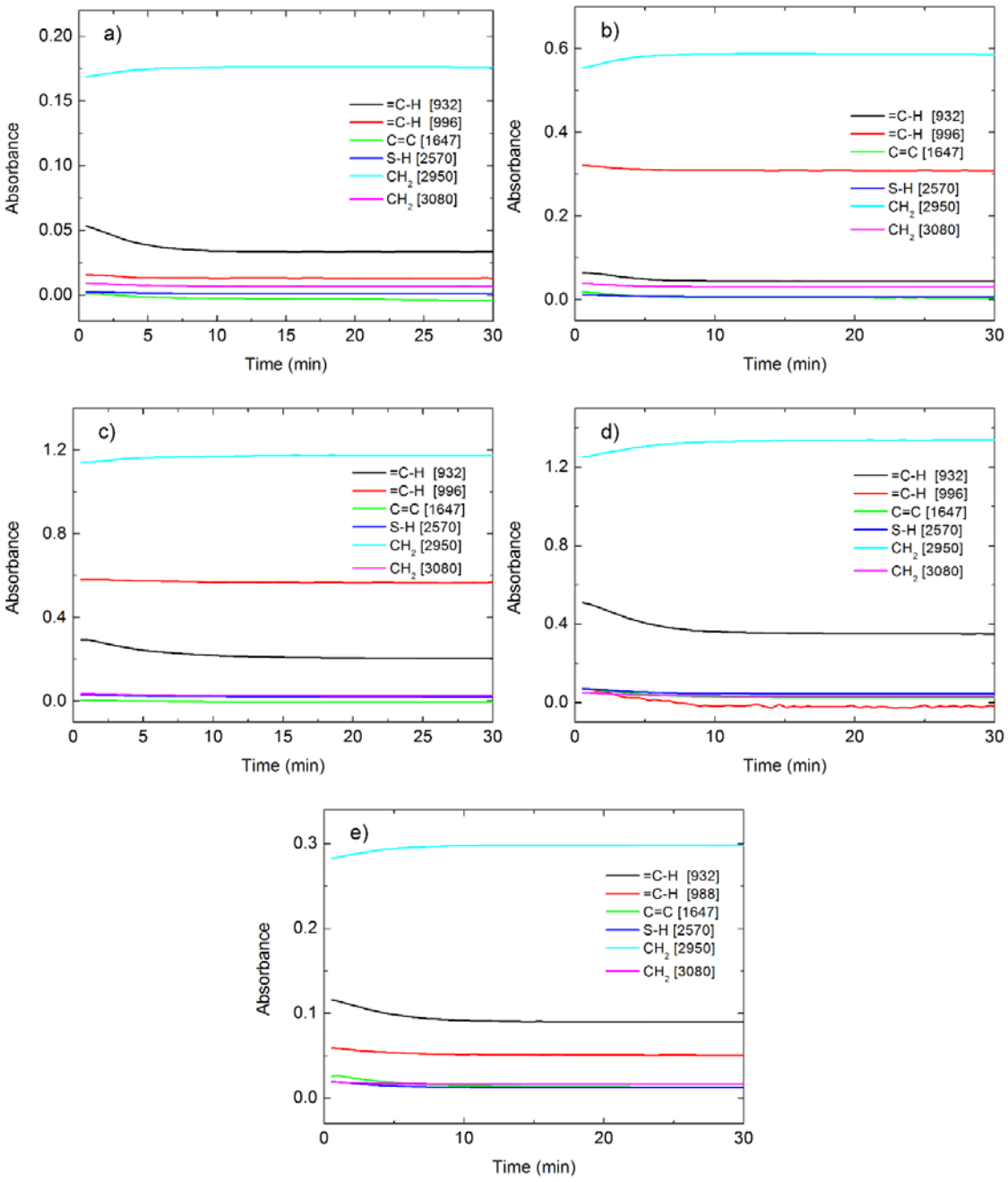

Figure 2.4: The FTIR absorbance as a function of time for selected peaks while curing at 150 °C (following 15 min of UV exposure) is shown in thiol-ene network derived from allylated a) SA, b) 3HBA, c) 4HBA, d) GenA and e) GalA.

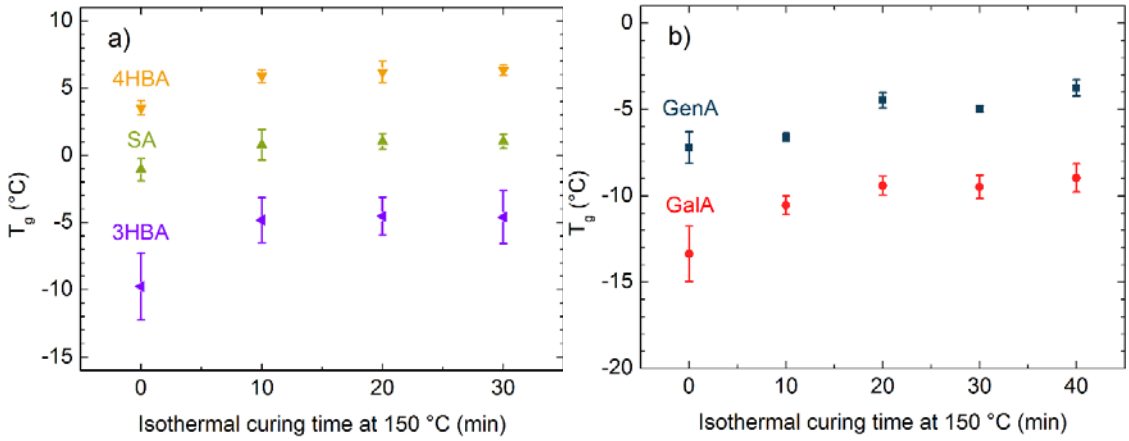

Figure 2.5: T_g as a function of isothermal curing time at 150 °C (following 15 min of UV exposure) for thiol-ene networks derived from allylated (a) SA (green ▲), 3HBA (purple ◂), 4HBA (orange ▼), (b) GenA (dark blue ■), GalA (red ●).

Table 2.3: Composition and Curing Protocol of Thiol-Ene Networks

Phenolic acid[a]	Molar ratio of reagents (allylated phenolic acid : PETMP : photoinitiator)	UV exposure time / Isothermal post-curing time at 150 °C
salicylic acid (SA)	1.0 : 0.50 : 0.018	15 min / 10 min
3-hydroxybenzoic acid (3HBA)	1.0 : 0.50 : 0.018	15 min / 10 min
4-hydroxybenzoic acid (4HBA)	1.0 : 0.50 : 0.018	15 min / 10 min
gentisic acid(GenA)	1.0 : 0.75 : 0.025	15 min / 20 min
gallic acid(GalA)	1.0 : 1.0 : 0.032	15 min / 20 min

[a]The phenolic acids were allylated and subsequently cured with pentaerythritol tetrakis(3-mercaptopropionate) (PETMP) and a photoinitiator, as described in the *Experimental Details*.

We quantified the biorenewable content in the thiol-ene networks, by calculating the wt% of phenolic acid in the final material. The biorenewable content (i.e. the contribution of the phenolic acids, which can be derived from plant sources) of the SA and 4HBA networks, both derived from difunctional phenolic acids, is calculated to be 29 wt%. We do not consider 3HBA to be a biorenewable chemical, as there is not a significant plant-based source to our knowledge. Rather, we have included this chemical in this study to highlight observed trends in the physical properties of the thiol-ene networks derived from difunctional phenolic acids, in which the relative placement of functional groups is varying (3HBA is the *meta*-hydroxybenzoic acid, complementing SA and 4HBA, which are

respectively *ortho*- and *para*-hydroxybenzoic acids). The biorenewable contents of the GenA and GalA networks (derived from trifunctional and tetrafunctional phenolic acids) are calculated to be 23 and 20 wt%, respectively. We conducted similar calculations for prior literature studies which report thiol-ene networks derived from biorenewable components, and found that the biorenewable content in prior studies on thiol-ene networks ranged from 20-58 wt%.[24-26, 28-32] One strategy to increase the total biorenewable content in our materials would be to employ a multifunctional thiol derived from a renewable resources, in addition to the allylated phenolic acids.

2.3 Synthesis of Epoxy Resins

2.3.1 Synthesis of Epoxy Resins from Epoxidized Soybean Oil

Epoxidized soybean oil (ESO) was kindly supplied free of charge by Arkema, Inc. (trade name Vikoflex 7170). Proton nuclear magnetic resonance experiments (using a JEOL ECA-500 instrument) were conducted on the Vikoflex 7170 and it was determined that there is an average of 4.27 epoxide groups per triglyceride molecule. MDA(4,4'-diaminodiphenylmethane, 97%, or MDA) was purchased from Alfa Aesar. The general curing reactions between DGEBA and MDA, as well as between ESO and MDA, are shown in Scheme 2.6. Three different protocols were used for the preparation of epoxy resins (Table 2.4). Protocols A and B were used to prepare samples for degradation experiments, as well as characterization of the glass transition temperature (through DSC) and thermal degradation properties (through TGA). Protocol C was used for the in-situ characterization of the curing process through DSC. In general, multistep reaction protocols were used following literature procedures.[40, 42, 43, 46, 47, 51, 58, 59] Through a multistep reaction, the time spent at the highest temperatures is minimized, avoiding

thermal degradation of the polymer. Specifically, we followed a previous study employing a four-step heating protocol for epoxy resins with < 50 wt% ESO,[59] and another study employing a two-step heating protocol for epoxy resins with > 50 wt% ESO.[51]

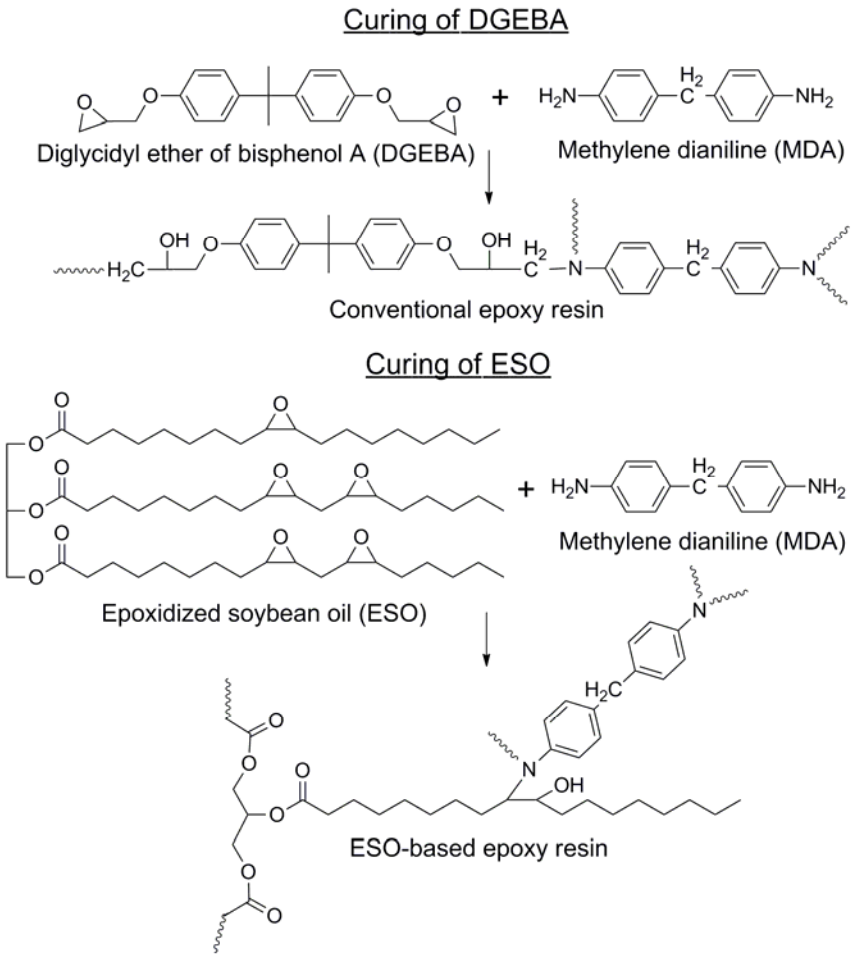

Scheme 2.6: Curing reactions for traditional epoxy resins (containing DGEBA and MDA) and triglyceride oil-based epoxy resins (containing ESO and MDA).

It was observed that MDA and ESO form an opaque solution at room temperature, likely due to lack of miscibility. Upon heating and stirring the mixture at 80 °C for 30 min, the solution becomes transparent and the components are likely miscible. If allowed to cool to room temperature prior to curing, the mixture becomes opaque once again. For this

reason, the samples were immediately transferred to the DSC after the 80 °C pre-mixing step and to the vacuum oven after the 80 °C degassing step (Table 2.4).

Table 2.4: Curing Protocols

Protocol	Description
A	DGEBA, MDA, and ESO were mixed together at 80 °C for 30 min (or until complete dissolution of the components) and degassed in a vacuum oven at 80 °C for 30 min. The mixture was then transferred to a convection oven and cured according to the following protocol: 101 °C for 3 h, 122 °C for 2 h, 141 °C for 1 h, and 153 °C for 30 min
B	DGEBA, MDA, and ESO were mixed together at 80 °C for 30 min (or until complete dissolution of the components) and degassed in a vacuum oven at 80 °C for 30 min. The mixture was then transferred to a convection oven and cured according to one of the following protocols: 1) 135 °C for 1 h and 198 °C for 3 h 2) 135 °C for 1 h and 198 °C for 9 h 3) 135 °C for 1 h and 198 °C for 21 h 4) 135 °C for 1 h and 198 °C for 3 days
C	DGEBA, MDA, and ESO were mixed together at 80 °C for 30 min (or until complete dissolution of the components) and transferred to an aluminum pan. The pan was subsequently sealed and transferred to the differential scanning calorimeter. The sample underwent one of the two following protocols: 1) heated at a constant rate of 10 °C/min from 50 °C to 360 °C 2) heated isothermally at a temperature of 200 °C

All epoxy resins contained a ratio of epoxide-bearing molecules (DGEBA and ESO) to amine-bearing molecules (MDA) of 100:30 (by weight). The total epoxide content is a mixture of DGEBA and ESO. Throughout this study, the concentration of ESO in the epoxy resin will be reported as a percentage of the total epoxide content (DGEBA + ESO), by weight. The ratio of 100:30 was chosen as it corresponds to a stoichiometrically balanced molar ratio of 0.97 epoxide groups to one active hydrogen atom (on a primary amine group) for a mixture of MDA and DGEBA. For a mixture of ESO and MDA, there are 0.76 epoxide groups to one active hydrogen atom (based upon the NMR

characterization of ESO which indicated the presence of an average of 4.27 epoxide groups per triglyceride molecule). Therefore, there is excess amine present in the samples containing ESO.

2.3.1 Synthesis of Epoxy Resins from Epoxidized Phenolic Acids

The epoxidized phenolic acid (1.00 g, 4.00 mmol) was mixed with Methylhexahydrophthalic Anhydrid (MHHPA, 1.35 g, 8.00 mmol, stoichiometry based on equal molar functional groups) and 3 phr (parts per hundred resin) of the catalyst 1-methylimidazole (1-MI, 0.03 g, 0.0365 mmol) at 50 °C in a 20 mL vial (using magnetic stirring). The mixture was placed in the following sample holders appropriate for each characterization experiment: a) in a preweighed Tzero aluminum pan for differential scanning calorimetry, b) in a pan for thermogravimetric analysis, c) between two NaCl windows (32 mm diameter, 3 mm thick) with a 0.05 mm Teflon spacer for transmission-mode FTIR, and d) in a aluminum dogbone-shaped mold following ASTM D638 (bar type 5, thickness 1.6 mm) for tensile testing. The sample was then transferred to a convection oven and cured according to the following protocol: 70 °C for 2 h, 170°C for 2 h.

2.4 Chemical Analysis

2.4.1 Nuclear Magnetic Resonance (NMR)

The following NMR experiments were performed on a JEOL ECA-400 or JEOL ECA-500 instrument using deuterated dimethyl sulfoxide (Cambridge Isotope Laboratories, Inc., 99.9% D) or deuterated chloroform (Cambridge Isotope Laboratories, Inc., 99.9 % D) as the solvent: ^{1}H NMR (400 MHz or 500 MHz), ^{13}C NMR (100 MHz or 125 MHz), DEPT 135, COSY, HSQC, and HMBC. Chemical shifts were referenced to the solvent proton resonance (2.5 ppm for dimethyl sulfoxide, 7.26 ppm for deuterated chloroform).

2.4.2 Fourier Transform Infrared Spectroscopy (FTIR)

FTIR spectra were recorded on a Thermo Scientific Nicolet 4700 spectrometer in transmission mode as well as using an attenuated total reflection (ATR) stage (containing a Germanium crystal). The OMNIC Series software was used to follow selected peaks at 1.928 cm^{-1} resolution using 32 scans.

2.5 Differential Scanning Calorimetry (DSC)

The glass transition temperature (T_g) was measured through DSC experiments. They are conducted using a TA Instruments Q2000 calorimeter, calibrated with an indium standard, with a nitrogen flow rate of 50 ml/min.

2.5.1 DSC Measurement of Thiol-ene Elastomers

The cured thiol-ene sample (following the protocol in the *Polymer Synthesis* section) was placed in the calorimeter (using a Tzero aluminum pan), equilibrated at 40 °C, cooled to -40 C at a rate of 10 °C /min and heated to 40 °C at a rate of 10°C/min. The cooling and heating scans were repeated for a total of three measurements. The value of the T_g was determined using the half extrapolated tangents method in the Universal Analysis software.[112] The onset and endset temperatures were also identified with the Universal Analysis software.

2.5.2 DSC Measurement of Epoxy Thermosets

The curing reactions between DGEBA, ESA and E4HBA and various curing agents were monitored through *in situ* DSC. The epoxy resin components (DGEBA, ESA or E4HBA, as well as curing agent and catalyst) were mixed at 50°C and placed in a preweighed Tzero hermetic aluminum pan. The pan was transferred to the differential

scanning calorimeter, equilibrated at 40 °C and heated to 200 °C at a rate of 10 °C /min to examine the curing behavior at constant heating rate.

The glass transition temperatures (T_g) of specimens prepared through various curing protocols (specimens cured at constant heating rate in the DSC, as well as specimens prepared in a convection oven for tensile testing) were measured through DSC experiments. The cured sample was placed in the calorimeter (using a Tzero aluminum pan), equilibrated at 40 °C, heated to 200 °C at a rate of 10 °C /min, cooled to 40 °C at a rate of 10°C/min and heated to 200 °C at a rate of 10°C/min. The value of the T_g was determined using the half extrapolated tangents method in the Universal Analysis software.

2.6 Thermogravimetric Analysis (TGA)

TGA experiments were conducted with a TA Instruments Q500 analyzer. The sample was heated from 30 °C to 800 °C at a rate of 10°C/min in an argon environment (the balance argon purge flow was 40 ml/min and the sample purge flow was 60 ml/min).

2.7 Dynamic Mechanical Analysis (DMA)

The dynamic mechanical behavior of cured thiol-ene films (following the protocol in the *Polymer Synthesis* section) was probed using a Q800 dynamic mechanical analyzer (TA Instruments) with a nitrogen environment. Specimens of 0.4 mm thickness were cut with a razor blade to have the following dimensions: 10 mm x 5 mm x 0.4 mm (length x width x thickness). Four experiments were conducted: 1) Isothermal strain sweeps were conducted at desired temperatures and using a frequency of 1 Hz to locate the range of strains in the linear viscoelastic region; 2) isothermal frequency sweeps were conducted from 0.1 to 10 Hz at desired temperatures, using a strain within the linear viscoelastic region; 3) time-temperature superposition of the data was performed at 0, 5, 10, 15, 20, 25,

30, and 40 °C, and 4) temperature ramps were conducted at a constant strain and frequency. In the case of time-temperature superposition, the master curve was prepared using the TA Instruments Rheology Advantage Data Analysis software with 30 °C chosen as the reference temperature.

2.8 Tensile Testing

2.8.1 Tensile Testing of Thiol-Ene Elastomers

Tensile testing was carried out with an Instron 5966 universal testing system containing a 2 kN load cell.Thiol-ene dogbone-shaped testing bars (ASTM D638, bar type 5, thickness 0.4 mm) were prepared following the procedure in the *Polymer Synthesis* section. Pneumatic grips (maximum force 2 kN) were used to affix the sample in the testing frame, at a compressed air pressure of 40 psi. The force and change in length were measured as the sample was elongated at a rate of 10 mm/min. Each measurement was repeated with 5-6 test specimens that broke in the gauge region and did not contain a visible defect at the point of fracture.

2.8.2 Tensile Testing of Epoxy Resins

Epoxy dogbone-shaped testing bars (ASTM D638, bar type 5, thickness 1.5 mm) were prepared following the curing protocol described above. Pneumatic grips (maximum force 2 kN) were used to affix the sample in the testing frame, at a compressed air pressure of 80 psi. The force and change in length were measured as the sample was elongated at a rate of 1 mm/min. The engineering stress was calculated using the measured force and cross-sectional area of the sample. The engineering strain was measured directly using an Instron extensometer (gauge length 0.3 inch, travel ± 0.15 inch). Each tensile measurement

was repeated with 5 test specimens that broke in the gauge region and did not contain a visible macroscopic defect (voids, bubbles, etc) at the point of fracture.

2.9 Hydrolytic Degradation

Hydrolytic degradation experiments were conducted in aqueous sodium hydroxide (NaOH) solutions, containing either 3 or 10 wt% NaOH, at 80 °C (0.04 wt% sodium azide was also added to the solution to prevent microbial growth), following literature procedures.[18] The sample weight was recorded (approximately 0.01 to 0.05 g) and it was placed in 10 mL of the NaOH solution for a predetermined time period. The sample was then removed from the solution, rinsed with deionized (DI) water, rinsed with a 1 wt% HCl solution, rinsed with DI water, and dried in a vacuum oven at 50 °C for 18-24 h. The sample weight was recorded and then the sample was placed back in the NaOH solution for additional days. This process was repeated until the sample was fully degraded, or up to a maximum of 72 days (in the NaOH solution).

2.10 Scanning Electron Microscopy

Scanning Electron Microscopy (SEM) micrographs of the fracture surfaces of tensile bars were imaged using a LEO 1525 field emission scanning electron microscope at a voltage of 15 kV. The fracture surface was etched with ionized argon gas and subsequently coated with gold using a Denton Vacuum Desk V sputter coater. The gold thickness was approximately 10 nm. The resulting micrographs were converted to binary images and analyzed with ImageJ to determine the areas of each feature (parabolic and elliptical features). Parabolic and elliptical features were manually distinguished from one another.

2.11 Density Measurement

The densities of phenolic acid-based thiol-ene networks were measured in a vial containing a calcium nitrate water solution of known concentration at room temperature. The water content was adjusted to determine the composition range over which the polymer transitioned from being suspended in the solvent to sinking in the solvent. This range was narrowed until the density could be determined to 2 significant digits after the decimal point. The exact density of calcium nitrate solution was determined through the quadratic equation fitting to the density-concentration data in a previous study.[113] The resulting densities were as follows: aSA-based thiol-ene networks, 1.22 g/mL; a3HBA-based thiol-ene networks, 1.22 g/mL; a4HBA-based thiol-ene networks, 1.22 g/mL; aGenA-based thiol-ene networks, 1.22 g/mL; aGalA-based thiol-ene networks, 1.22 g/mL.

Chapter 3 Effect of Functional Group Placement on Thiol-Ene Networks from Difunctional Allylated Phenolic Acids

3.1 Introduction

The synthesis of thiol-ene networks from difunctional allylated phenolic acids is described in Chapter 2. The phenolic acids were allylated and reactioned with a multifunctional thiol in the presence of a photoinitiator. Three phenolic acids were investigated: salicylic acid (SA or *ortho*-HBA), 3-hydroxybenzoic acid (3HBA or *meta*-HBA) and 4-hydroxybenzoic acid (4HBA or *para*-HBA). All phenolic acids contain two functional groups (one carboxylic acid group and one hydroxyl group), yet the relative placements of the functional groups vary (i.e. *ortho*, *meta*, *para* position). Synthetic conditions were developed to prepare thiol-ene networks with high yield and conversion. The thermal and mechanical behavior of the thiol-ene networks were investigated. This work develops fundamental relationships between functional group placement on the phenolic acids and the physical properties of thiol-ene networks. Such knowledge is an important first step toward the widespread implementation of biobased phenolic acids in thiol-ene elastomer applications.

3.2 Results and Discussion

3.2.1 Thermal Characterization

Differential scanning calorimetry (DSC) was employed to characterize the glass transition temperature (T_g) of thiol-ene networks that were prepared following the protocol in Table 2.3. The average and standard deviation values of T_g obtained during the first heating scan are provided in Table 3.1.

The T_g's of these networks are lower than room temperature, as is typically observed in thiol-ene networks, which contain flexible thioether linkages.[114] The 4HBA network exhibited the highest T_g, attributed to the high crosslink density of this network. Though the SA and 3HBA networks had similar crosslink densities (Table 3.2), the T_g of the SA network was significantly higher than that of the 3HBA network. Differences in the SA and 3HBA network T_g's may possibly be explained by differences in steric hindrance resulting from the relative placements of the allyl groups around the aromatic ring in the allylated monomer (*ortho* vs. *meta* positions). The average and standard deviation values obtained during the first heating scan are provided in Table 3.1.

Table 3.1: Thermal Properties of Thiol-Ene Networks Derived from Phenolic Acids[a]

phenolic acid	T_g (°C), as-prepared[b]	onset degradation temperature (°C)[c]
SA (*o*)	0.8 ± 2.1	341.9
3HBA (*m*)	-7.1 ± 1.9	349.2
4HBA (*p*)	5.5 ± 2.2	343.0

[a] Samples were prepared following the protocol in *Table 2.3*. *o*, *m,* and *p* indicate *ortho*, *meta*, and *para*.
[b] Nine total measurements using DSC were obtained for each sample, from three distinct regions of three separate specimens. The results presented in this table were obtained from the first heating scan.
[c] Determined from TGA.

The thermal degradation properties of the networks were explored with thermogravimetric analysis (TGA), and the results are summarized in Table 3.1. The three types of networks have similar onset degradation temperatures, around 342-349 °C, which is significantly higher than the chosen isothermal post-curing temperature of 150 °C. Therefore, it is expected that little sample degradation occurs during the curing process.

3.2.2 Network Structure and Homogeneity

The storage (E') and loss (E") moduli were probed as a function of strain (using frequency = 1 Hz) at selected temperatures. A strain in the linear viscoelastic region was

chosen at each temperature and used to examine the frequency-dependence of E' and E". Time-temperature superposition was applied to the frequency-dependent E' and E". Reduced moduli (E'_r and E''_r) were first obtained by multiplying each modulus by a vertical shift factor, b_T: [115, 116]

$$b_T = \frac{T_0}{T}, \qquad \text{(Equation 1)}$$

$$E'_r = b_T * E', \text{ and} \qquad \text{(Equation 2)}$$

$$E''_r = b_T * E'', \qquad \text{(Equation 3)}$$

where the reference temperature, T_o, was taken to be 30 °C. The reduced moduli were then shifted horizontally by applying a horizontal shift factor, a_T, at each temperature:

$$\omega_r = a_T\, \omega \qquad \text{(Equation 4)}$$

where ω_r are the reduced frequencies. At each temperature, a_T was identified as that required to produce a smooth and continuous master curve. The master curves containing the shifted data are shown in Figure 3.1a and Figure 3.1b.

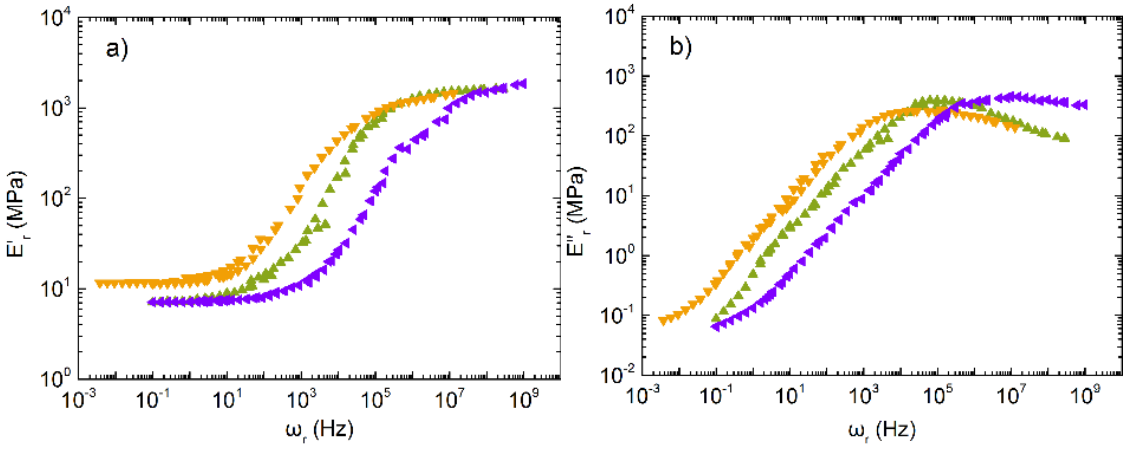

Figure 3.1: Master curves for the reduced (a) storage modulus (E'_r) and (b) loss modulus (E''_r) of thiol-ene networks derived from allylated SA (green ▲), 3HBA (purple ◂), and 4HBA (yellow ▼). Reference temperature was 30 °C.

The Williams–Landel–Ferry (WLF) equation is well-established for describing the temperature-dependence of a_T for polymers at temperatures above or in the vicinity of the T_g:[117]

$$\log a_T = \frac{-C_1(T-T_0)}{C_2+(T-T_0)}. \qquad \text{(Equation 5)}$$

The WLF equation fit to the shift factor as a function of temperature is shown in Figure 3.2. In all networks, the data are consistent with the WLF equation. C_1 is an empirical parameter, however C_2 can be described as $C_2 = f_r / \alpha_f$, where f_r is the fractional free volume of the material at the reference temperature and α_f is the coefficient of thermal expansion of the free volume ($\alpha_f \sim \alpha_l - \alpha_g$ where α_l and α_g are the coefficients of expansion of the liquid and glassy states, respectively). Significant differences are observed in the C_2 values for all five networks, possibly indicating differences in the values of f_r and α_f for these materials.

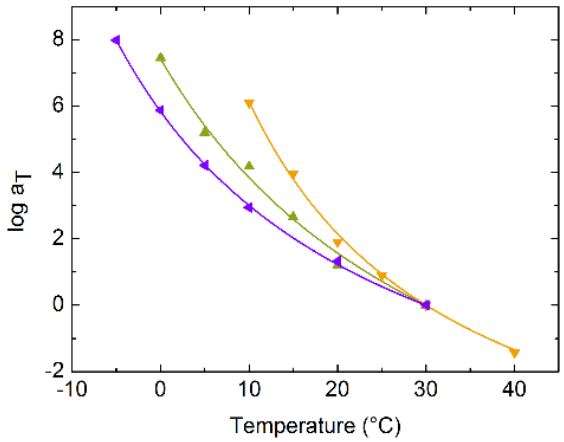

Figure 3.2: Temperature-dependent shift factor, a_T, for thiol-ene networks derived from allylated SA (green ▲), 3HBA (purple ◂), and 4HBA (yellow ▼). Curves indicate the fit of the WLF equation to the data.

Following the theory of rubber elasticity,[118] the crosslink density (υ_c) of a network is calculated from E' in the rubbery plateau region of the plot of E' vs. ω:

$$\upsilon_c = \frac{E'}{3RT}, \qquad \text{(Equation 6)}$$

where R is the gas constant. The crosslink densities calculated using the data from DMA, are summarized in Table 3.2.

Table 3.2 shows the resulting average values of the crosslink densities for the thiol-ene networks of varying functionality. The crosslink densities (and also plateau moduli) of the thiol-ene networks prepared from the difunctional allylated SA and 3HBA (*ortho* and *meta* placements of allyl groups, respectively) were quite similar to one another. A significant increase in crosslink density was observed for the thiol-ene network prepared from the difuctional allylated 4HBA (*para* placement of allyl groups). We propose that the lower crosslink density of the SA network as compared to the 4HBA network is due to the neighboring allyl groups found on allylated SA.[105] The structure of the SA network contains bulky aromatic groups intruded into network, reducing the crosslink density.[105] Surprisingly, we see that the *ortho* and *meta* placements of the allyl groups (allylated SA vs. 3HBA) result in very similar crosslink densities, which are lower than that of the network with *para* placements of allyl groups (using allylated 4HBA). The trend of modulus (Table 3.3) and T_g (Table 3.1) are consisitent to the crosslink density.[119, 120]

Previous studies on thiol-ene networks have indicated the presence of highly homogeneous networks, as evidence by the sharpness of the glass transition.[19, 21-23] In our study, a similarly sharp transition is observed in the DSC and DMA data. This is in contrast with the behavior observed in free radical and sulfur crosslinked networks with greater levels of inhomogeneity.[121-125] The SA, 3HBA, and 4HBA networks exhibit glass transitions with similar widths (Table 3.2), indicating comparable degrees of homogeneity

in the networks derived from difunctional allylated phenolic acids, regardless of the placement of functional groups (*ortho*, *meta*, *para*).

Table 3.2: Crosslink Density and Homogeneity of Thiol-Ene Networks Derived from Allylated Phenolic Acids[a]

Phenolic Acid	Crosslink Density		Width of Glass Transition (T_g)	
	E'_r in rubbery plateau (MPa)[b]	υ_c (mol/cm^3)[c]	T_g Width (°C) from DMA	T_g Width (°C) from DSC
SA (*o*)	8.9 ± 0.4	(1.18 ± 0.05) x 10^{-3}	9.6	5.8 ± 0.9
3HBA (*m*)	7.9 ± 0.5	(1.05 ± 0.07) x 10^{-3}	10.7	6.1 ± 0.3
4HBA (*p*)	10.2 ± 0.8	(1.35 ± 0.10) x 10^{-3}	10.0	6.3 ± 0.5

[a] Samples were prepared following the protocol in *Table 2.3*. *o*, *m,* and *p* indicate *ortho*, *meta*, and *para*.
[b] Reduced storage modulus in rubbery plateau at reference temperature 30 °C (at ω = 1 Hz).
[c] υ_c was Calculated using equation 6.

3.2.3 Tensile Behavior and the Ideal Elastomer Model

The mechanical properties of the networks were probed with tensile testing. Tensile experiments were conducted on multiple specimens for each network type; the average values of relevant parameters are shown in Table 3.3.

Table 3.3: Tensile Properties of Thiol-Ene Networks Derived from Phenolic Acids

Phenolic acid	Tensile strength (MPa)	% elongation at break	Modulus (MPa)	Toughness (MPa)
SA (*o*)	2.7 ± 0.3	25.0 ± 2.2	10.8 ± 0.4	0.36 ± 0.06
3HBA (*m*)	1.8 ± 0.1	20.4 ± 2.1	8.6 ± 0.5	0.20 ± 0.03
4HBA (*p*)	3.7 ± 0.3	29.6 ± 2.4	12.4 ± 0.3	0.57 ± 0.09

As the higher plateau modulus of the 4HBA network implies a greater crosslink density, the effect of crosslink density on the tensile parameters must first be considered. Refs.[126, 127] summarize the expected behavior of an elastomer as the crosslink density is increased: the tensile modulus increases with increasing crosslink density whereas both the tensile strength and toughness exhibit maximum values at intermediate crosslink densities. Therefore, the increase in the modulus, tensile strength and toughness of the 4HBA network, as compared to the SA network (Table 3.3), may simply be explained by

differences in crosslink density (where the 4HBA network has the higher crosslink density); however, in traditional rubber materials these trends are observed in the regime of relatively low crosslink densities. In the regime of high crosslink densities, it is expected that as the crosslink density increases, the modulus would increase, but the tensile strength and toughness would decrease.

We also consider the effect of the molecular structure of the phenolic acid on the tensile properties of the networks. When the material is macroscopically deformed, the strands within the network undergo microscopic changes which include alignment, rotation, displacement, bond rotation, and bond stretching, and the stress may become localized, particularly in the presence of a heterogeneous network.[128] The ultimate macroscopic rupture of the material at high elongations originates with the breaking of individual bonds.[129, 130] A microscopic view of the three phenolic acid-based networks shows important distinctions between them (Figure 3.3). In the 4HBA network, phenolic rings are aligned directly within the strand. In contrast, in the SA and 3HBA networks, the placement of the phenolic network is offset from the strand. Here we can conclude that both *meta* and *ortho* placements are less favorable arrangements of functional groups as compared to the *para* placement. We hypothesize that the relative placement of the bonds along the phenolic ring (i.e. *ortho* vs. *meta* vs. *para* position) may lead to differences observed in the mechanical behavior of the networks, such as the higher modulus and elongation at break observed in the 4HBA network.

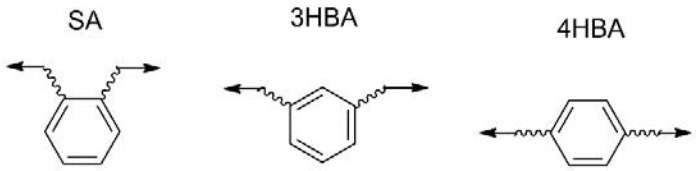

Figure 3.3: Diagram of expected forces exerted on an individual phenolic ring in a strand within the network that is aligned with the direction of applied force.

We now examine the stress-strain behavior of these networks with respect to the ideal elastomer model, described by:[118]

$$\sigma = \frac{E}{3}\left(\lambda - \frac{1}{\lambda^2}\right), \qquad \text{(Equation 7)}$$

where λ is the stretch ratio (λ=1+ε, where ε is the strain) and E is the tensile modulus (Young's modulus). Figure 3.4b shows a plot of the tensile data, formatted to highlight consistency with the ideal elastomer model. The tensile behavior of the SA and 3HBA network was consistent with the ideal elastomer model for the entire range of strains that were examined; the samples fractured at a strain of 0.250 ± 0.022 and 0.204 ± 0.021. The 4HBA network exhibited ideal behavior up to a strain of 0.202 ± 0.008, and became non-ideal at higher strain values.

The ideal elastomer model makes the following assumptions regarding the structure of the network:[118, 131] 1) all elastic chains in the network have the same length, 2) all crosslink junctions have the same functionality, 3) the network is homogeneous, and 4) each effective elastic chain obeys Gaussian statistics. Network imperfections such as dangling ends, loops, trapped entanglements, and other inhomogeneities are not accounted for in the ideal network model.[123, 132] In step-growth reactions such as in the formation of thiol-ene networks, the first two assumptions are likely valid, as the network is produced through the reaction of two complementary types of multifunctional molecules (where the functionality of each type of molecule is held constant). As discussed previously, the

narrowness of the glass transition implies the networks are relatively homogeneous (i.e. Table 3.2). We will now evaluate the network for the presence of defects and non-Gaussian strand conformations, which would lead to non-ideal behavior.

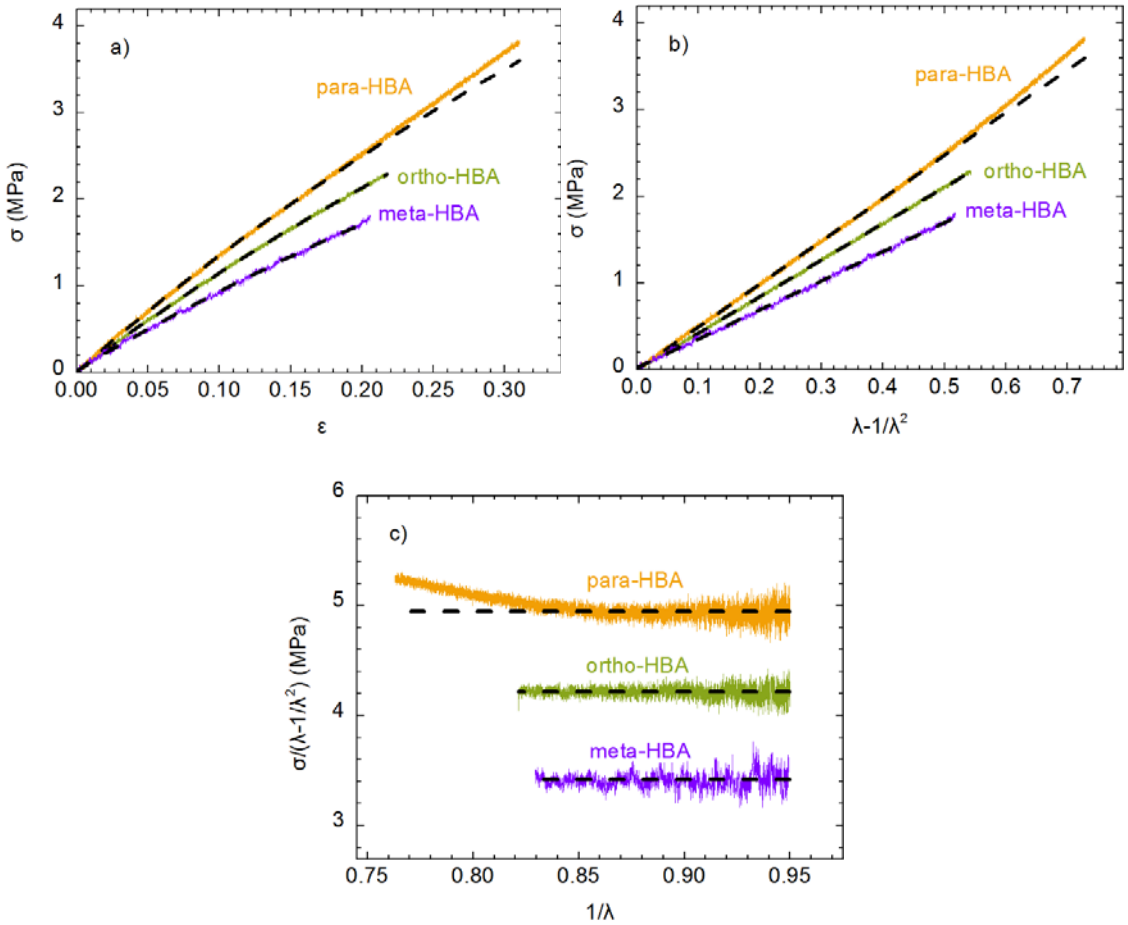

Figure 3.4: (a) Representative data showing tensile stress (σ) as a function of strain (ε); (b) tensile data plotted to highlight consistency with the ideal elastomer model; and (c) tensile data plotted in the Mooney-Rivlin format.[132]

A Mooney-Rivlin plot is a convenient method of identifying non-ideal behavior in networks:[133, 134]

$$\frac{\sigma_t}{\left(\lambda - \frac{1}{\lambda^2}\right)} = 2C_1 + \frac{2C_2}{\lambda}, \qquad \text{(Equation 5)}$$

where C_1 and C_2 are empirical constants. In the case of an ideal network, C_2 is equal to 0. The tensile data can be replotted in the Mooney-Rivlin format, as shown in Figure 3.4c. Over the full range of strain values examined, the SA and 3HBA network behavior was consistent with the ideal network model, in which $C_2 = -0.07 \pm 0.32$ for SA network and $C_2 = 0.12 \pm 0.18$ for SA network. At low to moderate strain values ($\varepsilon < 0.202 \pm 0.008$ and $1/\lambda > 0.832$), the behavior of the 4HBA network was also consistent with the ideal network model ($C_2 = -0.35 \pm 0.34$), and at high strain values ($\varepsilon > 0.202$ and $1/\lambda < 0.832$), the 4HBA network became non-Gaussian and deviated from the ideal network model ($C_2 = -5.05 \pm 0.13$).[132, 135] Agreement with the ideal network model is typically only observed for traditional networks in their highly swollen states;[136] such behavior in the non-swollen state is further evidence of the high degree of homogeneity and lack of defects in these thiol-ene systems.[137, 138]

3.3 Concluding Remarks

This chapter discussed thermal, mechanical and structural properties of thiol-ene network derived from mono-hydroxybenzoic acids, including the glass transition temperature, plateau modulus, corresponding crosslink density, tensile modulus, tensile strength, and elongation. All the properties above exhibited the same trend: *para* > *ortho* > *meta*. The networks derived from difunctional allylated phenolic acids exhibited narrow glass transitions (indicating a high degree of network homogeneity), and glass transition temperatures (T_g) which correlated with their crosslink density. The *para* placement of allyl groups on the allylated phenolic acid produced a network with the highest crosslink density, T_g, modulus, tensile strength, and elongation at break (followed by *ortho* and then *meta*). These variations in thermal and mechanical behavior were attributed to differences

in the crosslink densities of the networks as well as microscopic changes in the network upon deformation, which are likely impacted by the placement of functional groups around the aromatic ring. At the low to moderate strain, they behaved consistent with ideal elastic model. At high strain, *para*-HBA thiol-ene networks exhibited non-ideal behavior. Meanwhile, *meta*-HBA and *ortho*-HBA broke at lower strain and did not deviate from the ideal elastomer model.

Chapter 4 Effect of Monomer Functionality on Thiol-Ene Networks Derived From Phenolic Acids

4.1 Introduction

The synthesis of thiol-ene networks are described in Chapter 2. Thiol-ene networks were prepared through the photoinitiated reaction of allylated phenolic acids and a multifunctional thiol. A total of five phenolic acids were investigated: salicylic acid (SA or *ortho*-HBA), 3-hydroxybenzoic acid (3HBA or *meta*-HBA), 4-hydroxybenzoic acid (4HBA or *para*-HBA), gentisic acid (GenA), and gallic acid (GalA). Thiol-ene networks derived from difunctional allylated phenolic acids (SA, 3HBA, and 4HBA) were previously described in Chapter 2. Here, the properties of thiol-ene networks from multifunctional phenolic acids, GenA and GalA, containing 3 and 4 functional groups, respectively, are explored. Additionally, the effect of the number of functional groups on the phenolic acid (ranging from 2-4) on the properties of the thiol-ene networks is investigated.

Synthetic conditions were developed to prepare thiol-ene networks with high yield and conversion. The thermal and mechanical behavior of the thiol-ene networks was investigated. This work develops fundamental relationships between number of functional groups on the allylated phenolic acid and the physical properties of the thiol-ene networks.

4.2 Results and Discussion

4.2.1 Thermal Characterization

The glass transition temperatures (T_g) of thiol-ene networks (prepared following the protocol in Table 2.3) were explored through differential scanning calorimetry (DSC). The T_g values measured upon the first and second heating scans were comparable to one

another, within the error of the measurement. The average and standard deviation values obtained during the first heating scan are provided in Figure 4.3a and Figure 4.4. The T_g's of all networks were lower than room temperature, as is typically observed in thiol-ene networks, which contain flexible thioether linkages.[114] We examine the effect of increasing the functionality of the allylated phenolic acid on the network T_g. The GenA and GalA networks, derived from the allylated phenolic acids with the highest functionalities, exhibited high crosslink densities (comparable to the 4HBA network), yet low T_g values (comparable to the 3HBA network). However, these networks were all prepared at stoichiometric compositions (i.e., equal concentrations of allyl and thiol groups). As the functionality of the allylated phenolic acid increased, the molar concentration of allylated phenolic acid used to prepare the network (required for stoichiometric balance with the multifunctional thiol PETMP) thus decreased. We hypothesize that the presence of the aromatic rings on the allylated phenolic acids increase the glass transition of the networks. Thus, decreasing the molar concentration of aromatic rings throughout the network (through decreasing the concentration of allylated monomer) resulted in reduction of the T_g.

4.2.2 Network Structure and Homogeneity

The storage (E') and loss (E") moduli were probed as a function of strain (using frequency = 1 Hz) at selected temperatures. A strain in the linear viscoelastic region was chosen at each temperature and used to examine the frequency-dependence of E' and E". Time-temperature superposition was applied to the frequency-dependent E' and E". Reduced moduli (E'_r and E''_r) were first obtained by multiplying each modulus by a vertical shift factor, b_T, following Equation 6, Equation 7 and Equation 8.[115, 116] The reference

temperature, T_o, was taken to be 30 °C. The reduced moduli were then shifted horizontally by applying a horizontal shift factor, a_T, at each temperature following Equation 4. At each temperature, a_T was identified as that required to produce a smooth and continuous master curve. The master curves containing the shifted data are shown in Figure 3.1a and Figure 3.1b.

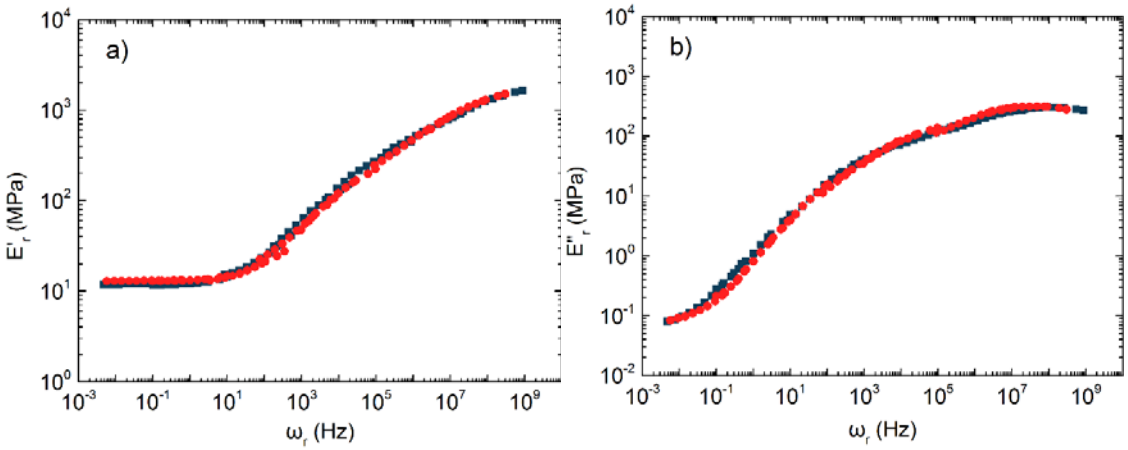

Figure 4.1: Master curves for the reduced (a) storage modulus (E'$_r$) and (b) loss modulus (E"$_r$) of thiol-ene networks derived from GenA (dark blue ■) and GalA (red ●). Reference temperature for time-temperature superposition was 30 °C.

The Williams–Landel–Ferry (WLF) equation is well-established for describing the temperature-dependence of a_T for polymers at temperatures above or in the vicinity of the T_g (Equation 5).[117]

The WLF equation fit to the shift factor as a function of temperature is shown in Figure 3.2. In all networks, the data are consistent with the WLF equation. C_1 is an empirical parameter, however C_2 can be described as $C_2 = f_r / \alpha_f$, where f_r is the fractional free volume of the material at the reference temperature and α_f is the coefficient of thermal expansion of the free volume ($\alpha_f \sim \alpha_l - \alpha_g$ where α_l and α_g are the coefficients of expansion of the liquid and glassy states, respectively). Significant differences are observed in the C_2

values for all five networks, possibly indicating differences in the values of f_r and α_f for these materials.

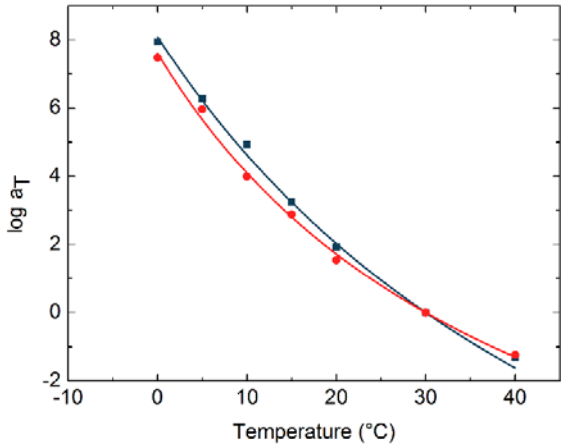

Figure 4.2: Temperature-dependent shift factor, a_T, for thiol-ene networks derived from allylated GenA (dark blue ■) and GalA (red ●). Curves indicate the fit of the WLF equation to the data.

Table 4.1: Homogeneity of Thiol-Ene Networks Derived from Allylated Phenolic Acids[a]

Phenolic Acid	f_{allyl}[b]	T_g Width (°C) from DMA[c]	T_g Width (°C) from DSC[d]
SA	2 (*o*)	9.6	5.8 ± 0.9
3HBA	2 (*m*)	10.7	6.1 ± 0.3
4HBA	2 (*p*)	10.0	6.3 ± 0.5
GenA	3	19.4	15.7 ± 0.8
GalA	4	17.1	14.5 ± 0.9

[a]Samples were prepared following the protocol in Table 2.3.
[b]f_{allyl} is the functionality (number of allyl groups) of the allylated phenolic acid used to prepare the thiol-ene network. *o*, *m* and *p* indicate *ortho*, *meta* and *para*.
[c]Full width at half maximum of peak observed in tan δ as a function of temperature
[d]Difference of the onset and endset temperatures

The crosslink density (υ_c) of each thiol-ene network was calculated from E' in the rubbery plateau region of the plot of E' vs. ω (Figure 3.1a), using the theory of rubber elasticity (Equation 5).[118] Figure 4.3b shows the resulting average values of the crosslink densities for the thiol-ene networks of varying functionality. Upon increasing the functionality (number of functional groups, f_{allyl}) to 3 and 4, the crosslink density remained

fairly consistent with that of the 4HBA network (compare values of the 4HBA, GenA and GalA networks in Figure 4.3b).

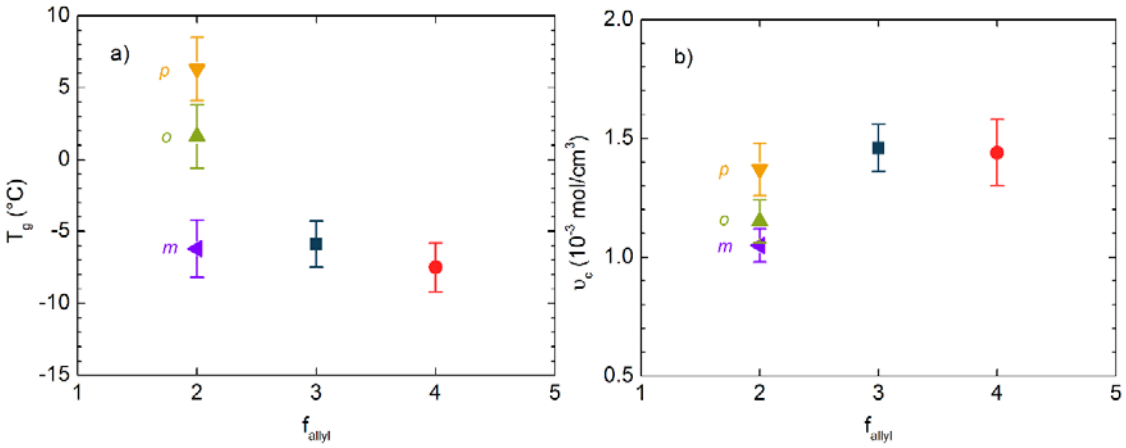

Figure 4.3: a) T_g and b) crosslink density (υ_c) of thiol-ene networks derived from allylated SA (green ▲), 3HBA (purple ◂), 4HBA (yellow ▼), GenA (dark blue ■) and GalA (red ●), where f_{allyl} is number of allyl groups.

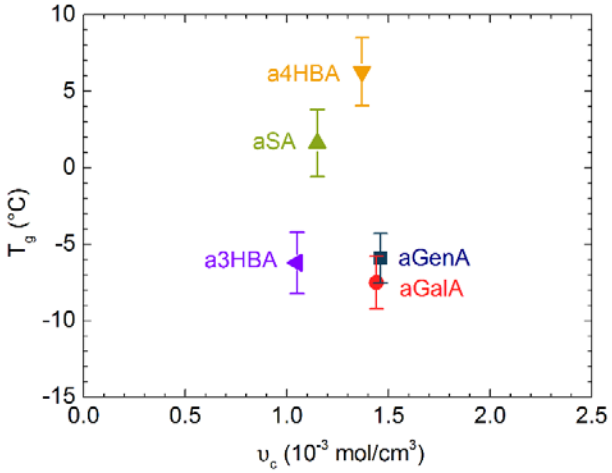

Figure 4.4: Glass transition temperature (T_g) of a function of crosslink density (υ_c) of thiol-ene networks derived from allylated SA (green ▲), 3HBA (purple ◂), 4HBA (yellow ▼), GenA (dark blue ■) and GalA (red ●).

Thiol-ene networks typically exhibit sharp glass transitions, indicating a high degree of network homogeneity.[19, 21-23] We observed similarly sharp transitions in the DSC and DMA data (Table 4.1). This is in contrast with the behavior observed in free radical and sulfur crosslinked networks with greater levels of inhomogeneity.[121-125] As the

functionality of the allylated phenolic acid was increased from 2 (SA, 3HBA and 4HBA) to 3 (GenA) and 4 (GalA), the T_g width increased, presumably indicating the formation of less homogeneous networks.

4.2.3 Tensile Behavior and the Ideal Elastomer Model

Tensile testing was employed to probe the mechanical behavior of the thiol-ene networks. Tensile experiments were conducted on multiple specimens for each network type (reported in Figure 4.5a); the average values of relevant parameters are shown in Table S11. The data in Figure 4.5a were fit to the ideal elastomer (affine network) model, described by Equation 6.[118] Figure 4.5b shows a plot of the tensile data, formatted to highlight consistency with the ideal elastomer model. The data are consistent with the ideal elastomer model and low to moderate strains for all five types of thiol-ene networks. At higher strains, in the vicinity of the elongation at break, some of the networks (4HBA, GenA, and GalA) exhibited a positive deviation from the ideal network model (at a given strain, stress was higher than predicted).

A Mooney-Rivlin plot is traditionally used to identify non-ideal behavior in networks. The Mooney-Rivlin model is defined in Equation 7.[133, 134] In the case of an ideal network, C_2 is equal to 0. The tensile data are plotted in the Mooney-Rivlin format, as shown in Figure 4.5c. The networks (4HBA, GalA and GenA) were consistent with the ideal elastomer model (and C_2 was close to 0) at low to moderate strains. As the strain was increased, the Mooney-Rivlin plots for the 4HBA, GalA and GenA networks exhibited a positive slope (and positive value of C_2 reported in Table S12). Networks traditionally exhibit strain softening at low to moderate strains, observed as a negative slope in the Mooney-Rivlin plot, attributed to trapped entanglements and described by models which

account for topological constraints.[139-141] The tensile behavior of the thiol-ene networks examined here is not consistent with trapped entanglements, but is similar to that reported previously for spatially homogenous gels[137, 138] and end-linked poly(dimethylsiloxane) networks.[142] At higher strain values, the deviations from the ideal network model observed in Figure 4.5 for the 4HBA, GalA, and GenA networks (showing a positive slope in Figure 4.5c) are indicative of strain hardening of the networks. Strain hardening is usually observed under two conditions: 1) strain-induced crystallization of the network[143] or 2) deviation from Gaussian strand conformations in the network[144] (both typically observed at much higher strain values than were achieved in Figure 4.5).

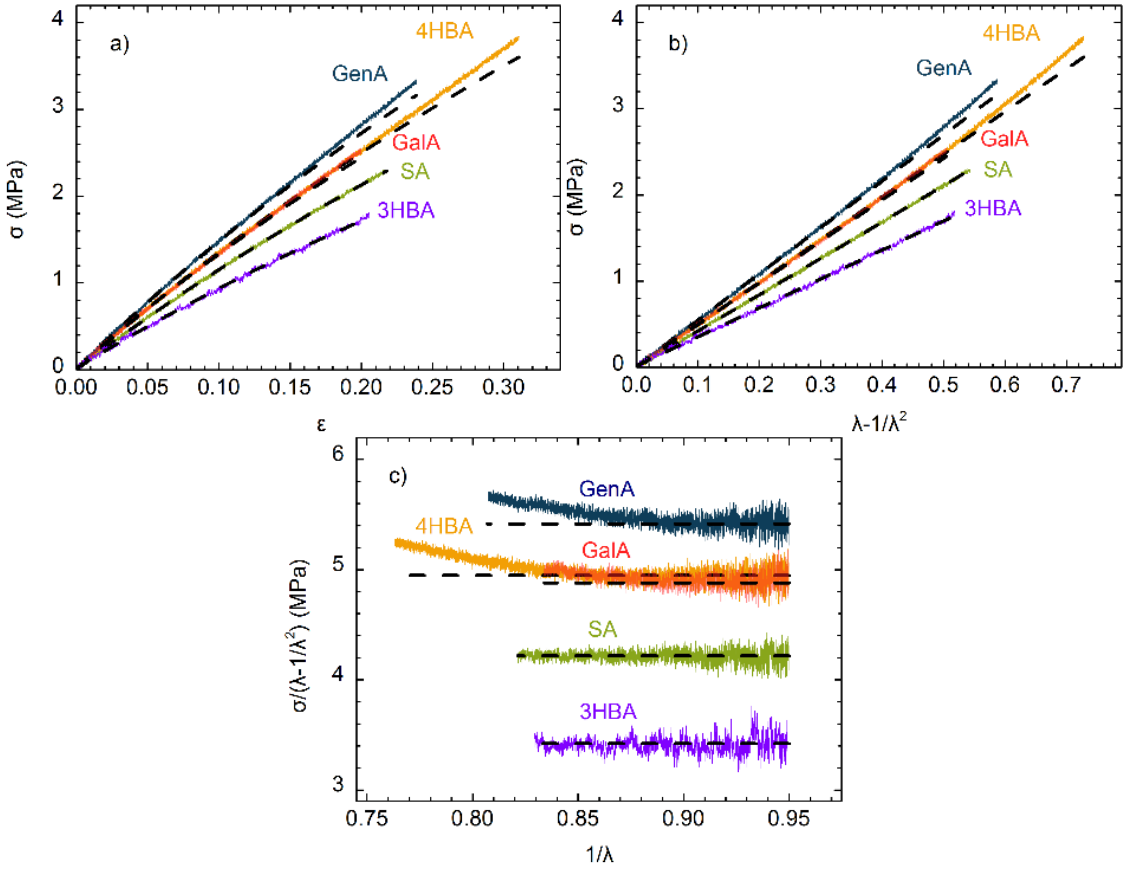

Figure 4.5: (a) Representative data showing tensile stress (σ) as a function of strain (ε); (b) tensile data plotted to highlight consistency with the ideal elastomer model; and (c) tensile data plotted in the Mooney-Rivlin format.

The ideal elastomer model (of an affine network) makes the following assumptions regarding the structure of the network: all elastic chains in the network have the same length, all crosslink junctions have the same functionality, the network is homogeneous, and each effective elastic chain obeys Gaussian statistics.[118, 131] Thiol-ene chemistry traditionally results in networks of high conversion of functional groups (in the range of 85-95% in our study; Tables S1-S5) and sharp glass transitions (Table 4.1), generally taken to be an indication of the high degree of homogeneity of the network. The agreement with the ideal elastomer model (and fit with the Mooney-Rivlin equation with C_2 close to 0) implies a lack of heterogeneities such as dangling ends and trapped entanglements in these networks.[123, 132]

Table 4.2: **Experimental** Crosslink Density and Molecular Weight Between Crosslinks[a]

Allylated phenolic acid	E' in rubbery plateau (MPa)[b]	υ_c (x 10^{-3} mol/cm^3)[c]	M_c (g/mol)[d]
aSA	8.46 ± 0.91	1.12 ± 0.12	1102 ± 131
a3HBA	7.91 ± 0.73	1.05 ± 0.10	1170 ± 109
a4HBA	10.5 ± 0.9	1.39 ± 0.12	882 ± 77
aGenA	11.2 ± 0.9	1.49 ± 0.12	825 ± 64
aGalA	11.3 ± 1.4	1.49 ± 0.19	828 ± 99

[a] Samples were prepared following the protocol in *Table 2.3*.
[b] Reduced storage modulus in rubbery plateau (DMA) at reference temperature 30 °C (ω = 1 Hz).
[c] υ_c was calculated using Eqn. 6. All data and calculations are shown in Appendix D
[d] Molecular weight between crosslinks (M_c), was calculated using E' in the rubbery plateau ($M_c = \rho / \upsilon_c$). The values of mass densities used in these calculations (ρ) were measured for the thiol-ene networks and reported in section 2.11.

However, there is one important inconsistency observed in fitting the model to the data. The molecular weight between crosslinks (M_c) can be readily calculated from the crosslink density ($M_c = \rho / \upsilon_c$) (in the range of 800-1,100 g/mol, Table 4.2). If we consider a perfect network (without any defects), then we can calculate the molecular weight between junctions in the network using the chemical structure of the network (in the range

of 200-500 g/mol, Figure 4.6 and Table 4.3). The experimental M_c is significantly higher than the predicted M_c for all networks (differing by factors of two and four for networks derived from difunctional [SA, 3HBA, 4HBA] and multifunctional [GenA, GalA] allylated phenolic acids, respectively). We hypothesize that primary loop formation[145-147] may be significant in these networks, thereby increasing M_c and lowering the modulus.

Table 4.3 **Theoretical** Crosslink Density and Molecular Weight Between Crosslinks

	Allylated phenolic acid	M_c (g/mol)[a]	υ_c (x 10^{-3} mol/cm^3)[c]	M_c (g/mol) average[b]	υ_c (x 10^{-3} mol/cm^3) average[c]
Assuming 100% Conversion of Functional Groups	aSA	456	2.68	456	2.68
	a3HBA	456	2.68	456	2.68
	a4HBA	456	2.68	456	2.68
	aGenA	176 / 204	6.93/5.98	185	6.61
	aGalA	176 / 204	6.93/5.98	183	6.69
Accounting for Measured Conversion of Functional Groups[d]	aSA	456	2.68	456	2.68
	a3HBA	456	2.68	456	2.68
	a4HBA	456	2.68	456	2.68
	aGenA	176 / 204 / 512	6.93/5.98/2.38	225	6.11
	aGalA	176 / 204	6.93/5.98	183	6.69

[a]The theoretical M_c was calculated considering a perfect network (without any defects) and using the chemical structures of the allylated phenolic acids and multifunctional thiol. Details are shown below in Figure 4.6.

[b]In the case of multiple values of M_c that are calculated theoretically, an average is reported here.
100% conversion:
For GenA: Average M_c = (1/3)(204)+(2/3)(176) = 185 g/mol
For GalA: Average M_c = (1/4)(204)+(3/4)(176) = 183 g/mol
Accounting for measured reaction conversion (more details included below Figure 4.6):
For GenA (88% conversion): Average M_c = (0.88)(1/3)(204)+(0.8)(2/3)(176)+(0.12)(512) = 225 g/mol

[c] υ_c is calculated from the theoretical M_c ($\upsilon_c = \rho / M_c$). The values of mass densities used in these calculations (ρ) were measured for the thiol-ene networks and reported in section 2.11.

[d] The experimentally measured conversions for each network type were considered in these calculations. More details are provided below Figure 4.6.

Figure 4.6: Theoretical M_c Calculations:

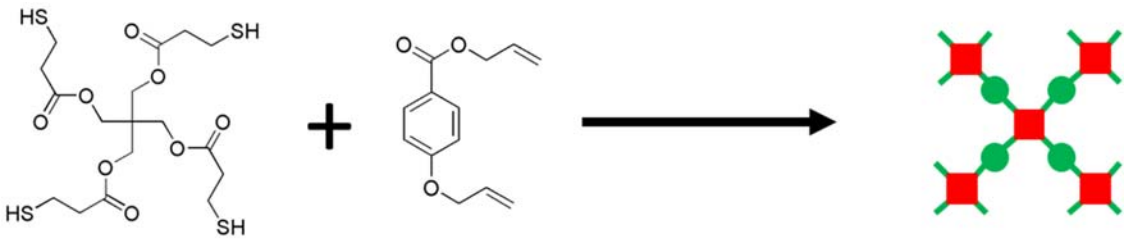

Figure 4.6i: Photoinitated thiol-ene reaction between allylated 4HBA and the tetra-functional thiol PETMP. The other difunctional allylated phenolic acids (SA, 3HBA) undergo comparable reactions.

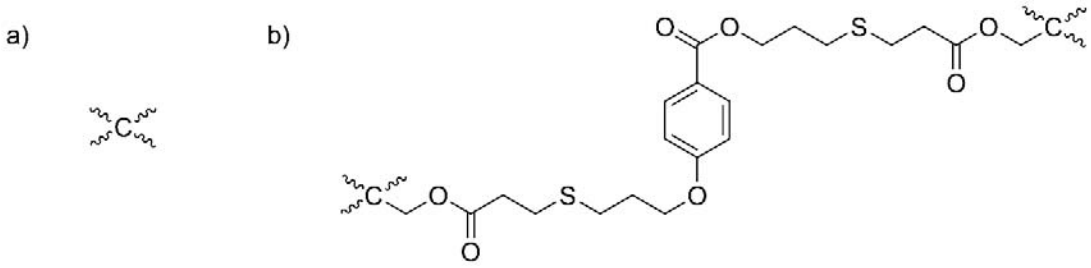

Figure 4.6ii: Chemical structures of a) junctions and b) strands in 4HBA thiol-ene networks. The molecular weight of a strand is 456 g/mol.

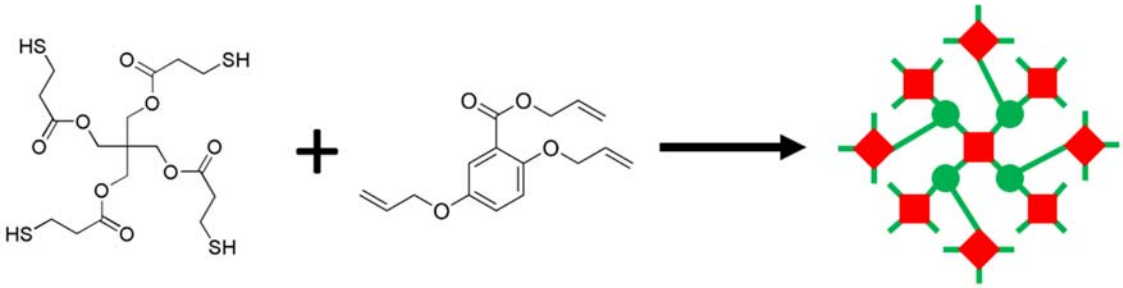

Figure 4.6iii: Photoinitated thiol-ene reaction between allylated GenA and the tetra-functional thiol PETMP.

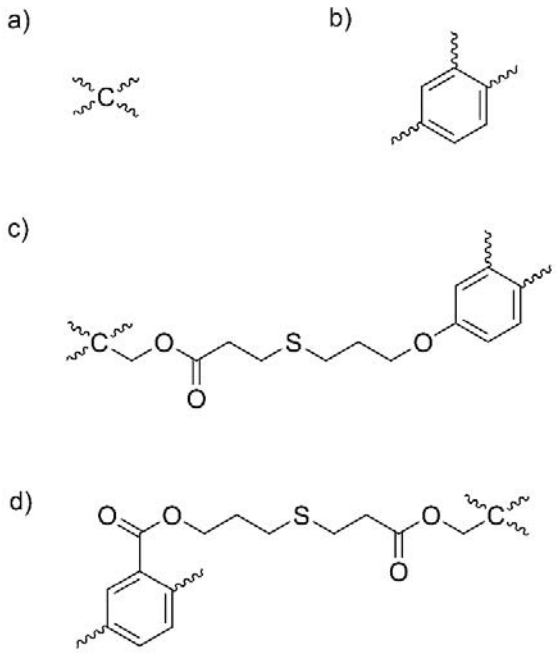

Figure 4.6iv: Chemical structures of a) b) junctions and c) d) strands in GenA thiol-ene networks. The molecular weights of strands are 176 or 204 g/mol.

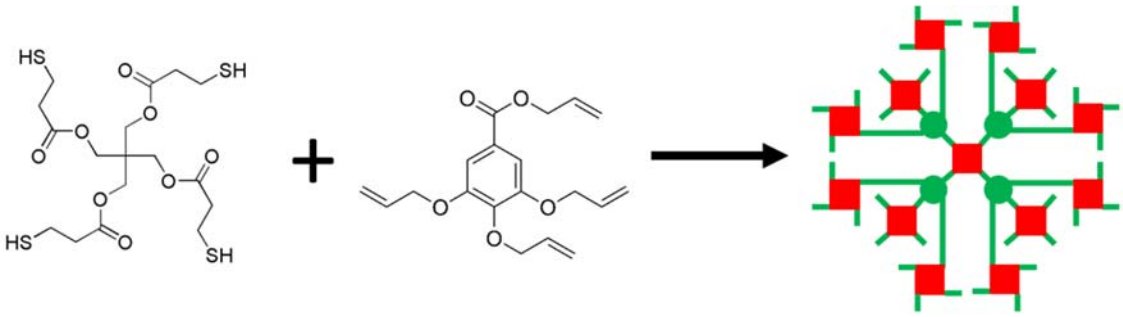

Figure 4.6v: Photoinitated thiol-ene reaction between allylated GalA and the tetra-functional thiol PETMP.

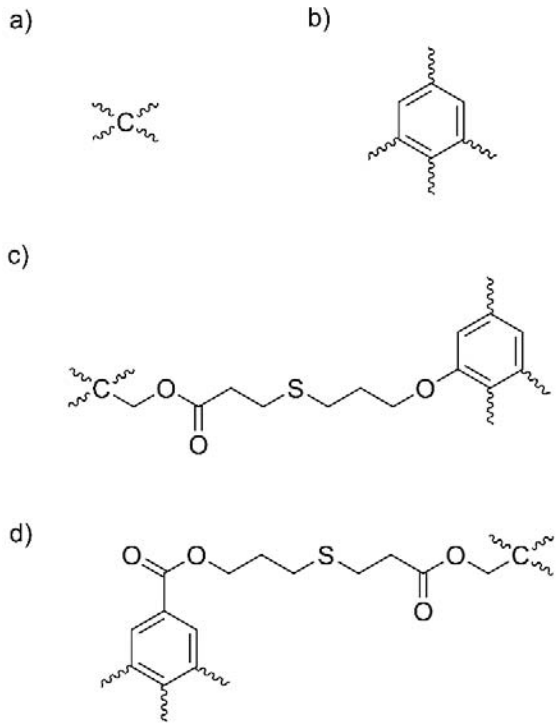

Figure 4.6vi: Chemical structures of i) ii) junctions and iii) iv) strands in GalA thiol-ene networks. The molecular weights of strands are 176 or 204 g/mol.

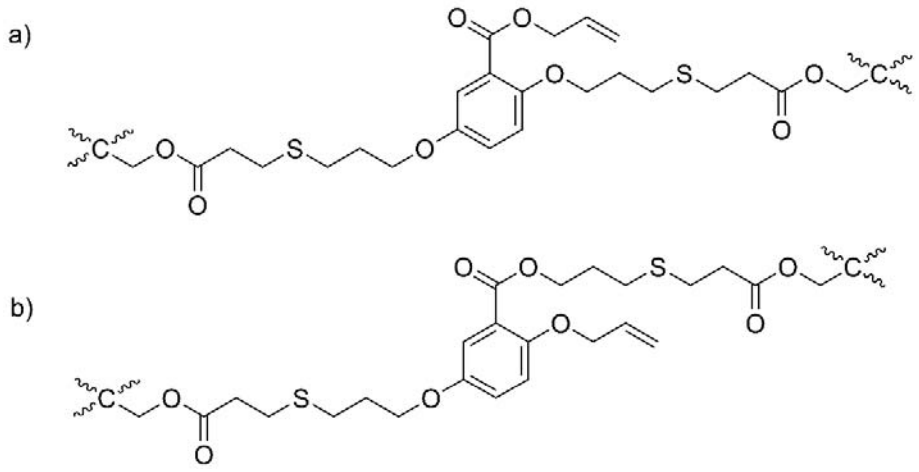

Figure 4.6vii: Chemical structures of strands in aGenA thiol-ene networks which are not fully reacted (i.e. one unreacted allyl group). The molecular weight of the strand is now 512 g/mol.

The tensile properties of the thiol-ene networks were characterized using measurements conducted on multiple test bars prepared from multiple independently prepared specimens (Figure 4.7). In the case of networks derived from multifunctional phenolic acids (GenA and GalA), the high tensile modulus and low elongation at break and toughness may be attributed to two factors: the high crosslink density (Figure 4.3b and Figure 4.8) and increased heterogeneity (evidenced by the higher glass transition width in Table 4.1) of the networks.

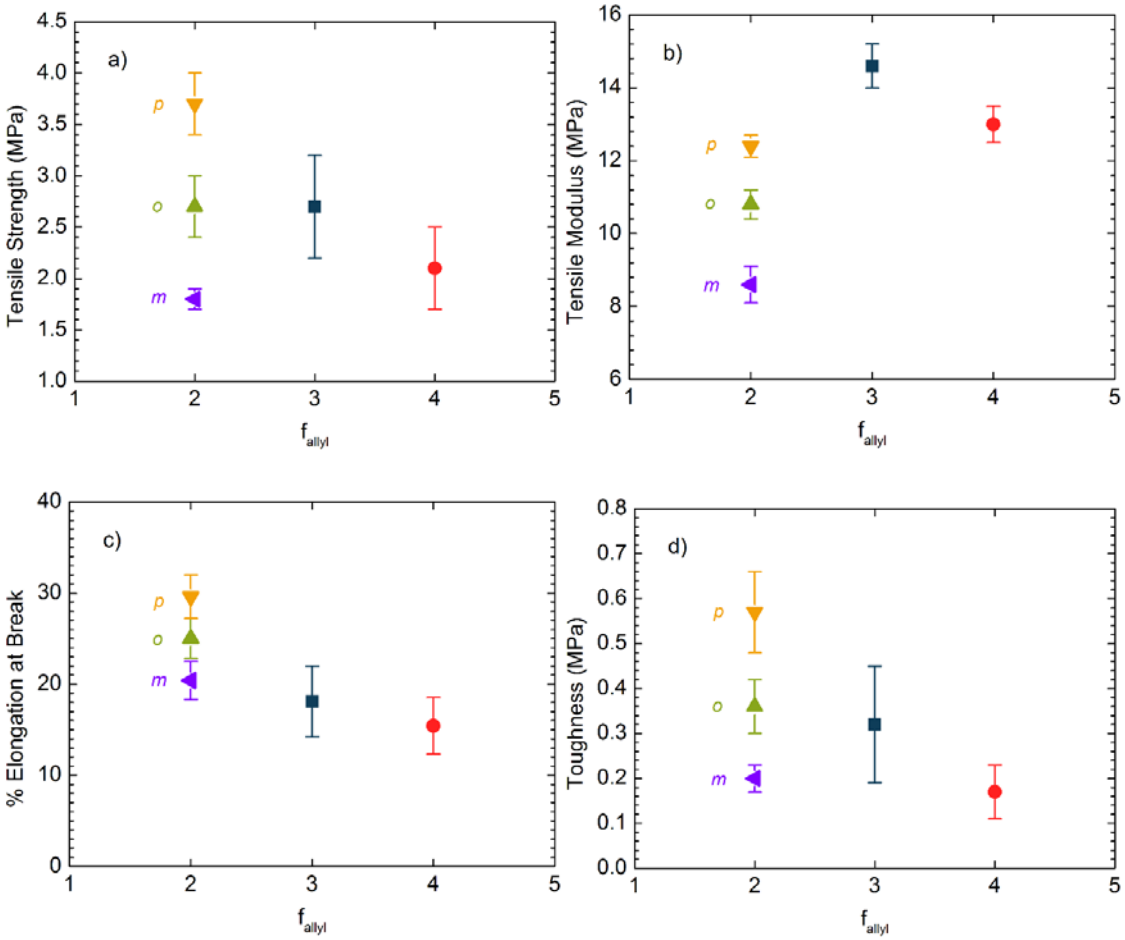

Figure 4.7: (a) Tensile strength, (b) tensile modulus, (c) % elongation at break and (d) toughness for as-prepared thiol-ene networks derived from phenolic acid. f_{allyl} is defined as the number of allyl groups per allylated phenolic acid.

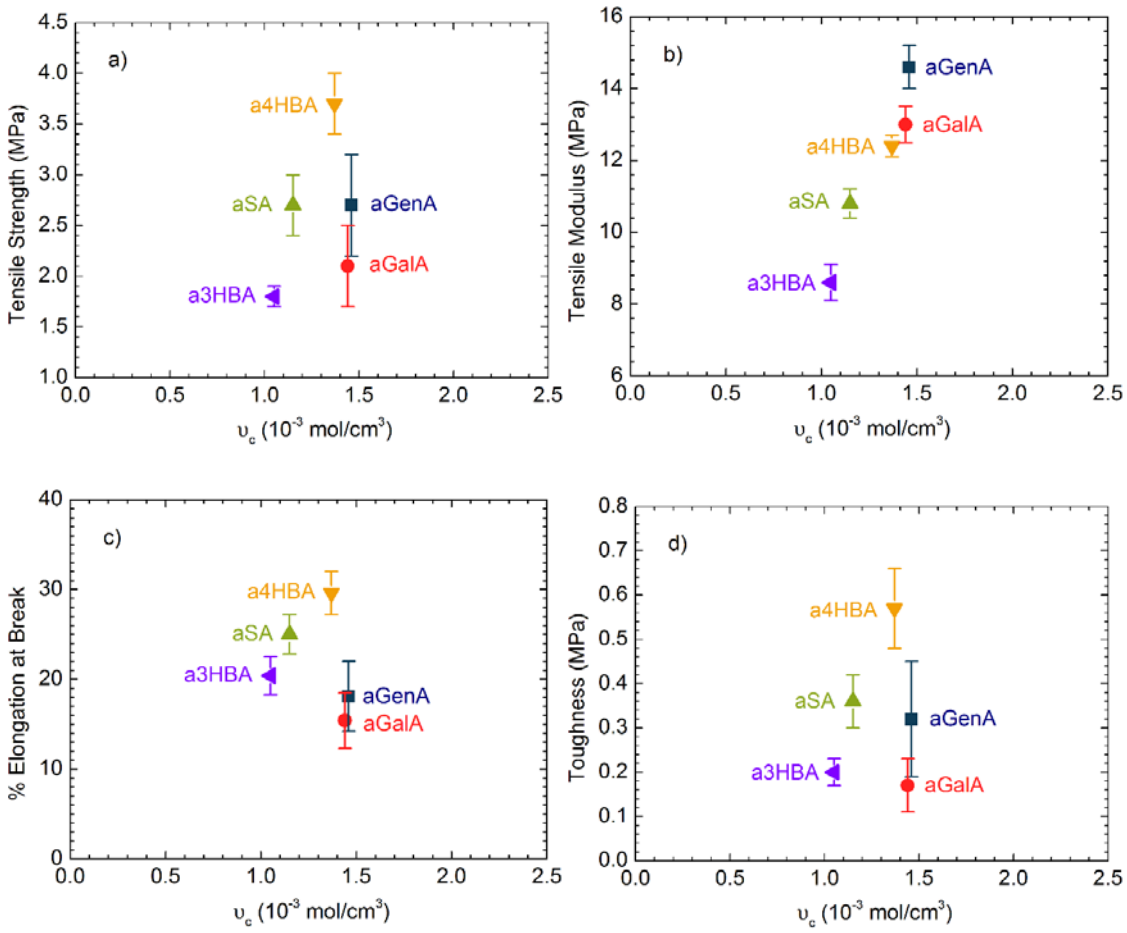

Figure 4.8: Mechanical properties of a function of crosslink density (υ_c) of thiol-ene networks derived from allylated SA (green ▲), 3HBA (purple ◂), 4HBA (yellow ▼), GenA (dark blue ■) and GalA (red ●).

4.3 Concluding Remarks

Biobased phenolic acids (found in plant sources) were allylated and subsequently reacted with a multifunctional thiol (in a photoinitiated reaction) to form networks. As the functionality of the allylated monomer increased (to 3-4 allyl groups per molecule), the crosslink density remained high yet the T_g decreased, attributed to a lower concentration of aromatic rings throughout the network structure (as all networks were prepared at the stoichiometric ratio of allyl and thiol functional groups). The networks derived from the higher functionality allylated phenolic acids also exhibited lower elongation at break and

associated tensile strength and tensile toughness, likely due to increased heterogeneity of the networks (indicated by higher glass transition widths compared to the networks derived from difunctional allylated phenolic acids). All networks exhibited behavior consistent with an ideal elastomer (affine network) at low to moderate strains, albeit with lower moduli than predicted from the monomer chemical structure. At the high end of the strain ranges achieved, some of the networks exhibited strain hardening behavior, in which the stress at a given strain was higher than that predicted for an ideal elastomer.

Chapter 5 Hydrolytic Degradation of Epoxy Resins Derived from Soybean Oil

5.1 Introduction

The development of renewable energy and material sources is of utmost importance due to the finite supply of petroleum and environmental implications of petroleum processing. Wind energy offers great potential as a sustainable alternative to petroleum energy sources.[148] The next generation of wind energy will depend on the design of new materials for turbine blades.[149] Epoxy resins are dominant materials in the fabrication of wind turbine blades, and are found in other applications including protective coatings, adhesives, and automotive materials. In a general epoxy resin synthesis, a molecule containing epoxide groups reacts with a multi-functional amine to form a network structure. Though the cured resin has desirable attributes such as chemical and heat resistance, electrical properties, adhesive properties, stiffness, and strength, the network structure prevents recycling or reuse of the material once the product has reached its useful lifetime.

This chapter focuses on the utilization of triglyceride vegetable oils as components of epoxy resins. The presence of ester linkages throughout the network structure are hypothesized to create epoxy resins which are degradable or recyclable. Triglyceride vegetable oils are an attractive alternative hydrocarbon source for polymers.[150-153] Triglyceride molecules contain varying numbers of carbon-carbon double bonds, allowing for functionalization through epoxidation, acrylation, maleination, and etc.[153] The functionalized oils can subsequently be polymerized through many techniques, including ring-opening polymerization,[154] urethane chemistry,[155] and free radical polymerization.[156-158] Degradation or re-processing of conventional petroleum-derived epoxy resins is prevented by the network structure. The triglyceride structure of a vegetable oil contains

ester linkages, which can be degraded through hydrolysis and enzymatic and bacterial degradation,[16] potentially opening up new routes for recycling or reuse of the materials after the product's useful lifetime.

The development of epoxy resins containing epoxidized triglyceride oils has been a recent focus in the literature.[37-59] The triglyceride-containing epoxy networks exhibit a higher fracture toughness and impact strength, with a corresponding decrease in the glass transition temperature, due to a decrease in the crosslink density and increase in chain flexibility.[37-45, 48, 50, 51] in general, triglyceride oil-based epoxy resins require higher curing temperatures than conventional diglycidyl ether of bisphenol A(DGEBA)-based epoxy resins.[47, 49] in addition, the morphology of epoxy resins containing epoxidized triglyceride oils has been examined. In general, the diglycidyl ether of bisphenol A (DGEBA) and epoxidized soybean oil (ESO; or other epoxidized triglyceride oils) are miscible prior to the crosslinking reaction.[37, 42] In some studies, the final resin was reported to be completely miscible, even post-cross-linking, and no phase separation was observed.[37, 42] In other cases, the DGEBA/triglyceride oil mixture was miscible initially, but underwent macroscopic phase separation during the cross-linking process as the polymer molecular weight increased.[44, 51] The inequality in the reactivity of the amine towards DGEBA, and the triglyceride oil can also lead to macrophase separation.[43, 44]

Few studies in the literature have characterized the hydrolytic degradation of epoxy resins containing vegetable-oil-derived components. One notable study characterized the biodegradability of various types of polymers synthesized from vegetable oils, using respirometry experiments in a soil medium.[16] Many of the polymerized oils were

biodegradable, similar to the neat oil. However, under the conditions used the amine-cured epoxy resins containing soybean oil showed similar CO_2 levels to the soil alone.[16]

Chapter 2 discusses the synthesis of ESO-based epoxy resins. All epoxy resins contained a ratio of epoxide-bearing molecules (DGEBA and ESO) to amine-bearing molecules (MDA) of 100 : 30 (by weight). The total epoxide content is a mixture of DGEBA and ESO. Throughout this study, the concentration of ESO in the epoxy resin will be reported as a percentage of the total epoxide content (DGEBA + ESO), by weight. The ratio of 100 : 30 was chosen as it corresponds to a stoichiometrically balanced molar ratio of 0.97 epoxide groups to one active hydrogen atom (on a primary amine group) for a mixture of MDA and DGEBA. For a mixture of ESO and MDA, there are 0.76 epoxide groups to one active hydrogen atom (based upon the NMR characterization of ESO which indicated the presence of an average of 4.27 epoxide groups per triglyceride molecule). Therefore, there is excess amine present in the samples containing ESO

In this chapter, basic NaOH solutions (3 and 10 wt%) were used to accelerate the degradation process, highlighting differences between polymers of varying soybean oil content. This study is the first to observe significant differences in the degradability of epoxy resins with varying oil content. The degradability of epoxy resins containing DGEBA, ESO, and a multifunctional amine, methylene dianiline (MDA) was probed through measuring the sample mass over time in the NaOH solution. In addition, the curing reaction was monitored through differential scanning calorimetry (DSC). The glass transition temperature and thermal degradation properties were also characterized through DSC and thermogravimetric analysis (TGA).

5.2 Results and Discussion

5.2.1 Dynamic DSC analysis of the curing kinetics

The curing reaction was monitored through in situ DSC, using a dynamic temperature scan. Previous studies have established that the curing of ESO occurs at higher temperatures than that of neat DGEBA.[47, 49] The curing reactions were monitored for epoxy resins with varying ESO content, in order to inform the choice of curing temperature utilized to prepare the polymers for characterization of degradation and thermal properties. The heat flow was measured as a function of temperature, at a heating rate of 10 °C/min (as the sample was heated from 50 to 360 °C), as shown in Figure 5.1a. The fraction of the total area under the curve was determined as a function of temperature, and the reaction conversion was calculated following Equation 9. Polymers containing both DGEBA and ESO exhibited two exothermic peaks during the curing process. For these samples, the total area (under both peaks) was utilized for calculation of the reaction conversion. The conversion as a function of temperature is plotted in Figure 5.1b for polymers with varying ESO content (the % ESO is reported relative to the total epoxide content in the polymer). Through comparison of the curves for polymers containing 0% and 100% ESO, it is clear that the reaction between ESO and MDA requires a significantly higher reaction temperature than the reaction between DGEBA and MDA. The temperature required for 50% conversion increases significantly at high ESO contents (80-100 wt%).

$$Conversion = \frac{\Delta H_T}{\Delta H_{total}}, \qquad \text{(Equation 9)}$$

where ΔH_{total} = the total heat flow during the temperature scan (area under the exothermic peak), ΔH_T = the area under the exothermic peak in the temperature range of room temperature to temperature T. Note that the values of ΔH_{total} used in calculating the

conversion were based on the temperature scans conducted at a rate of 10 °C/min. There are potential sources of deviation in these values from the theoretical heat of reaction due to the choice of heating rate, presence of excess amine in the samples containing ESO and inability to heat the samples to temperatures well above the location of the peak (the upper temperature limit of 360 °C was chosen to avoid degradation of the sample, based on TGA data).

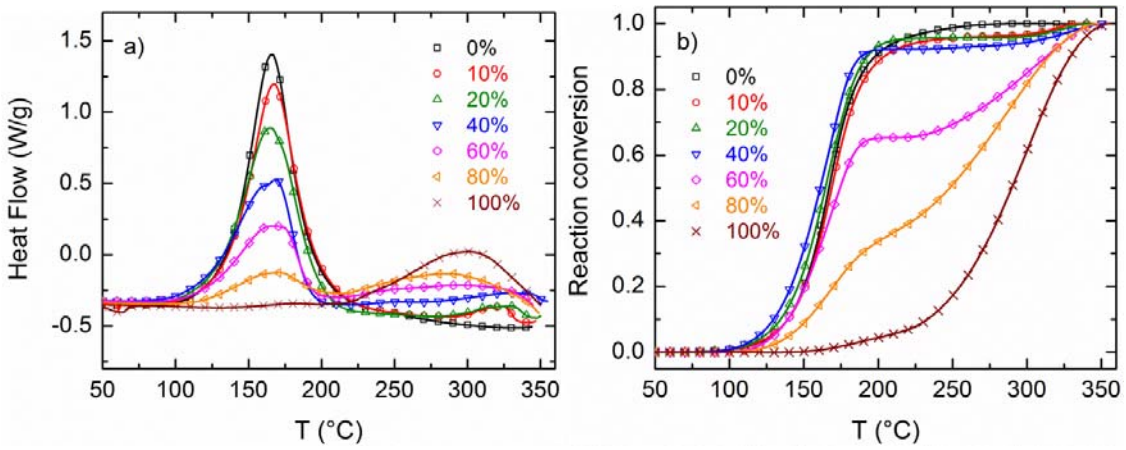

Figure 5.1: (a) Heat flow as a function of temperature for epoxy resins containing varying ESO content. (b) reaction conversion determined from the fraction of the total integral of the DSC exothermic peak as a function of temperature.

5.2.2 Glass transition temperatures of epoxy resins with varying ESO contents

DSC was utilized to determine the glass transition temperature (T_g) of the epoxy resins as a function of ESO content and curing protocol, as summarized in Table 2.4. Increasing the ESO content in the epoxy resin has a dramatic effect on the T_g, as the T_g decreased with increasing ESO content. Polymers containing 0-40 wt% ESO exhibited a slight increase in the T_g during the second heating ramp relative to the first, which could be attributed to the presence of additional curing during the first heating ramp, or enthalpic relaxation of the polymer. Subsequent heating ramps after the second ramp showed no further changes in the T_g.

The T_g of the polymers with 60-100 wt% ESO are reported in Table 5.1 for curing Protocols B1 – B4 (the protocols are described in Table 2.4). Polymers containing 60-100 wt% ESO exhibited an increase in the T_g as the time of the curing step at 198 °C was increased (comparing Protocols B1 – B4 in Table 5.1), indicating incomplete curing at shorter curing times. After 9 h of curing at 198 °C (following Protocol B2), no further change was observed in the T_g for polymers with 60 and 80 wt% ESO. In contrast, polymers with 100 wt% ESO continued to exhibit an increase in the T_g upon subsequent curing (compare Protocols B1 – B4 in Table 5.1). T_g values were measured on distinct specimens for many of the reaction conditions; error bars are included in Table 5.1 in the case of multiple measurements. In most cases multiple measurements under the same reaction conditions resulted in reproducible T_g values, with a standard deviation of 1-2 °C. Polymers with 100 wt% ESO were the exception, as a larger degree of variation in the measurements was observed (i.e. the standard deviation was as high as 5 °C for intermediate levels of curing).

The behavior of the polymers with 60 wt% ESO was distinct compared to all of the other polymers. Using a conventional DSC measurement, two features were observed in the heat flow vs. temperature curve upon the first heating ramp. MDSC was used to characterize the reversible and nonreversible heat flow during the first heating ramp, indicating that the glass transition is superimposed upon a peak related to the enthalpic relaxation of the polymer (observed clearly in the non-reversible heat flow). Further evidence for this conclusion is given by comparing conventional DSC data obtained within 1 day of curing the sample, and after 42 days of aging at room temperature. The longer aging time results in a greater enthalpic relaxation peak attributed to the reversal of the

aging process.[159] Once the polymers are cooled and reheated a second time through the transition, a single feature is observed (the T_g). The glass transition temperatures reported in Table 5.1 for the polymers with 60 wt% ESO were that obtained from the MDSC data. Polymers with 80-100 wt% ESO did not show a significant change in the T_g when comparing the first and subsequent heating ramps during the DSC measurement and exhibited only one feature in the conventional DSC data attributed to the T_g.

Table 5.1: Glass transition temperature (T_g) determined from DSC

% ESO (relative to total epoxide content)	Sample preparation method[a]	T_g (°C), first heating ramp	T_g (°C), second heating ramp
0	Protocol A	162	176
5		154	161
10		137	145
15		133	138
20		120	129
40		84	87
60	Protocol B1	55	65
	Protocol B2	59	72 ± 2.2
80	Protocol B1	25	29
	Protocol B2	40 ± 0.65	39
100	Protocol B1	3.3 ± 0.93	3.6 ± 1.4
	Protocol B2	15 ± 4.0	17 ± 4.8
	Protocol B3	21 ± 1.3	21 ± 1.3
	Protocol B4	26 ± 0.30	29 ± 2.7

Modulated DSC was used to characterize the T_g of polymers containing 60 wt% ESO. All other polymers were characterized with conventional DSC.Standard deviations were determined using measurements from multiple specimens. If the error is not reported, the measurement was conducted on a single specimen.
[a]Curing protocols are described in Table 2.4

5.2.3 Isothermal DSC analysis of the curing kinetics

Achieving complete curing for the polymer with 100 wt% ESO was significantly more challenging as compared to polymers with lower ESO contents. For this reason, additional experiments were conducted to explore the isothermal curing kinetics of this polymer. Initially, an insitu DSC experiment during curing was conducted at 200 °C, in

which the temperature was held constant at 200 °C for 60 min, after which the T_g was measured. This process was repeated until no change in the T_g was observed (Figure 5.2). The resulting Tg values are shown in Figure 5.3.

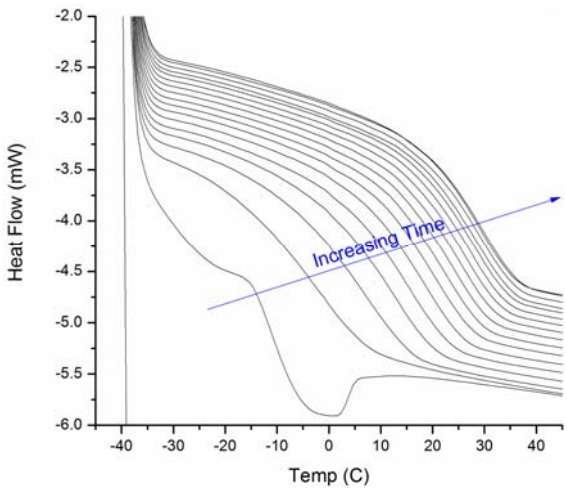

Figure 5.2: Isothermal DSC data obtained during the in-situ curing of an epoxy resin containing 100 wt% ESO (relative to total epoxide content in the polymer) at 200 °C.

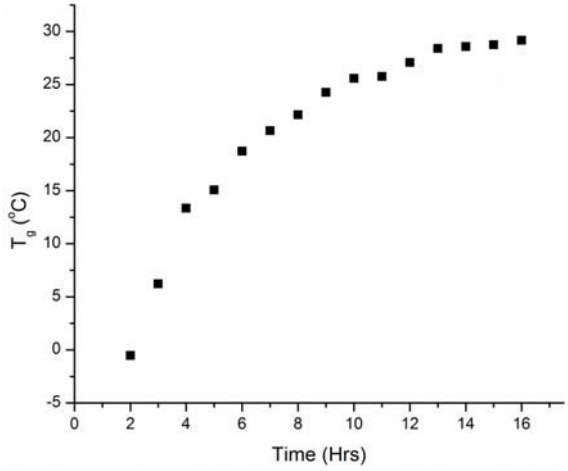

Figure 5.3: Glass transition temperatures determined from the in-situ DSC curing experiment conducted at 200 °C.

After approximately 16 hours of curing the T_g reached a limiting value of 30 °C. Subsequently, an *in situ* isothermal DSC experiment was conducted during curing, holding the temperature constant at 200 °C over a period of 17 hours. The final T_g of this sample

was 29 °C. The results of these experiments indicate that the degree of variability observed in the T_g measured for polymers containing 100 wt% ESO (Table 5.1) is likely due to variability in the degree of curing for each of the samples when shorter curing times are used. Multiple polymers containing 100 wt% ESO were also cured in a convection oven for 3 days at 198 °C (following Protocol B4), the results of which are reported in Table 5.1, achieving a similar T_g value as that in the isothermal DSC experiments (29 ± 2.7 °C).

5.2.4 Thermal degradation behavior

Thermogravimetric analysis (TGA) was used to monitor the thermal degradation of the polymers. TGA data for samples with varying ESO content are shown in Figure 5.4. The data included in Figure 5.4 were obtained from samples with the highest degree of curing from Table 5.1 (prepared through Protocol A for 0-40 wt% ESO, Protocol B2 for 60-80 wt% ESO and Protocol B4 for 100 wt% ESO). The weight % as a function of temperature is given in Figure 5.4a. The derivative of the weight % as a function of temperature is shown in Figure 5.4b. The position(s) of the peak maxima determined from the derivative plot are shown in Figure 5.4c. As a comparison, TGA data obtained from the epoxy resin components (DGEBA, MDA and ESO) are also shown in Figure 5.4. The TGA data obtained from the MDA and DGEBA monomers is attributed to evaporation and boiling of the molecules. Polymers containing 0-40 wt% ESO exhibited one peak in the derivative weight % (Figure 5.4b and Figure 5.4c). Interestingly, this degradation peak (located around 360-380 °C) exactly coincides with that of pure unreacted ESO (located at 374 °C). Polymers containing 60-100 wt% ESO exhibited two peaks: one located at around 360-380 °C, similar to the other samples, and a second peak located at a significantly higher temperature (around 420-450 °C).

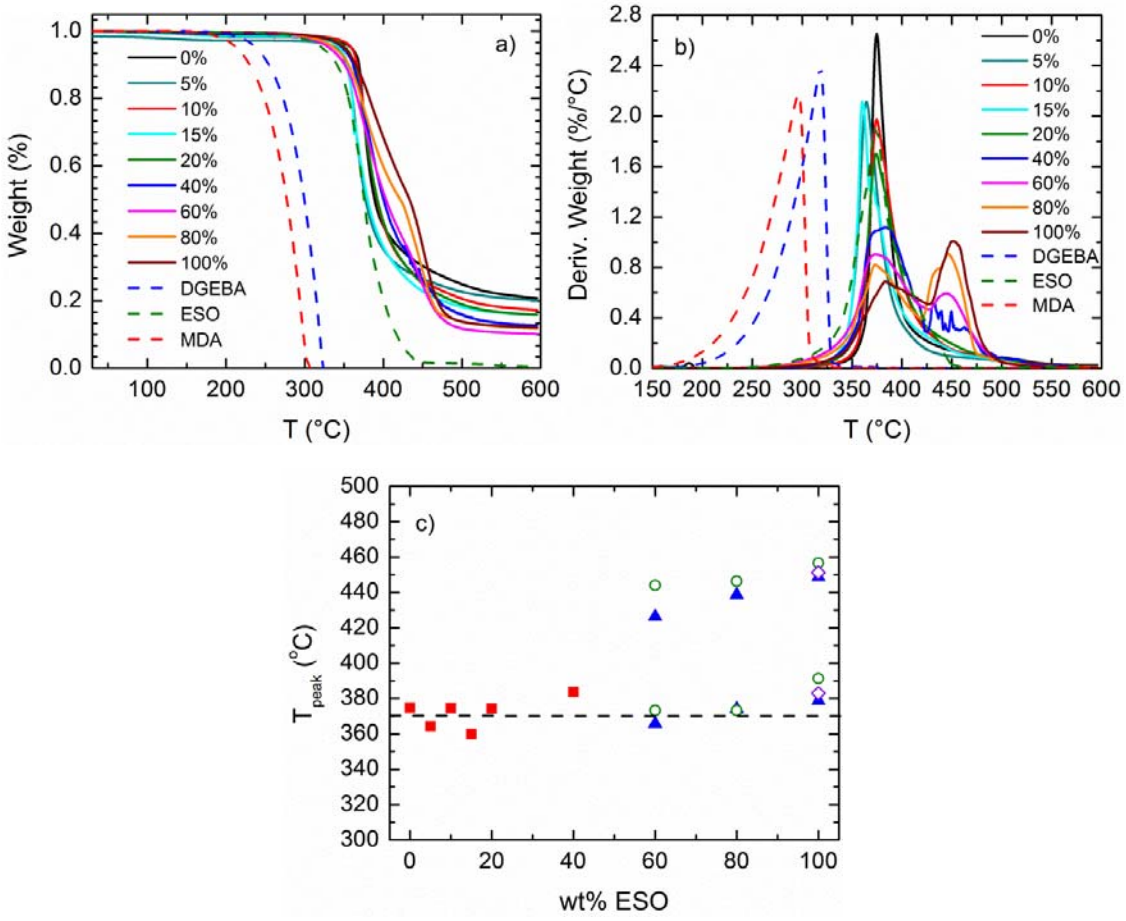

Figure 5.4: (a) Weight % as a function of temperature (obtained from TGA) for epoxy resins containing varying ESO content. b) Derivative of the weight % as a function of temperature. c) Position of the peak maxima.

Gupta and coworkers studied the thermal degradation of epoxy resins prepared through the curing of ESO with phthalic anhydride.[160] Similar to our data, weight loss was observed at two separate temperatures, for epoxy resins containing both stoichiometic and nonstoichiometic amounts of the functional groups. This was attributed to the presence of partially reacted curing agent.[160] In our case, there may be unreacted or partially reacted MDA present, which is the excess component for polymers containing ESO. In addition, there may be unreacted epoxide groups on ESO or DGEBA molecules if there are trapped segments in the network.

TGA data were obtained TGA data on epoxy resins containing 60-100 wt% ESO, prepared with various curing times (Protocol B1, B2 and B4). The peak locations for all curing protocols are shown in Figure 5.4c. Polymers with longer curing times tend to exhibit slightly higher degradation temperatures (comparing Protocols B1 and B2 in Figure 5.4c. In the case of the polymers with 100 wt% ESO, increasing the curing time further in Protocol B4 resulted in a slight reduction of the degradation temperature (Figure 5.4c).

5.2.5 Hydrolytic degradation in a NaOH solution

The hydrolytic degradation characteristics of the epoxy resins were characterized by placing the samples in a NaOH solution (either 3 or 10 wt% NaOH) and monitoring the mass of the sample over time. The base solutions were chosen to accelerate the hydrolytic degradation process, following literature procedures.[18] Polymers containing 0-40 wt% ESO (prepared with Protocol A) were monitored in both 3 and 10 wt% NaOH solutions. These samples showed little degradation over 72 days (the total time over which they were monitored), regardless of the NaOH concentration, as evidenced by the unchanging mass of the samples (Figure 5.5). It is worth noting that the polymers containing 0-40 wt% ESO were not completely cured, as evidenced by the change in the T_g during the first and second heating ramps of the DSC measurement, yet still exhibited little measureable mass loss.

In contrast, the polymers containing 60-100 wt% ESO rapidly degraded in the 3 wt% NaOH solution. Figure 5.5 illustrates the mass fraction of the polymers with 60-100 wt% ESO as a function of time in the 3 wt% NaOH solution. The degradation experiments were conducted on polymers prepared through Protocols B1 and B2. As there is a larger degree of variation in the T_g's for the samples containing 100 wt% ESO, the T_g values for the samples measured in the degradation experiments are indicated in the caption to Figure 5.5.

Both 80 and 100 wt% ESO polymers fully degraded within two weeks in the 3 wt% NaOH solution. The polymers with 60 wt% ESO exhibited an initial loss of mass during the degradation experiment. After loss of approximately 40-50% of the sample mass, no further loss was observed (measured up to 22 days as indicated in Figure 5.5 of the Supporting Information). This is consistent with the conclusion that only the strands in the networks containing ESO molecules are degradable, and strands containing only DGEBA and MDA molecules will not be degradable. In general, the degradation rate is highly dependent on the concentration of ESO in the sample, yet appears unaffected by the curing protocol used (B1 vs. B2) and resulting degree of curing and T_g of the resin (Figure 5.5).

In summary, there appears to be significant differences between polymers with 0-40 wt% ESO, which exhibited little degradation, in both the 3 and 10 wt% NaOH solutions, and the polymers with 60-100 wt% ESO, which exhibited significant degradation within a two-week period in the 3 wt% NaOH solution. The polymers with 60 wt% ESO are only partially degradable.

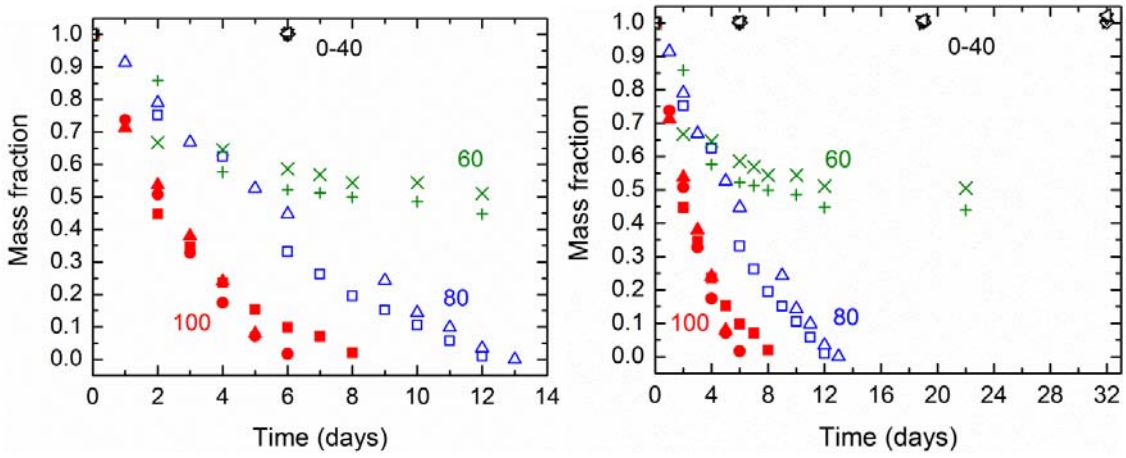

Figure 5.5: Fraction of mass remaining as a function of time in a 3 wt% NaOH solution at 80 °C. The same data are shown in the left and right figures, over different time ranges.

5.3 Concluding Remarks

Epoxy resins were prepared containing varying concentrations of ESO. The thermal degradation properties and glass transition temperature were found to be highly dependent on the ESO content in the polymer. Polymers with large ESO contents (60-100 wt%) exhibited a higher thermal degradation temperature than polymers with lower ESO contents (0-40 wt%). In addition, the glass transition temperature significantly decreased, as the ESO concentration was increased. The accelerated hydrolytic degradation of the polymers was observed through mass loss experiments in a NaOH solution. Polymers containing 0-40 wt% ESO exhibited little measurable mass loss (in both 3 and 10 wt% NaOH solutions) over 72 days (the total experimental time). In stark contrast, polymers with 60-100 wt% exhibited significant mass loss in a 3 wt% NaOH solution within two weeks.

Chapter 6 Thermal and Mechanical Properties of Epoxy Resins derived from Phenolic Acids

6.1 Introduction

Plant-derived phenolic acids are an attractive substitute for petroleum sources for the derivation of polymers, due to their rigid aromatic rings and chemical groups amenable to functionalization. Difunctional phenolic acids were investigated as replacements for the diglycidyl ether of bisphenol A (DGEBA) in anhydride-cured epoxy resins. Functionalization of each phenolic acid was carried out through allylation, followed by epoxidization. Epoxy resins were synthesized containing epoxidized salicylic acid (ESA) and epoxidized 4-hydroxybenzoic acid (E4HBA), cured with methylhexahydrophthalic anhydride (MHHPA) and 1-methyl-imidazole (1-MI) catalyst. The curing reaction with various curing agents was monitored with *in situ* differential scanning calorimetry. A two-step protocol was developed to avoid monomer evaporation and polymer vitrification during curing. The physical properties of these biorenewable epoxy resins are benchmarked to that of a conventional DGEBA-based epoxy resin. This work explores strategies for developing sustainable epoxy resins with thermal and mechanical behaviors that are competitive to traditional materials.

6.2 Results and Discussion

6.2.1 Selection of Curing Agent for Epoxidized Phenolic Acids

The curing reactions between DGEBA, ESA and E4HBA and various curing agents were monitored through *in situ* DSC, using a dynamic temperature scan: the temperature was heated from 40 to 200 ^{o}C, cooled back to 40 ^{o}C, and subsequently heated to 200 ^{o}C; each step was conducted at a rate of 10 ^{o}C/min. The curing reactions between ESA and

various curing agents were explored in order to inform the choice of proper curing agent (Figure 6.2a): aliphatic amines (DETA, TETA), a cycloaliphatic amine (IPDA), an aliphatic aromatic amine (MXDA), and anhydrides with catalyst (MHHPA + 3 phr 1-MI, NMA + 3 phr Ancamine K54). The ratio of epoxy resin to curing agent was held at the stoichiometric ratio of respective functional groups. When ESA was cured with an amine, the resin exhibited a relatively low curing temperature (maximum of the exothermic peak was below 100 ^{o}C), regardless of the choice of amine. By contrast, when ESA was cured with anhydride in a catalyzed reaction, the required curing temperature was higher (maximum of the exothermic peak was above 100 ^{o}C). We note that 200 °C was specified as the upper temperature limit of these experiments, to avoid thermal degradation of the polymer within the calorimeter. For this reason, not all specimens were fully cured after the heating scan (in particular, when the NMA curing agent was used the curve did not return to the baseline at high temperatures as shown in Figure 6.2a).The T_g's of each ESA-based epoxy resin, cured with various choices of curing agents, were also characterized (Table 6.1). The T_g of the ESA-based epoxy resins were systematically lower than that of DGEBA-based epoxy resins (cured with the same choices of curing agents). In the case of the amine curing agents, the differences in T_g of the two types of epoxy resins (ESA and DGEBA-based) were quite large (in the range of 30-50 °C), whereas the anhdride curing agents produced epoxy resins with more similar T_g's (differing by < 20 °C). The MHHPA anhydride curing agent (catalyzed by 1-MI) was chosen for subsequent studies due to the advantageous high T_g of the ESA epoxy resin (138 °C, compared to 155 °C for the DBEGA-based epoxy resin cured with the same curing agent). A comparison of the DSC data obtained during curing of ESA, E4HBA, and DGEBA with MHHPA (catalyzed by 1-

MI) is shown in Figure 6.2b; the ESA and E4HBA-based epoxy resins exhibited comparable T_g's (138 and 140 °C, respectively).

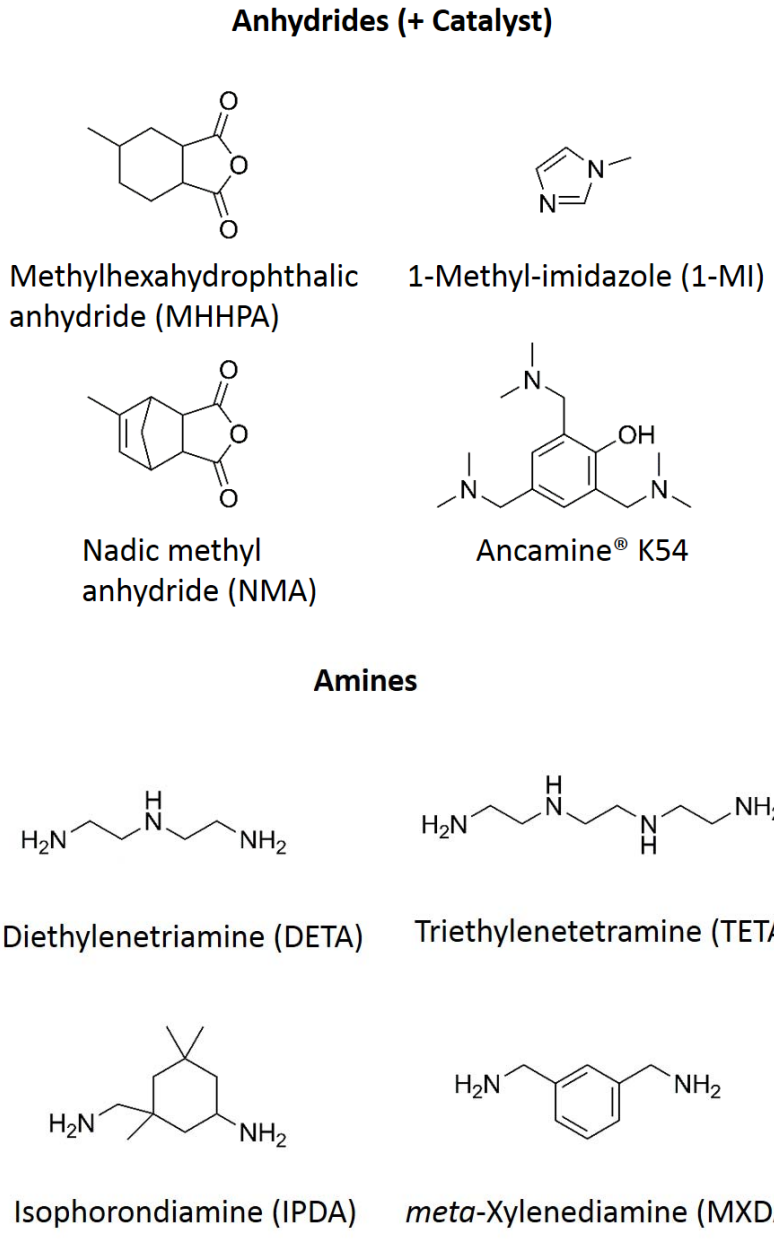

Figure 6.1 Chemical structures of curing agents used in this study.

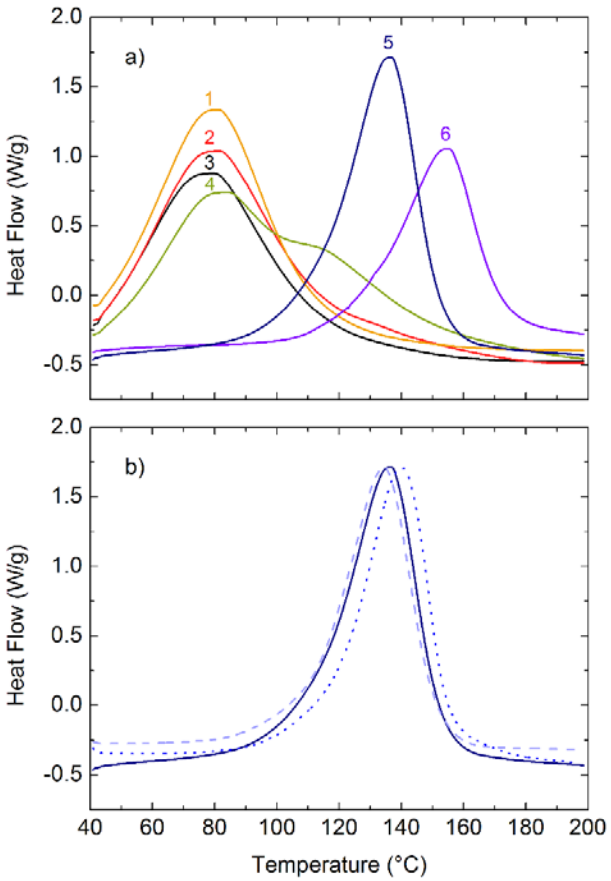

Figure 6.2: a) *In-situ* DSC data of ESA cured with: MXDA (1), TETA (2), DETA (3), IPDA (4), MHHPA (5), NMA (6). b) cured with MHHPA (+ 3 phr 1-MI): DGEBA (dotted curve), ESA (solid curve), E4HBA (dashed curve).

Table 6.1: Glass Transition Temperatures (T_g, °C) of Epoxy Resins Derived from Phenolic Acids Using Various Curing Agents[a]

Epoxy Monomer	TETA	DETA	MXDA	IPDA	MHHPA[b]	NMA[c]
DGEBA	118	137	119	156	155	99
ESA (E4HBA)	81	86	90	112	138 (140)	96

[a] samples were cured using *in situ* DSC dynamic temperature scan from 40 to 200 °C at a rate of 10 °C /min.
[b]catalyzed by 3 phr 1-MI
[c]catalyzed by 3 phr Ancamine K54

6.2.2 Optimization of Curing Protocol for Anhydride-Cured Epoxidized Phenolic Acids

The epoxy resins were cured through a two-stage process in which a lower temperature stage was first employed to cure the resin without significant loss of monomer,

and a second, higher temperature stage was then used to achieve high conversion of monomer. The potential evaporation of monomer was monitored with TGA during the first (lower temperature) curing stage (Figure 6.3a). The onset monomer evaporation temperatures were observed to be 90.1 and 96.5 ^{o}C for the ESA-based and E4HBA-based epoxy resins, respectively. To avoid significant monomer evaporation, 70 ^{o}C was choosen as the temperature of the first step in the curing protocol. The reactant mixture for both ESA-based and E4HBA-based epoxy resins was cured in a convection oven at 70 ^{o}C for various time periods until solidification (gelation) was observed visually. The ESA-based and E4HBA-based epoxy resins solidified after 1.5 and 2 h, respectively, at 70 ^{o}C. The first stage in the curing protocol was therefore specified as 70 ^{o}C for 2 h.

To avoid vitrification and achieve high conversion, a curing temperature higher than the T_g of the final epoxy networks is required. The second curing stage was therefore selected to occur at 170 ^{o}C, well above the T_g's observed in the *in situ* DSC experiments (Figure 6.2 and Table 6.1). The three types of epoxy resins (ESA, E4HBA and DGEBA) were cured at 70 ^{o}C in the convection oven, and then were subsequently cured at 170 ^{o}C in the convection oven for various time periods ranging from 1-5 h. The T_g of each resin was monitored as a function of the second stage (170 ^{o}C) curing time (Figure 6.3b). The T_g's showed little change after the first hour of curing at 170 ^{o}C, and therefore 2 h was chosen. The final curing protocol was therefore selected to be: 2 h isothermal curing at 70 ^{o}C (first stage), followed by 2 h isothermal curing at 170 ^{o}C (second stage). The synthetic scheme for the curing of ESA and E4HBA using MHHPA is shown in Scheme 6.1.

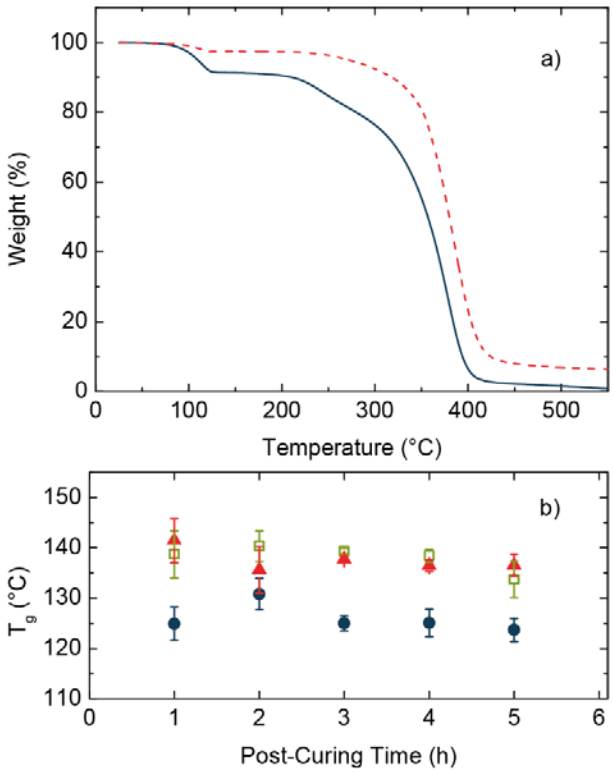

Figure 6.3: a) TGA of epoxy resins containing ESA (dark curve) and E4HBA (red curve). b) T_g as a function of post-curing time at 170 ºC (following pre-curing for 2 h at 70 ºC) for ESA (dark blue ●), E4HBA (red ▲) and DGEBA (green □).

FTIR was used to monitor the curing reactions between MHHPA and ESA, E4HBA, and DGEBA (Figure 6.4). Spectra were obtained following 1 and 2 h of curing at 70 °C (the temperature of the first stage in our curing protocol), which showed a systematic decrease (yet not disappearance) in intensities of peaks associated with anhydride groups (1857 and 1787 cm^{-1}, anhydride C=O stretching;[161] 1007-900 cm^{-1}, anhydride C-O and C-O-C stretching;[161, 162] as well as a systematic decrease in intensities of peaks associated with epoxide groups (915 cm^{-1}, epoxide C-O stretching and 845 cm^{-1}, epoxide C-O-C stretching[161, 163, 164]). Similarly, systematic increases in intensities of peaks associated with formation of the epoxy network were observed (1210 – 1036 cm^{-1}, ester C-O and ether C-O stretching; 1736 cm^{-1}, ester C=O stretching). Upon heating the sample at 170 °C (the

second stage in our curing protocol), the peaks associated with anhydride and epoxide groups drastically reduced after 1 h, showing high conversion of fucntional groups (in the range of 96-100%, Table 6.2). Increasing the curing time to 2 and 3 h had little impact on the conversion of functional groups(Table 6.2).

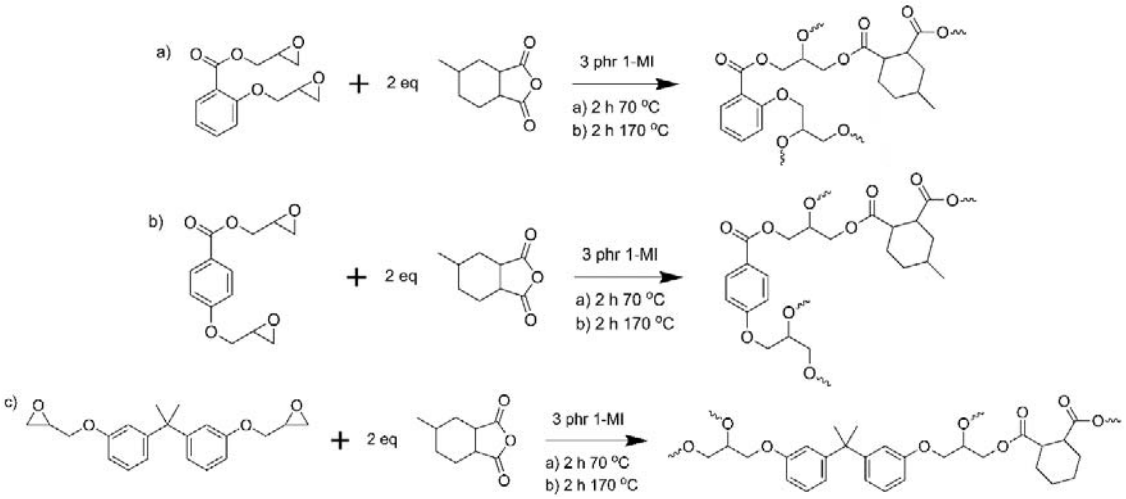

Scheme 6.1: Synthesis of epoxy resins through curing of a) ESA, b) E4HBA and c) DGEBA with MHHPA (catalyzed by 3 phr 1-MI).

Table 6.2: Conversion of Epoxy Resins Quantified through FTIR[a]

Curing Time (h)[b] at 70 °C / 170 °C	ESA		E4HBA		DGEBA	
	1857 cm^{-1}	1787 cm^{-1}	1857 cm^{-1}	1787 cm^{-1}	1857 cm^{-1}	1787 cm^{-1}
1 / 0	28 ± 3%	26 ± 2%	36 ± 3%	34 ± 2%	29 ± 2%	29 ± 1%
2 / 0	44 ± 3%	40 ± 2%	55 ± 3%	53 ± 2%	43 ± 2%	40 ± 1%
2 / 1	94 ± 3%	90 ± 2%	97 ± 3%	96 ± 2%	99.5 ± 0.8%	97 ± 1%
2 / 2	96 ± 3%	93 ± 2%	97 ± 3%	97 ± 2%	100[c]	97 ± 1%
2 / 3	96 ± 3%	94 ± 2%	97 ± 3%	97 ± 2%	100[c]	97 ± 1%

[a] Error bars represent error on analysis of conversion from FTIR peak areas.
[b] Samples were cured in the convection oven.
[c] Peak could not be detected.

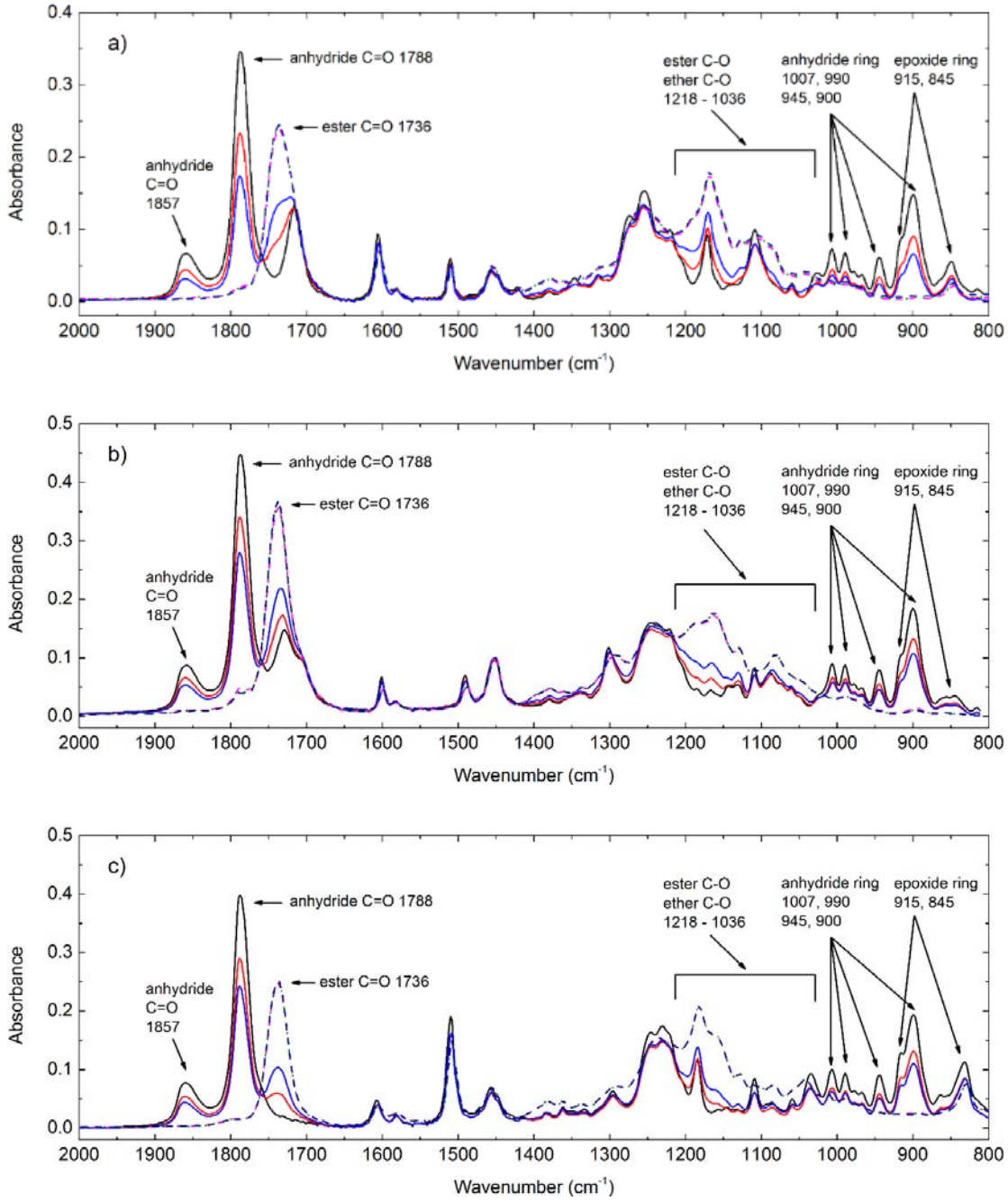

Figure 6.4: FTIR data for (a) ESA, (b) E4HBA and (c) DGEBA: before curing (black solid), 1 h 70 ºC (red solid), 2 h 70 ºC (blue solid), + 1 h 170 ºC (pink dash), + 2 h 170 ºC (green dot) and + 3 h 170 ºC (dark blue dash).

6.2.3 Characterization of Epoxy Resin Mechanical Properties

The mechanical properties of the epoxy resins were probed with tensile testing. Tensile experiments were conducted on multiple specimens for each network type; the average values of relevant parameters are shown in Table 6.3.

Table 6.3: Tensile Properties of Epoxy Resins[a]

Epoxy monomer	Tensile strength (MPa)	% Elongation at break	Modulus (GPa)	Tensile toughness (MPa)
ESA	85 ± 6	5 ± 1	3.0 ± 0.3	3 ± 1
E4HBA	90 ± 2	8 ± 1	2.9 ± 0.2	5 ± 1
DGEBA	80 ± 2	8 ± 2	2.5 ± 0.2	5 ± 1

[a] Samples were prepared using the following curing protocol: 2 h at 70 °C, followed by 2 h at 170 °C. The error of the measurement represents the standard deviation of measurements obtained on multiple test specimens.

We find that ESA and E4HBA-based epoxy resins are desirable replacements for DGEBA-based epoxy resins due to their high moduli (around 3 GPa) and tensile strengths (around 85-90 MPa). These attractive properties are likely attributed to the presence of rigid aromatic rings in the network, regardless of whether ESA, E4HBA or DGEBA is used in the resin synthesis. The E4HBA and DGEBA-based epoxy resins also fractured at comparable elongation at break values. We note, however, that epoxy resins derived from ESA broke at lower elongation compared to E4HBA and DGEBA-based epoxy resins. We hypothesize that differences in the elongation at break originate from differences in the relative placement of functional groups on the epoxy monomers. E4HBA and DGEBA contain epoxide groups at the *para* positions around the aromatic ring, whereas ESA contains epoxide groups at the *ortho* position.

Chapter 7 Summary and Future Work

7.1. Conclusions of this work

Biomass-based molecules were explored as potential replacements for petroleum-derived components in polymers. In the first project, five types of biomass-derived phenolic acids were utilized as ene-bearing molecules in the sustainable thiol-ene elastomers to explore the relationship between the physical properties of thiol-ene elastomers and the chemical structures of phenolic acids. The phenolic acids contained varying functional group placement (*ortho*, *meta*, and *para*) and functionality (2-4 functional groups per molecule). In the second project, sustainable and degradable epoxy thermosets were synthesized from soybean oil (containing degradable ester groups) and plant-derived phenolic acids (containing rigid aromatic rings) as substitutes for DGEBA, a petrochemical based monomer traditionally used in epoxy resins.

7.1.1 Thiol-ene networks

Biobased phenolic acids (found in plant sources) were allylated and subsequently reacted with a multifunctional thiol (in a photoinitiated reaction) to form networks. A series of phenolic acids were explored in which the relative number (2-4) and placement (*ortho*, *meta*, *para*) of functional groups was varied. The networks derived from difunctional allylated phenolic acids exhibited narrow glass transitions (indicating a high degree of network homogeneity), and glass transition temperatures (T_g) which correlated with their crosslink density. The *para* placement of allyl groups on the allylated phenolic acid produced a network with the highest crosslink density, T_g, modulus, tensile strength, and elongation at break (followed by *ortho* and then *meta*). These variations in thermal and mechanical behavior were attributed to differences in the crosslink densities of the

networks as well as microscopic changes in the network upon deformation, which are likely impacted by the placement of functional groups around the aromatic ring. As the functionality of the allylated monomer increased (to 3-4 allyl groups per molecule), the crosslink density remained high yet the T_g decreased, attributed to a lower concentration of aromatic rings throughout the network structure (as all networks were prepared at the stoichiometric ratio of allyl and thiol functional groups). The networks derived from the higher functionality allylated phenolic acids also exhibited lower elongation at break and associated tensile strength and tensile toughness, likely due to increased heterogeneity of the networks (indicated by higher glass transition widths compared to the networks derived from difunctional allylated phenolic acids). All networks exhibited behavior consistent with an ideal elastomer (affine network) at low to moderate strains, albeit with lower moduli than predicted from the monomer chemical structure. At the high end of the strain ranges achieved, some of the networks exhibited strain hardening behavior, in which the stress at a given strain was higher than that predicted for an ideal elastomer.

7.1.2 Epoxy resins

Epoxy resins were prepared containing varying concentrations of epoxidized soybean oil (ESO). The thermal degradation properties and glass transition temperature were found to be highly dependent on the ESO content in the polymer. Polymers with large ESO contents (60-100 wt%) exhibited a higher thermal degradation temperature than polymers with lower ESO contents (0-40 wt%). In addition, the glass transition temperature significantly decreased, as the ESO concentration was increased. The accelerated hydrolytic degradation of the polymers was observed through mass loss experiments in a NaOH solution. Polymers containing 0-40 wt% ESO exhibited little measurable mass loss

(in both 3 and 10 wt% NaOH solutions) over 72 days (the total experimental time). In stark contrast, polymers with 60-100 wt% exhibited significant mass loss in a 3 wt% NaOH solution within two weeks.

Biobased phenolic acids (SA and 4HBA, found in plant sources) were allylated, epoxidized and subsequently reacted with MHHPA and catalyst 1-MI to form epoxy networks. The curing reactions between ESA and various curing agents were explored, and the MHHPA anhydride curing agent (catalyzed by 1-MI) was chosen due to the advantageous high glass transitions of the resulting epoxy resins. ESA, E4HBA and DGEBA underwent similar curing behavior with MHHPA, monitored through *in situ* DSC. In order to avoid monomer evaporation and polymer vitrification during curing, the a two-stage curing protocol was established: 2 h at 70 ^{o}C and 2 h at 170 ^{o}C. ESA and E4HBA-baesd epoxy resins exhibited comparable moduli and tensile strengths to a conventional DGEBA-based epoxy resin, likely attributed to the presence of rigid aromatic rings in the network. The epoxy resin derived from ESA broke at lower elongation compared to E4HBA and DGEBA-based epoxy resins.

7.2. Outlook and future challenges

Due to the potentially significant effect of network imperfections and heterogeneity within thiol-ene elastomers on their physical properties, challenges remain in understanding the thiol-ene network morphology. Exploration of network defects will provide more detailed information to explain the effect of chemical structure of phenolic acids on the thiol-ene elastomer properties. Improving the understanding of the effect of monomer molecular structure on the thiol-ene network properties will be a helpful

reference to target proper thiol- and ene-bearing molecules for future elastomer development.

The development of degradable epoxy thermosets while increasing both biorenewable content and tensile strength is an ongoing challenge in this field. Other bio-based molecules containing aromatic and alicyclic components may be promising alternatives to replace DGEBA as sustainable substitutes. One promising approach is to explore the degradation of the phenolic acid-based epoxy resins, which contain ester groups (indeed, ethyl benzoate was reported to hydrolyze in a NaOH solution[165]). In addition, the biorenewable content in SA-based and E4HBA-based epoxy resins is only 23.2 wt% when a conventional curing agent is used. The development of curing agents (amine and anhydride) from biomass are attractive routes to sustainable materials.

Although the phenolic acid-derived epoxy resins exhibit comparable mechanical performance to DGEBA epoxy resins, there is a long journey to achieve their commercialization. Nowadays the commercial salicylic acid and 4-hydroxybenzoic acid are synthesized from petroleum-sourced molecules, even if they are available in vegetables and fruits. An alternative route has been reported for SA and 4HBA through fermentation.[166, 167] Phenolic acid fermentation is a promising method to decrease the cost and increase the production efficiency of biomass-derived phenolic acids.

References

1. Wilbon, P. A.; Chu, F.; Tang, C., Progress in Renewable Polymers from Natural Terpenes, Terpenoids, and Rosin. *Macromolecular Rapid Communications* **2013,** *34* (1), 8-37.

2. Gandini, A., The Irruption of Polymers From Renewable Resources on the Scene of Macromolecular Science and Technology. *Green Chemistry* **2011,** *13* (5), 1061-1083.

3. Narayan, R., Polymeric Materials from Agricultural Feedstocks. **1994,** *575*, 2-28.

4. Shibata, M.; Yoshihara, S.; Yashiro, M.; Ohno, Y., Thermal and Mechanical Properties of Sorbitol-Based Epoxy Resin Cured with Quercetin and the Biocomposites with Wood Flour. *Applied Polymer Science* **2012**.

5. Atta, A. M.; Mansour, R.; Abdou, M. I.; Sayed, A. M., Epoxy Resins from Rosin Acids: Synthesis and Characterization. *Polymers for Advanced Technologies* **2004,** *15* (9), 514-522.

6. Deng, L.; Shen, M.; Yu, J.; Wu, K.; Ha, C., Preparation, Characterization, and Flame Retardancy of Novel Rosin-Based Siloxane Epoxy Resins. *Industrial & Engineering Chemistry Research* **2012,** *51* (24), 8178-8184.

7. Liu, X.; Xin, W.; Zhang, J., Rosin-Based acid Anhydrides as Alternatives to Petrochemical Curing Agents. *Green Chemistry* **2009,** *11* (7), 1018.

8. Liu, X.; Xin, W.; Zhang, J., Rosin-Derived Imide-Diacids as Epoxy Curing Agents for Enhanced Performance. *Bioresource technology* **2010,** *101* (7), 2520-4.

9. Fache, M.; Darroman, E.; Besse, V.; Auvergne, R.; Caillol, S.; Boutevin, B., Vanillin, A Promising Biobased Building-Block for Monomer Synthesis. *Green Chemistry* **2014,** *16* (4), 1987.

10. Aouf, C.; Nouailhas, H.; Fache, M.; Caillol, S.; Boutevin, B.; Fulcrand, H., Multi-functionalization of Gallic Acid. Synthesis of a Novel Bio-Based Epoxy Resin. *European Polymer Journal* **2013,** *49* (6), 1185-1195.

11. Mitrus, M.; Wojtowicz, A.; Moscicki, L., Biodegradable Polymers and Their Practical Utility. In *Thermoplastic Starch*, Wiley-VCH Verlag GmbH & Co. KGaA: 2010; pp 1-33.

12. Vroman, I.; Tighzert, L., Biodegradable Polymers. *Materials* **2009,** *2* (2), 307-344.

13. Derraik, J. G. B., The Pollution of the Marine Environment by Plastic Debris: a Review. *Marine Pollution Bulletin* **2002,** *44*, 842–852.

14. Khosravi, E.; Musa, O. M., Thermally Degradable Thermosetting Materials. *European Polymer Journal* **2011,** *47* (4), 465-473.

15. Hita, C.; Parlanti, E.; Jambu, P.; Joffre, J.; Ambli, A., Triglyceride Degradation in Soil. *Org. Geochem.* **1996,** *25*, 19-28.

16. Shogren, R. L.; Petrovic, Z.; Liu, Z.; Erhan, S. Z., Biodegradation Behavior of Some Vegetable Oil-Based Polymers. *Journal of Polymers and the Environment* **2004,** *12* (3), 173-178.

17. Buchwalter, S. L.; Kosbar, L. L., Cleavable Epoxy Resins Design for Disassembly of a Thermoset. *Journal of Polymer Science: Part A Polymer Chemistry* **1996,** *34*, 249-260.

18. Umare, S. S.; Chandure, A. S., Synthesis, Characterization and Biodegradation Studies of Poly(Ester Urethane)s. *Chemical Engineering Journal* **2008,** *142* (1), 65-77.

19. Hoyle, C. E.; Lee, T. Y.; Roper, T., Thiol–enes: Chemistry of the Past With Promise For the Future. *Journal of Polymer Science Part A: Polymer Chemistry* **2004,** *42* (21), 5301-5338.

20. Lu, H.; Carioscia, J. A.; Stansbury, J. W.; Bowman, C. N., Investigations of Step-Growth Thiol-Ene Polymerizations for Novel Dental Restoratives. *Dental Materials* **2005,** *21* (12), 1129-1136.

21. Hoyle, C. E.; Bowman, C. N., Thiol-ene Click Chemistry. *Angewandte Chemie* **2010,** *49* (9), 1540-73.

22. Kade, M. J.; Burke, D. J.; Hawker, C. J., The Power of Thiol-Ene Chemistry. *Journal of Polymer Science Part A: Polymer Chemistry* **2010,** *48* (4), 743-750.

23. Li, Q.; Zhou, H.; Wicks, D. A.; Hoyle, C. E., Thiourethane-Based Thiol-Ene High Tg Networks: Preparation, Thermal, Mechanical, and Physical Properties. *Journal of Polymer Science Part A: Polymer Chemistry* **2007,** *45* (22), 5103-5111.

24. Samuelsson, J.; Jonsson, M.; Brinck, T.; Johansson, M., Thiol-Ene Coupling Reaction of Fatty Acid Monomers. *Journal of Polymer Science Part A: Polymer Chemistry* **2004,** *42* (24), 6346-6352.

25. Black, M.; Rawlins, J. W., Thiol–Ene UV-Curable Coatings ssing Vegetable Oil Macromonomers. *European Polymer Journal* **2009,** *45* (5), 1433-1441.

26. Chen, Z.; Chisholm, B.; Patani, R.; Wu, J.; Fernando, S.; Jogodzinski, K.; Webster, D., Soy-Based UV-Curable Thiol–Ene Coatings. *J Coat Technol Res* **2010,** *7* (5), 603-613.

27. Lligadas, G.; Ronda, J. C.; Galià, M.; Cádiz, V., Monomers and Polymers from Plant Oils Via Click Chemistry Reactions. *Journal of Polymer Science Part A: Polymer Chemistry* **2013,** *51* (10), 2111-2124.

28. Türünç, O.; Meier, M. A. R., The Thiol-Ene (Click) Reaction for The Synthesis of Plant Oil Derived Polymers. *European Journal of Lipid Science and Technology* **2013,** *115* (1), 41-54.

29. Acosta Ortiz, R.; Martinez, A. Y. R.; García Valdez, A. E.; Berlanga Duarte, M. L., Preparation of a Crosslinked Sucrose Polymer by Thiol–Ene Photopolymerization using Dithiothreitol as Comonomer. *Carbohydrate Polymers* **2010,** *82* (3), 822-828.

30. Ortiz, R. A.; Garcia Valdéz, A. E.; Martinez Aguilar, M. G.; Berlanga Duarte, M. L., An Effective Method to Prepare Sucrose Polymers by Thiol-Ene Photopolymerization. *Carbohydrate Polymers* **2009,** *78* (2), 282-286.

31. Hearon, K.; Nash, L. D.; Rodriguez, J. N.; Lonnecker, A. T.; Raymond, J. E.; Wilson, T. S.; Wooley, K. L.; Maitland, D. J., A High-Performance Recycling Solution for Polystyrene Achieved by the Synthesis of Renewable Poly(thioether) Networks Derived from d-Limonene. *Advanced Materials* **2014,** *26* (10), 1552-1558.

32. Link, L. A.; Lonnecker, A. T.; Hearon, K.; Maher, C. A.; Raymond, J. E.; Wooley, K. L., Photo-Cross-Linked Poly(Thioether-Co-Carbonate) Networks Derived from The Natural Product Quinic Acid. *ACS applied materials & interfaces* **2014,** *6* (20), 17370-5.

33. Fertier, L.; Koleilat, H.; Stemmelen, M.; Giani, O.; Joly-Duhamel, C.; Lapinte, V.; Robin, J.-J., The Use of Renewable Feedstock In UV-Curable Materials – A New Age for Polymers and Green Chemistry. *Progress in Polymer Science* **2013,** *38* (6), 932-962.

34. Pham, H. Q.; Marks, M. J., Epoxy Resins. In *Encyclopedia of Polymer Science and Technology*, John Wiley & Sons, Inc.: 2002.

35. Haymana, B.; Wedel-Heinen, J.; Brøndsted, P., Materials Challenges in Present and Future Wind Energy. *MRS Bulletin* **2008,** *33* (0.4), 343-353.

36. Vandenberg, L. N.; Maffini, M. V.; Sonnenschein, C.; Rubin, B. S.; Soto, A. M., Bisphenol-A and the Great Divide: a Review of Controversies in the Field of Endocrine Disruption. *Endocrine reviews* **2009,** *30* (1), 75-95.

37. Czub, P., Application of Modified Natural Oils as Reactive Diluents for Epoxy Resins. *Macromol. Symp.* **2006,** *242*, 60-64.

38. Frischinger, I.; Dirlikov, S., Toughening of Epoxy-Resins by Epoxidized Vegetable-Oils. *Polymer Communications* **1991,** *32* (17), 536-537.

39. Jin, F. L.; Park, S. J., Thermomechanical Behavior of Epoxy Resins Modified with Epoxidized Vegetable Oils. *Polymer International* **2008,** *57* (4), 577-583.

40. Jin, F. L.; Park, S. J., Impact-strength Improvement of Epoxy Resins Reinforced with a Biodegradable Polymer. *Mater. Sci. Eng. A-Struct. Mater. Prop. Microstruct. Process.* **2008,** *478* (1-2), 402-405.

41. Miyagawa, H.; Misra, M.; Drzal, L. T.; Mohanty, A. K., Fracture Toughness and Impact Strength of Anhydride-Cured Biobased Epoxy. *Polym. Eng. Sci.* **2005,** *45* (4), 487-495.

42. Park, S. J.; Jin, F. L.; Lee, J. R., Effect of Biodegradable Epoxidized Castor Oil on Physicochemical and Mechanical Properties of Epoxy Resins. *Macromol. Chem. Phys.* **2004,** *205* (15), 2048-2054.

43. Park, S. J.; Jin, F. L.; Lee, J. R., Thermal and Mechanical Properties of Tetrafunctional Epoxy Resin Toughened with Epoxidized Soybean Oil. *Mater. Sci. Eng. A-Struct. Mater. Prop. Microstruct. Process.* **2004,** *374* (1-2), 109-114.

44. Frischinger, I.; Dirlikov, S., Toughening of Epoxy-Resins By Epoxidized Soybean Oil. *Adv. Chem. Ser.* **1993,** (233), 451-489.

45. Raquez, J. M.; Deléglise, M.; Lacrampe, M. F.; Krawczak, P., Thermosetting (Bio)Materials Derived From Renewable Resources: A Critical Review. *Progress in Polymer Science* **2010,** *35* (4), 487-509.

46. Tan, S. G.; Chow, W. S., Curing Characteristics and Thermal Properties of Epoxidized Soybean Oil Based Thermosetting Resin. *J. Am. Oil Chem. Soc.* **2011,** *88* (7), 915-923.

47. Mustata, F.; Tudorachi, N.; Rosu, D., Curing and Thermal Behavior of Resin Matrix for Composites Based on Epoxidized Soybean Oil/Diglycidyl Ether of Bisphenol A. *Compos. Pt. B-Eng.* **2011,** *42* (7), 1803-1812.

48. Gupta, A. P.; Ahmad, S.; Dev, A., Modification of Novel Bio-Based Resin-Epoxidized Soybean Oil by Conventional Epoxy Resin. *Polymer Engineering & Science* **2011,** *51* (6), 1087-1091.

49. Espinoza-Perez, J. D.; Nerenz, B. A.; Haagenson, D. M.; Chen, Z. G.; Ulven, C. A.; Wiesenborn, D. P., Comparison of Curing Agents for Epoxidized Vegetable Oils Applied to Composites. *Polym. Compos.* **2011,** *32* (11), 1806-1816.

50. Cheng, X.; Chen, Y. X.; Du, Z. L.; Zhu, P. X.; Wu, D. C., Effect of the Structure of Curing Agents Modified by Epoxidized Oleic Esters on the Toughness of Cured Epoxy Resins. *J. Appl. Polym. Sci.* **2011,** *119* (6), 3504-3510.

51. Altuna, F. I.; Espósito, L. H.; Ruseckaite, R. A.; Stefani, P. M., Thermal and Mechanical Properties of Anhydride-Cured Epoxy Resins with Different Contents of Biobased Epoxidized Soybean Oil. *Journal of Applied Polymer Science* **2011,** *120* (2), 789-798.

52. Tan, S. G.; Chow, W. S., Biobased Epoxidized Vegetable Oils and Its Greener Epoxy Blends: A Review. *Polymer-Plastics Technology and Engineering* **2010,** *49* (15), 1581-1590.

53. Czub, P., Synthesis of High-Molecular-Weight Epoxy Resins from Modified Natural Oils and Bisphenol A or Bisphenol A-Based Epoxy Resins. *Polym. Adv. Technol.* **2009,** *20* (3), 194-208.

54. Supanchaiyamat, N.; Shuttleworth, P. S.; Hunt, A. J.; Clark, J. H.; Matharu, A. S., Thermosetting Resin Based on Epoxidised Linseed Oil and Bio-Derived Crosslinker. *Green Chemistry* **2012,** *14* (6), 1759.

55. Sarwono, A.; Man, Z.; Bustam, M. A., Blending of Epoxidised Palm Oil with Epoxy Resin: The Effect on Morphology, Thermal and Mechanical Properties. *J. Polym. Environ.* **2012,** *20* (2), 540-549.

56. Samper, M. D.; Fombuena, V.; Boronat, T.; Garcia-Sanoguera, D.; Balart, R., Thermal and Mechanical Characterization of Epoxy Resins (ELO and ESO) Cured with Anhydrides. *J. Am. Oil Chem. Soc.* **2012,** *89* (8), 1521-1528.

57. Espana, J. M.; Sanchez-Nacher, L.; Boronat, T.; Fombuena, V.; Balart, R., Properties of Biobased Epoxy Resins from Epoxidized Soybean Oil (ESBO) Cured with Maleic Anhydride (MA). *J. Am. Oil Chem. Soc.* **2012,** *89* (11), 2067-2075.

58. Liu, Z. S.; Erhan, S. Z.; Calvert, P. D., Solid Freeform Fabrication of Epoxidized Soybean Oil/Epoxy Composites with Di-, Tri-, And Polyethylene Amine Curing Agents. *Journal of Applied Polymer Science* **2004,** *93* (1), 356-363.

59. El Gouri, M.; El Bachiri, A.; Hegazi, S. E.; Rafik, M.; El Harfi, A., Thermal Degradation of A Reactive Flame Retardant Based on Cyclotriphosphazene and Its Blend With DGEBA Epoxy Resin. *Polymer Degradation and Stability* **2009,** *94* (11), 2101-2106.

60. Yang, G.; Rohde, B. J.; Robertson, M. L., Hydrolytic Degradation and Thermal Properties of Epoxy Resins Derived from Soybean Oil. *Green Materials* **2013,** *1* (2), 125-134.

61. Feng, X.; East, A. J.; Hammond, W. B.; Zhang, Y.; Jaffe, M., Overview of Advances in Sugar-Based Polymers. *Polymers for Advanced Technologies* **2011,** *22* (1), 139-150.

62. Feng, X.; East, A.; Hammond, W.; Ophir, Z.; Zhang, Y.; Jaffe, M., Thermal Analysis Characterization of Isosorbide-Containing Thermosets. *Journal of Thermal Analysis and Calorimetry* **2012,** *109* (3), 1267-1275.

63. Liu, X.; Zhang, J., High-performance Biobased Epoxy Derived from Rosin. *Polymer International* **2010**, n/a-n/a.

64. Busto, G.; Saini, P.; Feng, X.; Hammond, W. B.; East, A. J.; Jaffe, M.; Ieee, *Controlling Water Uptake of Sugar Based Epoxy Resins*. Ieee: New York, 2011.

65. Chrysanthos, M.; Galy, J.; Pascault, J.-P., Preparation and Properties of Bio-based Epoxy Networks Derived from Isosorbide Diglycidyl Ether. *Polymer* **2011,** *52* (16), 3611-3620.

66. Łukaszczyk, J.; Janicki, B.; Kaczmarek, M., Synthesis and Properties of Isosorbide Based Epoxy Resin. *European Polymer Journal* **2011,** *47* (8), 1601-1606.

67. Nelson, A. M.; Long, T. E., A Perspective on Emerging Polymer Technologies for Bisphenol-A Replacement. *Polymer International* **2012,** *61* (10), 1485-1491.

68. Varma, A. J.; Chavan, V. B., Cellulosic Diamines as Reaction-Incorporated Fillers in Epoxy Composites. *CELLULOSE* **1994,** *1*, 215-219.

69. Simionescu, C. I.; Rusan, V.; Macoveanu, M. M.; Cazacu, G.; Lipsa, R.; Vasile, C.; Stoleriu, A.; Ioanid, A., Lignin epoxy composites. *Composites Science and Technology* **1993,** *48*, 317-323.

70. Sun, H.; Sun, G.; Lv, H.; Liu, Y.; Zhao, B.; Zhu, N.; Hu, K., DSC Study on The Effect of Cure Reagents on The Lignin Base Epoxy Cure Reaction. *Journal of Applied Polymer Science* **2007,** *105* (4), 2332-2338.

71. Ruamcharoen, P.; Umare, S.; Ruamcharoen, J., Relationship between Tensile Properties and Morphology of Epoxy Resin Modified by Epoxidised Natural Rubber. *Journal of Materials Science and Engineering* **2011,** *5*, 504-510.

72. Hong, S.-G.; Chan, C.-K., The Curing Behaviors of The Epoxy/Dicyanamide System Modified with Epoxidized Natural Rubber. *Thermochimica Acta* **2004,** *417* (1), 99-106.

73. Alamri, H.; Low, I. M., Characterization of Epoxy Hybrid Composites Filled with Cellulose Fibers And Nano-Sic. *Journal of Applied Polymer Science* **2012,** *126* (S1), E222-E232.

74. Amor, I. B.; Ghallabi, Z.; Kaddami, H.; Raihane, M.; Arous, M.; Kallel, A., Experimental Study of Relaxation Process In Unidirectional (Epoxy/Palm Tree Fiber) Composite. *Journal of Molecular Liquids* **2010,** *154* (2-3), 61-68.

75. Liao, H.; Wu, Y.; Wu, M.; Zhan, X.; Liu, H., Aligned Electrospun Cellulose Fibers Reinforced Epoxy Resin Composite Films with High Visible Light Transmittance. *Cellulose* **2011,** *19* (1), 111-119.

76. Omrani, A.; Simon, L. C.; Rostami, A. A., Influences of Cellulose Nanofiber on The Epoxy Network Formation. *Materials Science and Engineering: A* **2008,** *490* (1-2), 131-137.

77. Tang, L.; Weder, C., Cellulose Whisker/Epoxy Resin Nanocomposites. *ACS applied materials & interfaces* **2010,** *2* (4), 1073-80.

78. Russell, W. R.; Labat, A.; Scobbie, L.; Duncan, G. J.; Duthie, G. G., Phenolic acid Content of Fruits Commonly Consumed and Locally Produced in Scotland. *Food Chemistry* **2009,** *115* (1), 100-104.

79. Manach, C.; Scalbert, A.; Morand, C.; Rémésy, C.; Jiménez, L., Polyphenols: Food Sources and Bioavailability. *The American Journal of Clinical Nutrition* **2004,** *79* (5), 727-747.

80. Schieber, A.; Stintzing, F. C.; Carle, R., By-products of Plant Food Processing as A Source of Functional Compounds — Recent Developments. *Trends in Food Science & Technology* **2001,** *12* (11), 401-413.

81. Naczk, M.; Shahidi, F., Phenolics in Cereals, Fruits and Vegetables: Occurrence, Extraction and Analysis. *Journal of Pharmaceutical and Biomedical Analysis* **2006,** *41* (5), 1523-1542.

82. Aouf, C.; Lecomte, J.; Villeneuve, P.; Dubreucq, E.; Fulcrand, H., Chemo-Enzymatic Functionalization of Gallic And Vanillic Acids: Synthesis of Bio-Based Epoxy Resins Prepolymers. *Green Chemistry* **2012,** *14* (8), 2328.

83. Hou, G.; Gao, J.; Xie, J.; Li, B., Preparation and Properties Characterization of Gallic Acid Epoxy Resin/Succinic Anhydride Bionanocomposites Modified by Green Reduced Graphene Oxide. *Soft Materials* **2016,** *14* (1), 27-37.

84. Cao, L.; Liu, X.; Na, H.; Wu, Y.; Zheng, W.; Zhu, J., How A Bio-Based Epoxy Monomer Enhanced the Properties of Diglycidyl Ether of Bisphenol A (DGEBA)/Graphene Composites. *Journal of Materials Chemistry A* **2013,** *1* (16), 5081.

85. Chen, S.; Lv, S.; Hou, G.; Huo, L.; Gao, J., Mechanical and Thermal Properties of Biphenyldiol Formaldehyde Resin/Gallic Acid Epoxy Composites Enhanced by Graphene Oxide. *Journal of Applied Polymer Science* **2015**, 42637-42637.

86. Fourcade, D.; Ritter, B. S.; Walter, P.; Schönfeld, R.; Mülhaupt, R., Renewable Resource-Based Epoxy Resins Derived from Multifunctional Poly(4-Hydroxybenzoates). *Green Chemistry* **2013,** *15* (4), 910.

87. IBRAHIM, A. M.; SEFERIS, J. C., Salicylic Acid Modified High Performance Epoxy Matrices. *Polymer Composites* **1985,** *6*, 47 - 53.

88. Motawie, A. M.; Sadek, E. M., Adhesives and Coatings Based on Phenolic/Epoxy Resins. *POLYMERS FOR ADVANCED TECHNOLOGIES* **1999,** *10*, 223-228.

89. Abbasi, E.; Vatankhah, M.; Hosseini, Y.; Ariana, M. A.; Ayazi, M., Synthesis, Structure, and Mechanical Properties of Castor Oil-Based Polyamidoamines Toughened Epoxy Coatings. *Journal of Applied Polymer Science* **2013**, 4023-4030.

90. Lambert, C.; Larroque, M.; Lebruna, J.-C.; Gérard, J.-F., Food-contact Epoxy Resin: Co-Variation Between Migration and Degree of Cross-Linking. *Food Additives and Contaminants* **2009,** *14* (2), 199-208.

91. Seniha Güner, F.; Yağcı, Y.; Tuncer Erciyes, A., Polymers from Triglyceride Oils. *Progress in Polymer Science* **2006,** *31* (7), 633-670.

92. Mustata, F.; Tudorachi, N.; Rosu, D., Curing and Thermal Behavior of Resin Matrix For Composites Based on Epoxidized Soybean Oil/Diglycidyl Ether of Bisphenol A. *Composites Part B: Engineering* **2011,** *42* (7), 1803-1812.

93. Czub, P., Application of Modified Natural Oils as Reactive Diluents for Epoxy Resins. *Macromolecular Symposia* **2006,** *242* (1), 60-64.

94. Tan, S. G.; Chow, W. S., Curing Characteristics and Thermal Properties of Epoxidized Soybean Oil Based Thermosetting Resin. *Journal of the American Oil Chemists' Society* **2010,** *88* (7), 915-923.

95. Park, S.-J.; Jin, F.-L.; Lee, J.-R., Effect of Biodegradable Epoxidized Castor Oil on Physicochemical and Mechanical Properties of Epoxy Resins. *Macromolecular Chemistry and Physics* **2004,** *205* (15), 2048-2054.

96. Miyagawa, H.; Misra, M.; Drzal, L. T.; Mohanty, A. K., Fracture Toughness and Impact Strength of Anhydride-Cured Biobased Epoxy. *Polymer Engineering & Science* **2005,** *45* (4), 487-495.

97. Jin, F.-L.; Park, S.-J., Impact-strength Improvement of Epoxy Resins Reinforced with A Biodegradable Polymer. *Materials Science and Engineering: A* **2008,** *478* (1-2), 402-405.

98. Park, S.-J.; Jin, F.-L.; Lee, J.-R., Thermal and Mechanical Properties of Tetrafunctional Epoxy Resin Toughened with Epoxidized Soybean Oil. *Materials Science and Engineering: A* **2004,** *374* (1-2), 109-114.

99. Yang, S.; Chen, J.-S.; Korne, H.; Breiner, T.; Ober, C. K., Reworkable Epoxies Thermosets with Thermally Cleavable Groups for Controlled Network Breakdown. *Chemistry of Material* **1998,** *10* (6), 1475-1482.

100. Li, H.; Wang, L.; Jacob, K.; Wong, C. P., Syntheses and Characterizations of Thermally Degradable Epoxy Resins. III. *Journal of Polymer Science Part A: Polymer Chemistry* **2002,** *40* (11), 1796-1807.

101. Griffith, J. R. Org Coat Plast 1978, 39, 209

102. Rivaton, A.; Moreau, L.; Gardette, J.-L., Photo-Oxidation of Phenoxy Resins at Long and Short Wavelengths- II. Mechanisms of Formation of Photoproducts. *Polymer Degradation and Stabiltiy* **1997,** *58*, 333-339.

103. Tesoro, G. C.; Sastri, V., Reversible Cross-linking in Epoxy-resin .1. Feasibility Studies. *Journal of Applied Polymer Science* **1990,** *39* (7), 1425 - 1437.

104. Sastri, V.; Tesoro, G. C., Reversible Cross-linking in Epoxy-resin .2. New Appoaches. *Journal of Applied Polymer Science* **1990,** *39* (7), 1439 - 1457.

105. Yang, G.; Kristufek, S. L.; Link, L. A.; Wooley, K. L.; Robertson, M. L., Synthesis and Physical Properties of Thiol–Ene Networks Utilizing Plant-Derived Phenolic Acids. *Macromolecules* **2015,** *48* (23), 8418-8427.

106. Brown, D. P.; Duong, H. Q., Synthesis of Novel Aromatic Macrolactones via Ring Closing Metathesis of Substituted Phenylalkanoic Acid Allylic Esters. *J. Heterocyclic Chem* **2008,** *45*, 435.

107. Murakami, H.; Minami, T.; Ozawa, F., Facile and Selective Deallylation of Allyl Ethers Using Diphosphinidenecyclobutene-Coordinated Palladium Catalysts. *Journal of Organic Chemistry* **2004,** *69*, 4482.

108. Hoyle, C. E.; Lee, T. Y.; Roper, T., Thiol-Enes: Chemistry of The Past with Promise for The Future. *Journal of Polymer Science Part A: Polymer Chemistry* **2004,** *42* (21), 5301-5338.

109. Cramer, N. B.; Reddy, S. K.; O'Brien, A. K.; Bowman, C. N., Thiol−Ene Photopolymerization Mechanism and Rate Limiting Step Changes for Various Vinyl Functional Group Chemistries. *Macromolecules* **2003,** *36* (21), 7964-7969.

110. Silverstein, R. M.; Webster, F. X.; Kiemle, D., *Spectrometric Identification of Organic Compounds*. 7th Edition ed.; John Wiley & Sons Hoboken, NJ, 2005.

111. Claudino, M.; van der Meulen, I.; Trey, S.; Jonsson, M.; Heise, A.; Johansson, M., Photoinduced Thiol-Ene Crosslinking of Globalide/E-Caprolactone Copolymers: Curing Performance and Resulting Thermoset Properties. *Journal of Polymer Science Part A: Polymer Chemistry* **2012,** *50* (1), 16-24.

112. Jean-Pierre Pascault; Henry Sautereau; Jacques Verdu; Williams, R. J. J., *Thermosetting Polymers*. Marcel Dekker, Inc: New York, 2002.

113. Ewing, W. W.; Mikovsky, R. J., Calcium Nitrate. V. Partial Molal Volumes of Water and Calcium Nitrate in Concentrated Solutions. *J. Am. Chem. Soc.* **1950,** *72* (3), 1390–1393.

114. Li, Q.; Zhou, H.; Wicks, D. A.; Hoyle, C. E., Thiourethane-Based Thiol-Ene Hightg Networks: Preparation, Thermal, Mechanical, And Physical Properties. *Journal of Polymer Science Part A: Polymer Chemistry* **2007,** *45* (22), 5103-5111.

115. Dealy, J.; Plazek, D., Temperature-Time Superposition - A User Guide. *Rheology Bulletin* **2009,** *78* (2), 16 - 31.

116. Malkin, A. Y.; Isayev, A. I., *Rheology - Concepts, Methods, & Applications*. ChemTec Publishing: Toronto, 2006.

117. Williams, M. L.; Landel, R. F.; Ferry, J. D., The Temperature Dependence of Relaxation Mechanisms in Amorphous Polymers and Other Glass-forming Liquids. *Journal of the American Chemical Society* **1955,** *77* (14), 3701-3707.

118. Flory, P. J., *Principles of Polymer Chemistry*. Cornell University Press: Ithaca, NY, 1953.

119. Hale, A.; Macosko, C. W.; Bair, H. E., Glass Transition Temperature as A Function of Conversion in Thermosetting Polymers. *Macromolecules* **1991,** *24* (9), 2610-2621.

120. Simon, S. L.; McKenna, G. B.; Sindt, O., Modeling The Evolution of the Dynamic Mechanical Properties of a Commercial Epoxy During Cure After Gelation. *Journal of Applied Polymer Science* **2000,** *76* (4), 495-508.

121. Kannurpatti, A. R.; Anseth, J. W.; Bowman, C. N., A Study of the Evolution of Mechanical Properties and Structural Heterogeneity of Polymer Networks Formed by Photopolymerizations of Multifunctional (Meth)Acrylates. *Polymer* **1998,** *39* (12), 2507-2513.

122. Senyurt, A. F.; Wei, H.; Hoyle, C. E.; Piland, S. G.; Gould, T. E., Ternary Thiol−Ene/Acrylate Photopolymers: Effect of Acrylate Structure on Mechanical Properties. *Macromolecules* **2007,** *40* (14), 4901-4909.

123. Shibayama, M., Spatial Inhomogeneity and Dynamic Fluctuations of Polymer Gels. *Macromolecular Chemistry and Physics* **1998,** *199* (1), 1-30.

124. Kannurpatti, A. R.; Anderson, K. J.; Anseth, J. W.; Bowman, C. N., Use of "Living" Radical Polymerizations to Study the Structural Evolution and Properties of Highly Crosslinked Polymer Networks. *Journal of Polymer Science Part B: Polymer Physics* **1997,** *35* (14), 2297-2307.

125. Ikeda, Y.; Higashitani, N.; Hijikata, K.; Kokubo, Y.; Morita, Y.; Shibayama, M.; Osaka, N.; Suzuki, T.; Endo, H.; Kohjiya, S., Vulcanization: New Focus on a Traditional Technology by Small-Angle Neutron Scattering. *Macromolecules* **2009,** *42* (7), 2741-2748.

126. Hamed, G. R., Materials and Compounds. In *Engineering with Rubber (Third Edition)*, Gent, A. N., Ed. Hanser: 2012; pp 11-36.

127. Coran, A. Y., 7 - Vulcanization. In *Science and Technology of Rubber (Second Edition)*, Eirich, J. E. M. E. R., Ed. Academic Press: San Diego, 1994; pp 339-385.

128. Caruso, M. M.; Davis, D. A.; Shen, Q.; Odom, S. A.; Sottos, N. R.; White, S. R.; Moore, J. S., Mechanically-Induced Chemical Changes in Polymeric Materials. *Chemical Reviews* **2009,** *109* (11), 5755-5798.

129. Zhurkov, S. N.; Korsukov, V. E., Atomic Mechanism of Fracture of Solid Polymers. *Journal of Polymer Science: Polymer Physics Edition* **1974,** *12* (2), 385-398.

130. Beyer, M. K.; Clausen-Schaumann, H., Mechanochemistry: The Mechanical Activation of Covalent Bonds. *Chemical Reviews* **2005,** *105* (8), 2921-2948.

131. Hild, G., Model Networks Based On `Endlinking' Processes: Synthesis, Structure and Properties. *Progress in Polymer Science* **1998,** *23* (6), 1019-1149.

132. Schlogl, S.; Trutschel, M. L.; Chasse, W.; Riess, G.; Saalwachter, K., Entanglement Effects in Elastomers: Macroscopic vs Microscopic Properties. *Macromolecules* **2014,** *47* (9), 2759-2773.

133. Mooney, M., A Theory of Large Elastic Deformation. *Journal of Applied Physics* **1940,** *11* (9), 582-592.

134. Rivlin, R. S., The Elasticity of Rubber. *Rubber Chemistry and Technology* **1992,** *65* (3), 51-66.

135. Wu, P. D.; Van Der Giessen, E., On Improved Network Models for Rubber Elasticity and Their Applications to Orientation Hardening in Glassy Polymers. *Journal of the Mechanics and Physics of Solids* **1993,** *41* (3), 427-456.

136. Mark, J. E., The Constants 2C1 and 2C2 in Phenomeno-Logical Elasticity Theory and Their Dependence on Experimental Variables. *Rubber Chemistry and Technology* **1975,** *48* (3), 495-512.

137. Akagi, Y.; Katashima, T.; Katsumoto, Y.; Fujii, K.; Matsunaga, T.; Chung, U.-i.; Shibayama, M.; Sakai, T., Examination of the Theories of Rubber Elasticity Using an Ideal Polymer Network. *Macromolecules* **2011,** *44* (14), 5817-5821.

138. Oshima, K.; Fujimoto, T.; Minami, E.; Mitsukami, Y., Model Polyelectrolyte Gels Synthesized by End-Linking of Tetra-Arm Polymers with Click Chemistry: Synthesis and Mechanical Properties. *Macromolecules* **2014,** *47* (21), 7573-7580.

139. Rubinstein, M.; Panyukov, S., Nonaffine Deformation and Elasticity of Polymer Networks. *Macromolecules* **1997,** *30* (25), 8036-8044.

140. Rubinstein, M.; Panyukov, S., Elasticity of Polymer Networks. *Macromolecules* **2002,** *35* (17), 6670-6686.

141. Edwards, S. F., Statistical Mechanics of Polymerized Material. *Proceedings of the Physical Society of London* **1967,** *92* (575P), 9-16.

142. Mark, J. E.; Tang, M. Y., Dependence of The Elastomeric Properties of Bimodal Networks On the Lengths and Amounts of the Short Chains. *Journal of Polymer Science: Polymer Physics Edition* **1984,** *22* (11), 1849-1855.

143. Trabelsi, S.; Albouy, P. A.; Rault, J., Crystallization and Melting Processes in Vulcanized Stretched Natural Rubber. *Macromolecules* **2003,** *36* (20), 7624-7639.

144. Gordon, M., The Physics of Rubber Elasticity (Third Edition). L. R. G. Treloar, Clarendon Press, Oxford. 1975 pp. xii + 370. Price: £14.00. *British Polymer Journal* **1976,** *8* (1), 39-39.

145. Zhou, H.; Woo, J.; Cok, A. M.; Wang, M.; Olsen, B. D.; Johnson, J. A., Counting Primary Loops in Polymer Gels. *Proceedings of the National Academy of Sciences* **2012,** *109* (47), 19119-19124.

146. Wang, R.; Alexander-Katz, A.; Johnson, J. A.; Olsen, B. D., Universal Cyclic Topology in Polymer Networks. *Physical Review Letters* **2016,** *116* (18), 188302.

147. Kawamoto, K.; Zhong, M.; Wang, R.; Olsen, B. D.; Johnson, J. A., Loops versus Branch Functionality in Model Click Hydrogels. *Macromolecules* **2015,** *48* (24), 8980-8988.

148. NREL, Large-Scale Offshore Wind Power in the United States. **2010**.

149. Hayman, B.; Wedel-Heinen, J.; Brondsted, P., Materials Challenges in Present And Future Wind Energy. *Mrs Bulletin* **2008,** *33* (4), 343-353.

150. Biermann, U.; Bornscheuer, U.; Meier, M. A. R.; Metzger, J. O.; Schäfer, H. J., Oils and Fats as Renewable Raw Materials in Chemistry. *Angewandte Chemie International Edition* **2011,** *50* (17), 3854-3871.

151. Xia, Y.; Larock, R. C., Vegetable Oil-Based Polymeric Materials: Synthesis, Properties, And Applications. *Green Chemistry* **2010,** *12* (11), 1893-1909.

152. Galia, M.; de Espinosa, L. M.; Ronda, J. C.; Lligadas, G.; Cadiz, V., Vegetable Oil-Based Thermosetting Polymers. *European Journal of Lipid Science and Technology* **2010,** *112* (1), 87-96.

153. Meier, M. A. R.; Metzger, J. O.; Schubert, U. S., Plant Oil Renewable Resources as Green Alternatives In Polymer Science. *Chemical Society Reviews* **2007,** *36*, 1788-1802.

154. Park, S. J.; Jin, F. L.; Lee, J. R., Synthesis and Thermal Properties of Epoxidized Vegetable Oil. *Macromolecular Rapid Communications* **2004,** *25* (6), 724-727.

155. Ionescu, M.; Petrovic, Z. S.; Wan, X. M., Ethoxylated Soybean Polyols for Polyurethanes. *J. Polym. Environ.* **2010,** *18* (1), 1-7.

156. Sen, S.; Cayli, G., Synthesis of Bio-Based Polymeric Nanocomposites from Acrylated Epoxidized Soybean Oil and Montmorillonite Clay in The Presence of a Bio-Based Intercalant. *Polym. Int.* **2010,** *59* (8), 1122-1129.

157. David, S. B.; Sathiyalekshmi, K.; Raj, G. A. G., Studies On Acrylated Epoxydised Triglyceride Resin-Co-Butyl Methacrylate Towards the Development of Biodegradable Pressure Sensitive Adhesives. *J. Mater. Sci.-Mater. Med.* **2009,** *20*, 61-70.

158. La Scala, J.; Wool, R. P., Property Analysis of Triglyceride-Based Thermosets. *Polymer* **2005,** *46* (1), 61-69.

159. Odegard, G. M.; Bandyopadhyay, A., Physical Aging of Epoxy Polymers and Their Composites. *Journal of Polymer Science Part B: Polymer Physics* **2011,** *49* (24), 1695-1716.

160. Gupta, A. P.; Ahmad, S.; Dev, A., Development of Novel Bio-Based Soybean Oil Epoxy Resins as a Function of Hardener Stoichiometry. *Polym.-Plast. Technol. Eng.* **2010,** *49* (7), 657-661.

161. Mertzel, E.; Koenig, J. L., Application of FT-IR and NMR to Epoxy Resins. In *Epoxy Resins and Composites II*, Dušek, K., Ed. Springer Berlin Heidelberg: 1986; pp 73-112.

162. Silverstein, R. M.; Webster, F. X., *Spectrometric Identification of Organic Compounds*. 6th ed.; John Wiley & Sons, Inc.: New York, 1998.

163. González, M. G.; Cabanelas, J. C.; Baselga, J., Applications of FTIR on Epoxy Resins – Identification, Monitoring the Curing Process, Phase Separation and Water Uptake. In

Infrared Spectroscopy - Materials Science, Engineering and Technology, Theophile, T., Ed. InTech: Spain, 2012.

164. Nikolic, G.; Zlatkovic, S.; Cakic, M.; Cakic, S.; Lacnjevac, C.; Rajic, Z., Fast Fourier transform IR characterization of epoxy GY systems crosslinked with aliphatic and cycloaliphatic EH polyamine adducts. *Sensors* **2010,** *10* (1), 684-96.

165. Pečar, D.; Goršek, A., Alkaline Hydrolysis of an Aromatic Ester: Kinetic Studies Using Thermal Power Profiles. *Chemical Engineering & Technology* **2011,** *34* (12), 2033-2036.

166. HOSLEK, P.; Hook, M., Kinetic Study of the Salicylic Acid Fermentation. *Biotechnology_and_Bioengineering* **1963,** *V*, 243-251.

167. Barker, J. L.; Frost, J. W., Microbial Synthesis of p-HydroxybenzoicAcid from Glucose. *Biotechnology_and_Bioengineering* **2001,** *76*, 376-390.

Appendix A. 2D NMR Spectra

Section 1: NMR Characterization of Allyl (2-allyloxy)benzoate

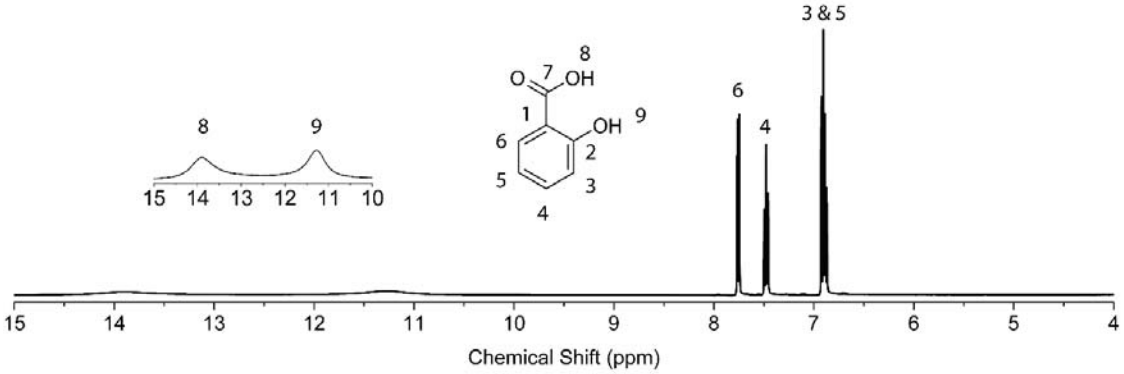

Figure S1a: Chemical structure of and ^{1}H NMR data obtained from salicylic acid.

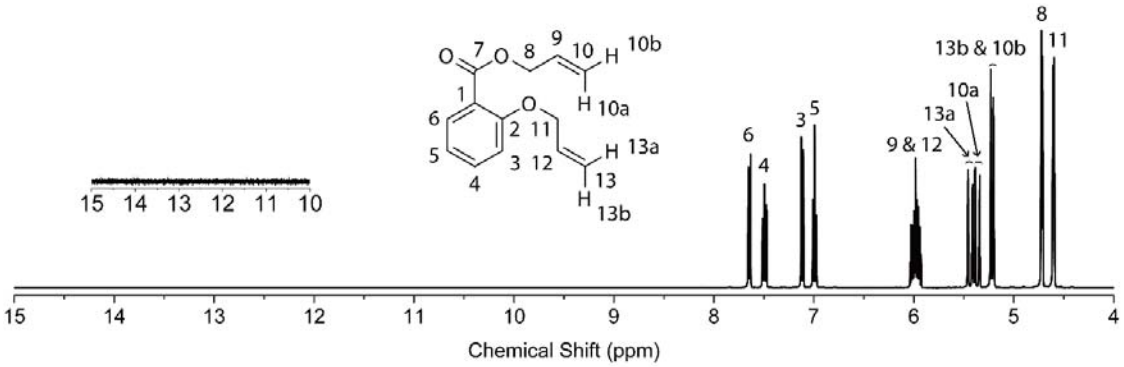

Figure S1b: Chemical structure of and ^{1}H NMR data obtained from allyl (2-allyloxy)benzoate. Data were obtained from final purified product.

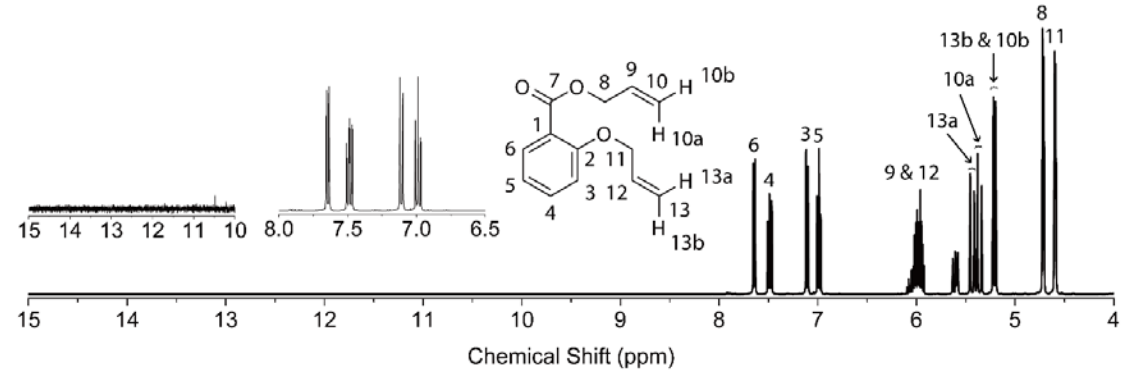

Figure S1c: Chemical structure of and ^{1}H NMR data obtained from allyl (2-allyloxy)benzoate. Data were obtained prior to extraction. Refer to Figure S1d for a closer view.

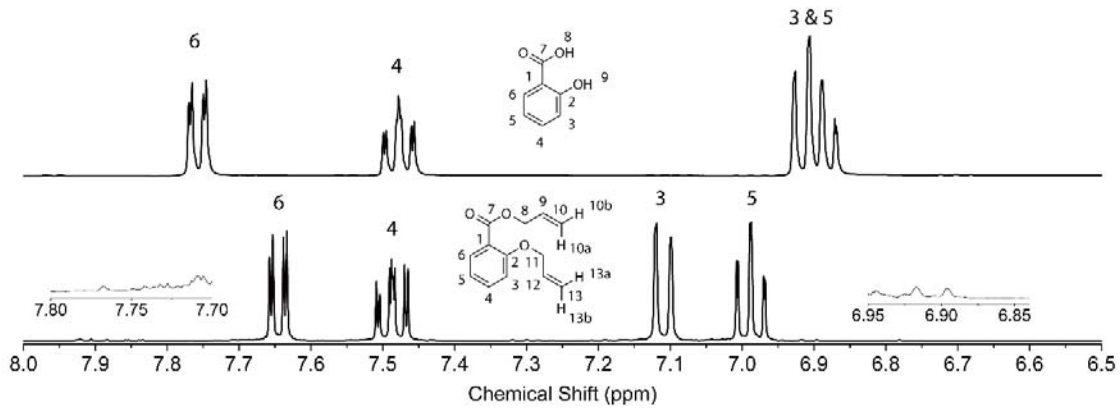

Figure S1d: ^{1}H NMR data obtained from (top) salicylic acid and (bottom) allyl (2-allyloxy)benzoate. The spectrum of allyl (2-allyloxy)benzoate was obtained prior to extraction for the purposes of determining the reaction conversion.

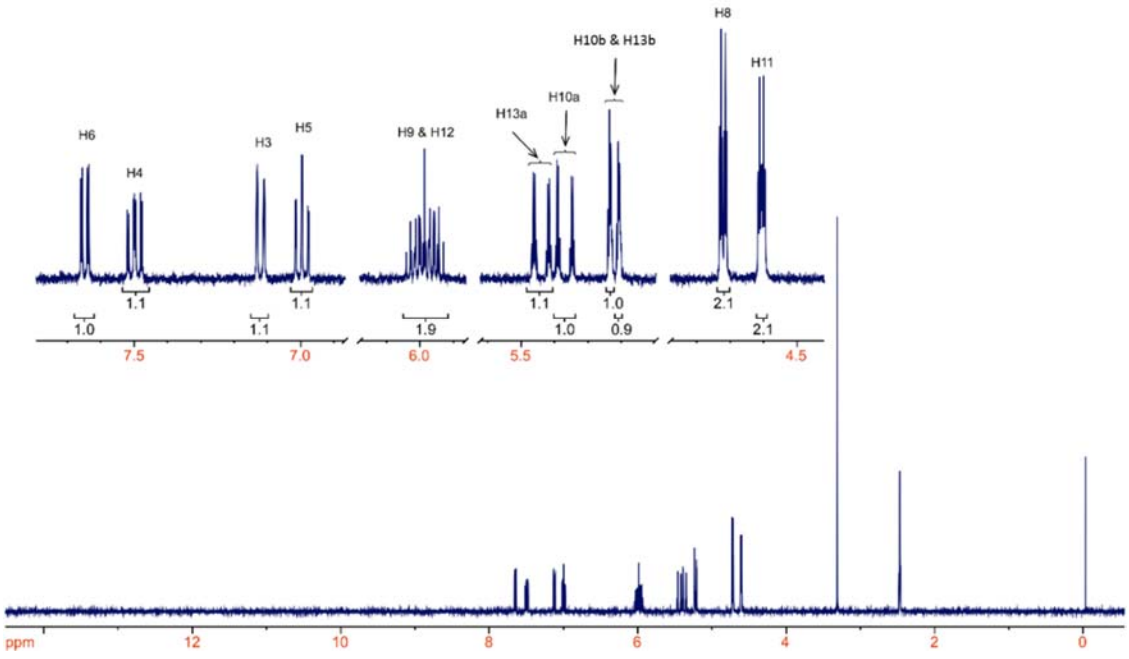

Figure S1e: ^{1}H NMR data obtained from allyl (2-allyloxy)benzoate.

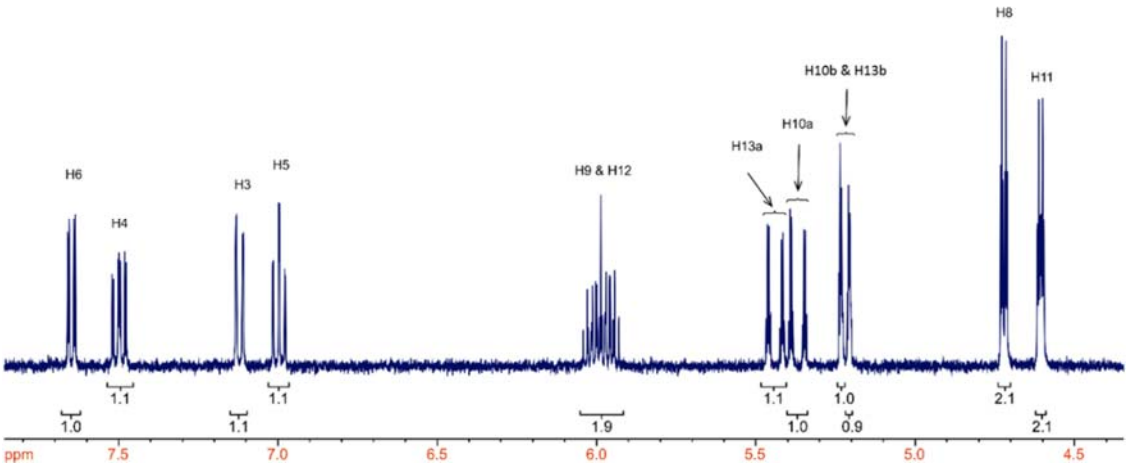

Figure S1f: ^{1}H NMR data obtained from allyl (2-allyloxy)benzoate (closer view).

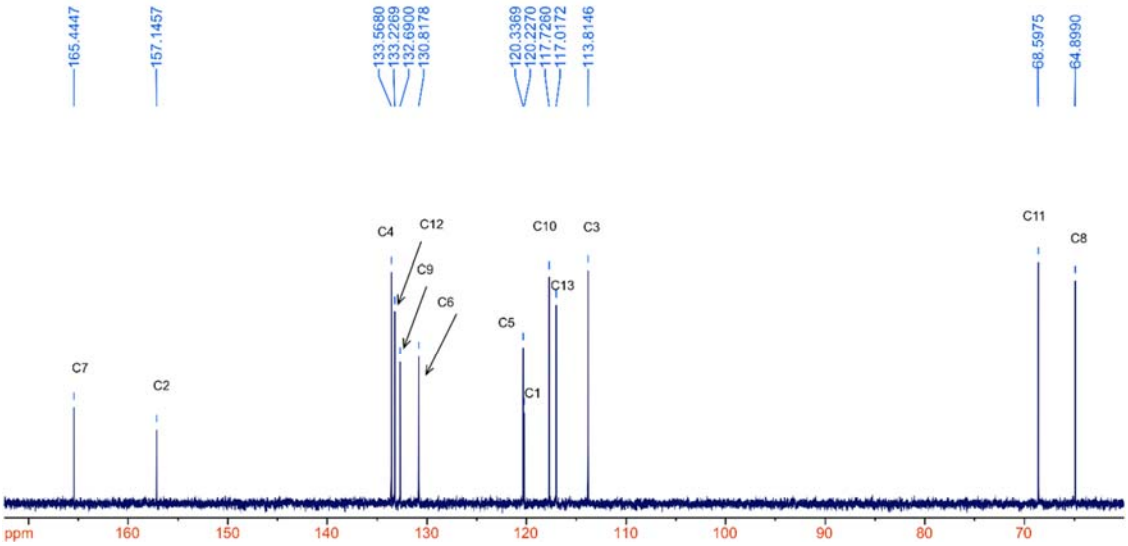

Figure S1g: ^{13}C NMR data obtained from allyl (2-allyloxy)benzoate.

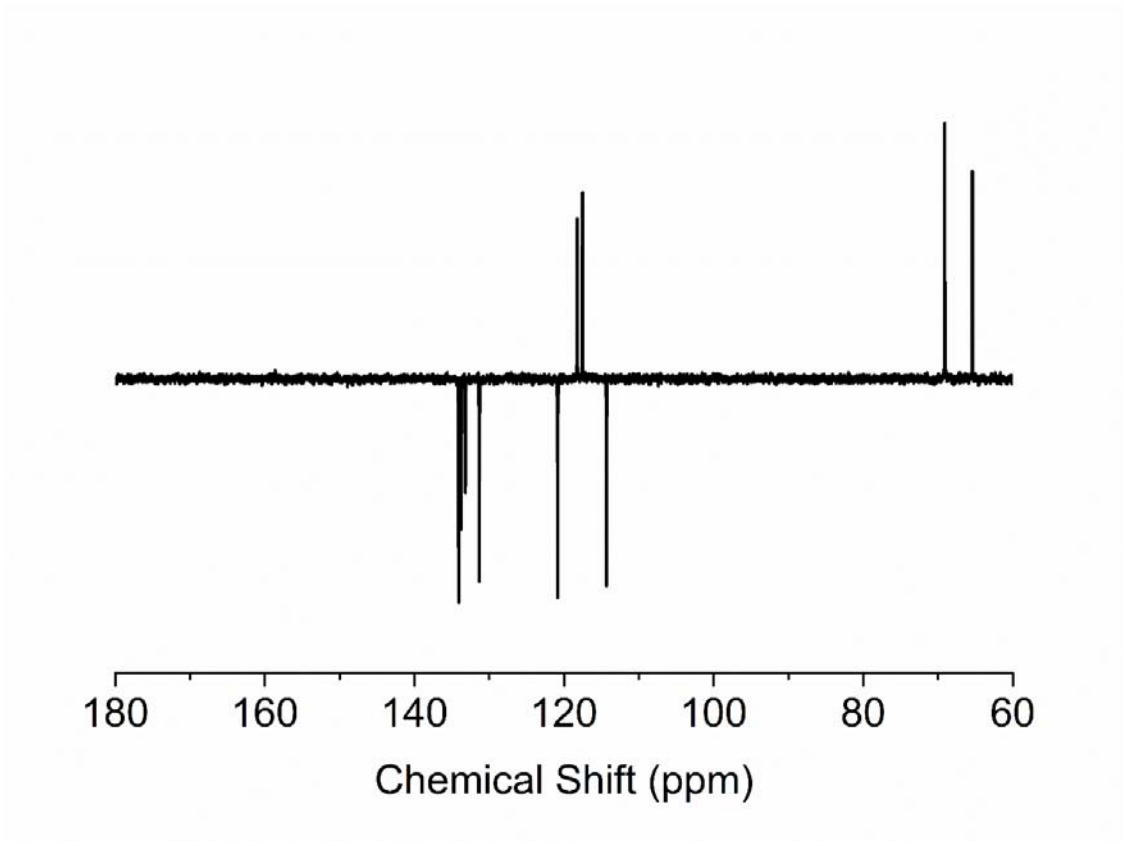

Figure S1h: DEPT 135 data obtained from allyl (2-allyloxy)benzoate.

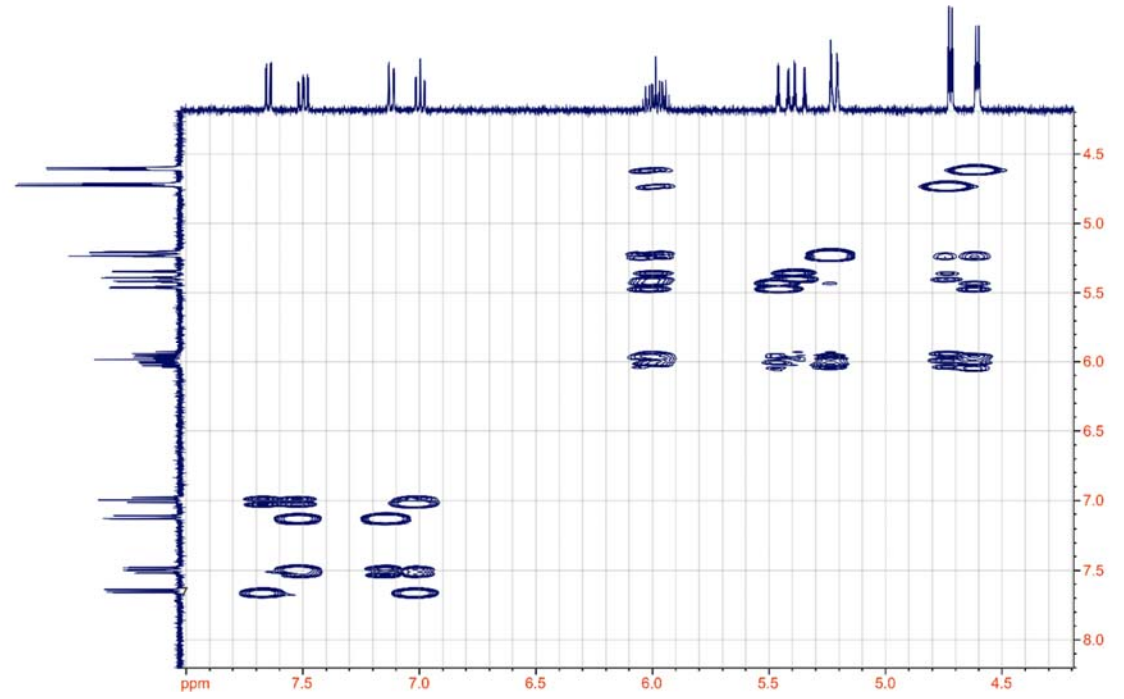

Figure S1i: COSY data obtained from allyl (2-allyloxy)benzoate.

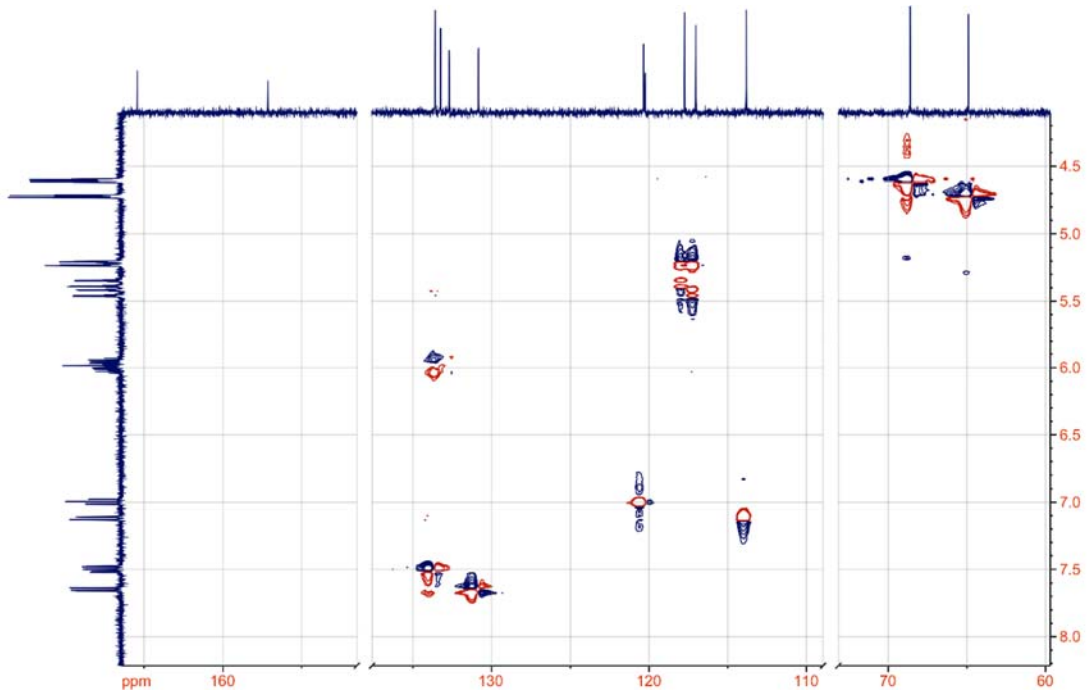

Figure S1j: HSQC data obtained from allyl (2-allyloxy)benzoate.

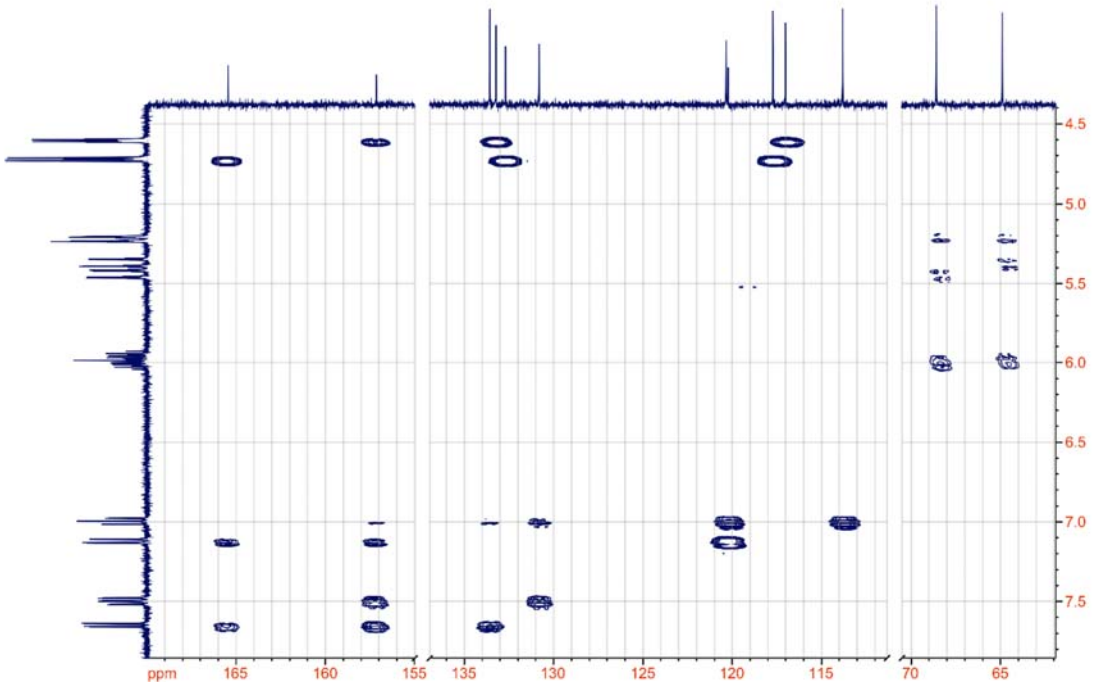

Figure S1k: HMBC data obtained from allyl (2-allyloxy)benzoate.

Section 2: NMR Characterization of Allylated 3-Hydroxybenzoic Acid

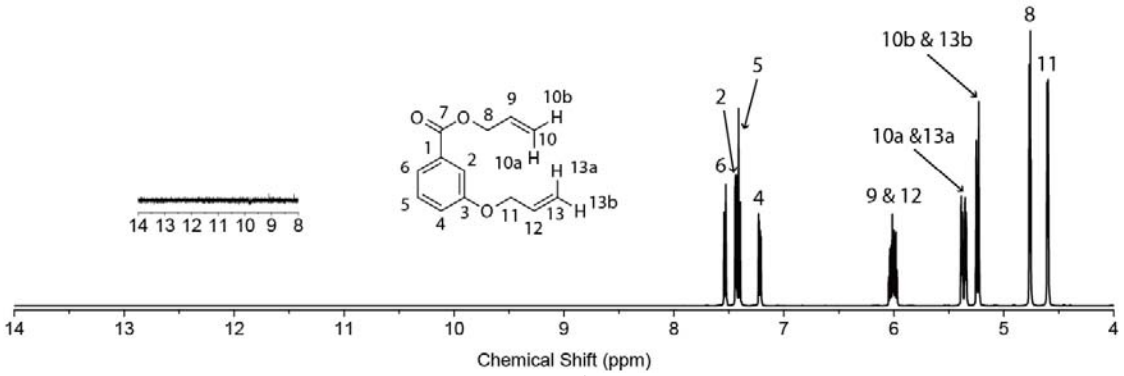

Figure S2a: Chemical structure of and ^{1}H NMR data obtained from allyl 3-allyloxybenzoate. Data were obtained from final purified product.

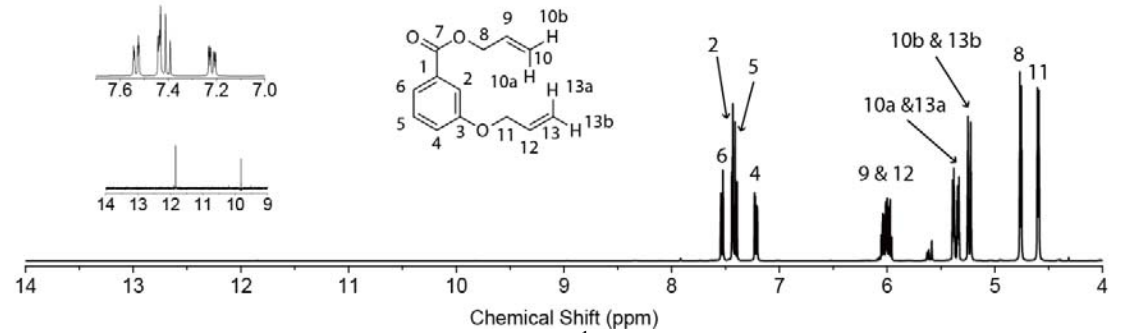

Figure S2b: Chemical structure of and ^{1}H NMR data obtained from allyl 3-allyloxybenzoate. Data were obtained prior to extraction.

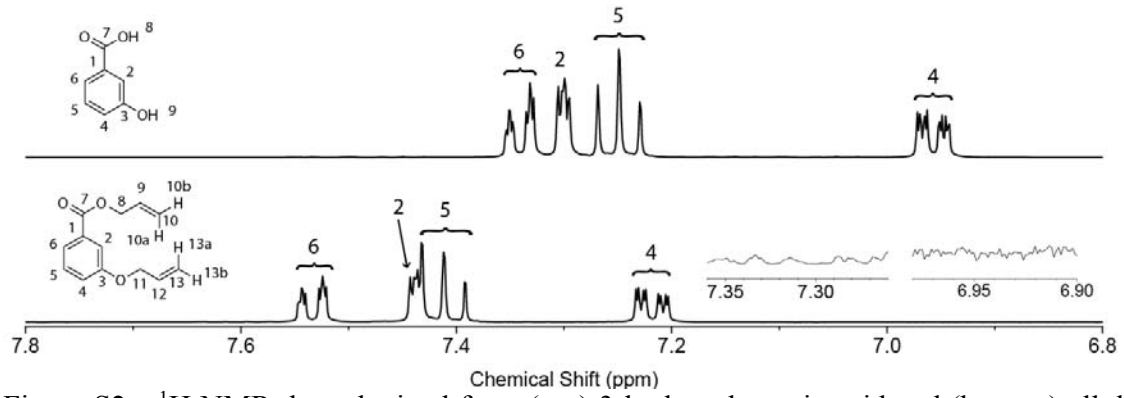

Figure S2c: ^{1}H NMR data obtained from (top) 3-hydroxybenzoic acid and (bottom) allyl 3-allyloxybenzoate. The spectrum of allyl 3-allyloxybenzoate was obtained prior to extraction for the purposes of determining the reaction conversion.

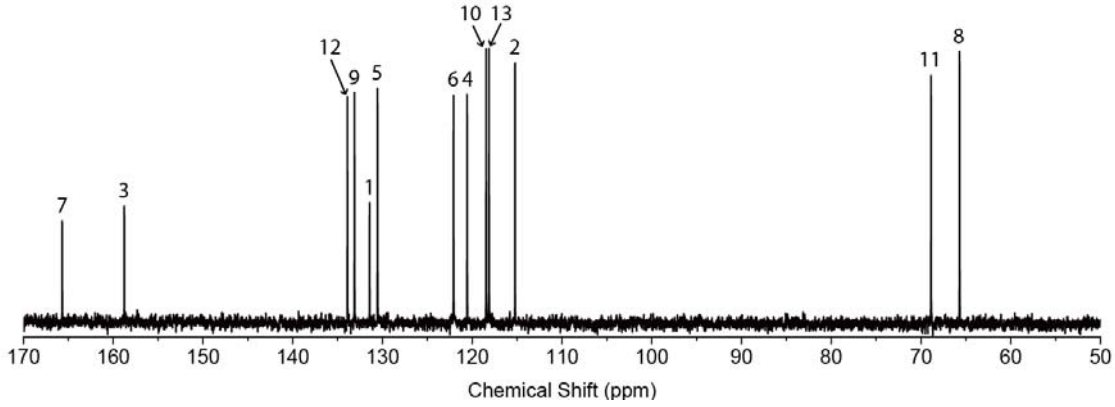

Figure S2d: ^{13}C NMR data obtained from allyl 3-allyloxybenzoate.

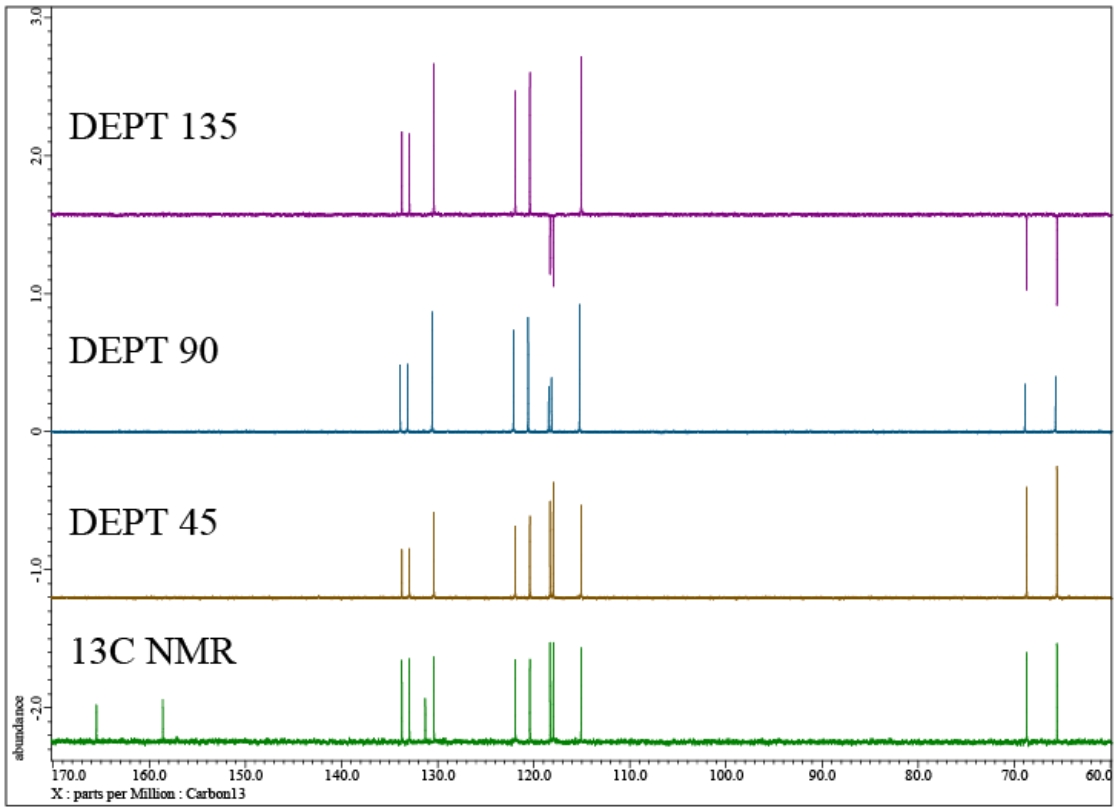

Figure S2e: ^{13}C NMR, DEPT 45, 90, 135 data obtained from allyl 3-allyloxybenzoate

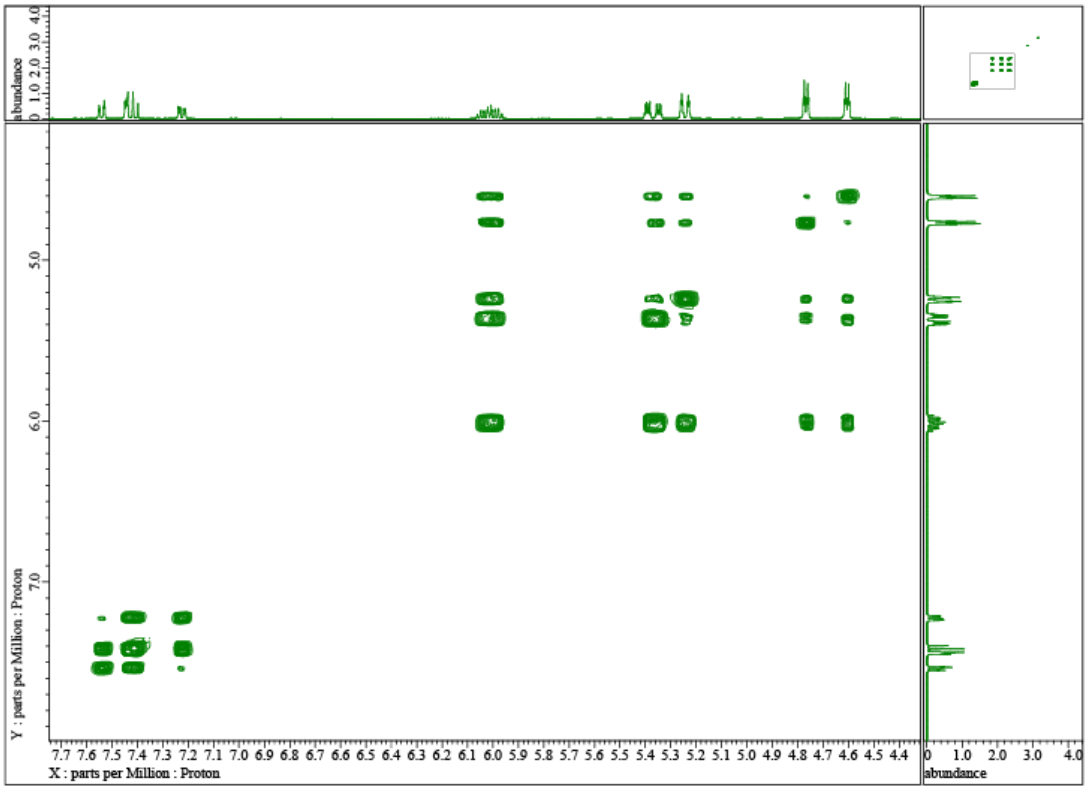

Figure S2f: COSY data obtained from allyl 3-allyloxybenzoate

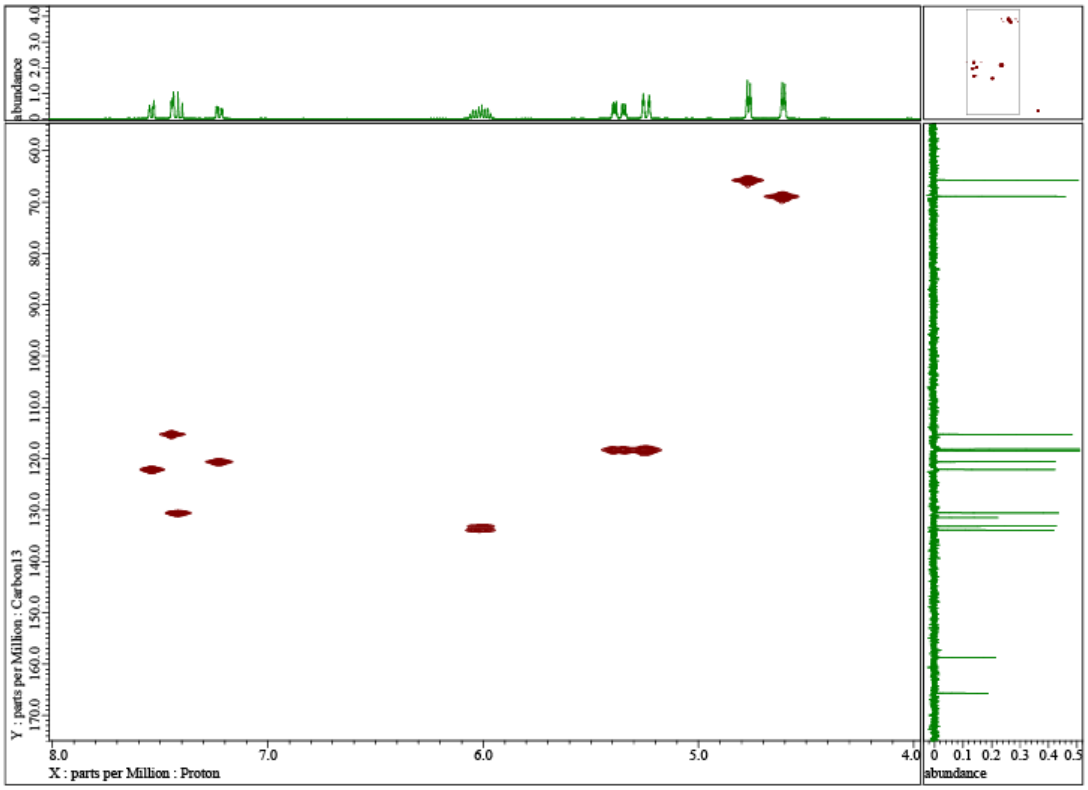

Figure S2g: HSQC data obtained from allyl 3-allyloxybenzoate

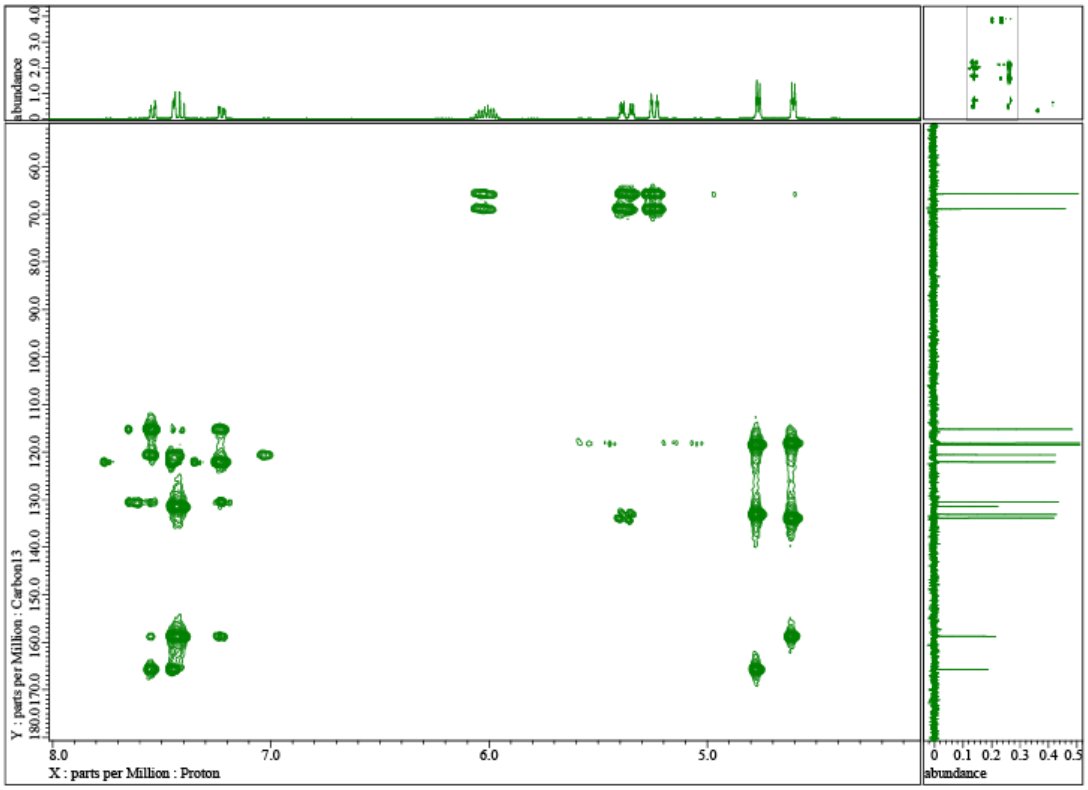

Figure S2h: HMBC data obtained from allyl 3-allyloxybenzoate

Section 3: NMR Characterization of Allyl (4-allyloxy)benzoate

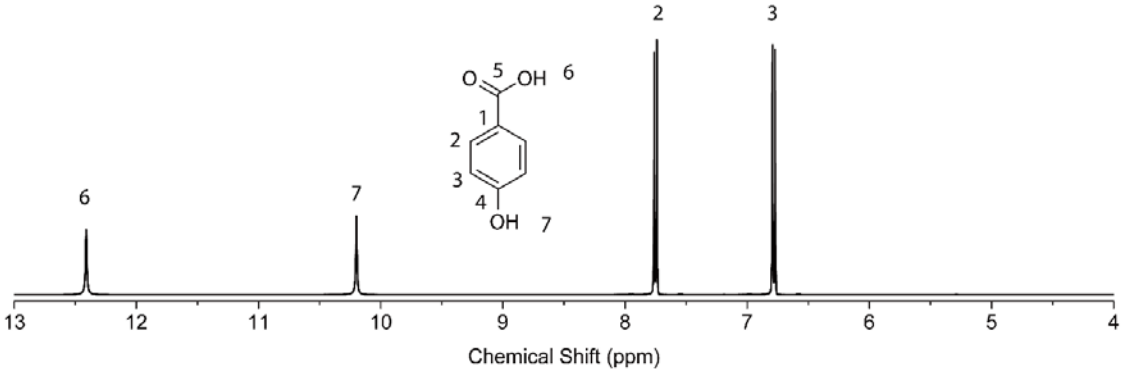

Figure S3a: Chemical structure of and ^{1}H NMR data obtained from 4-hydroxybenzoic acid.

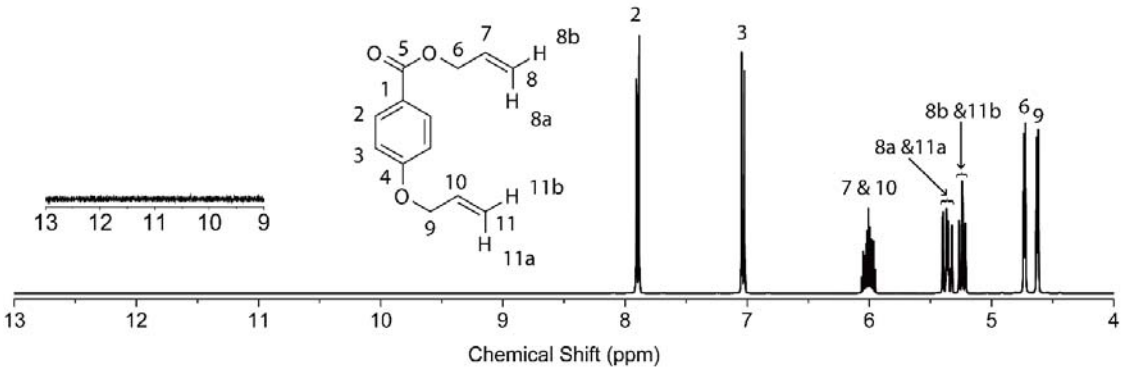

Figure S3b: Chemical structure of and ^{1}H NMR data obtained from allyl (4-allyloxy)benzoate. Data were obtained from final purified product.

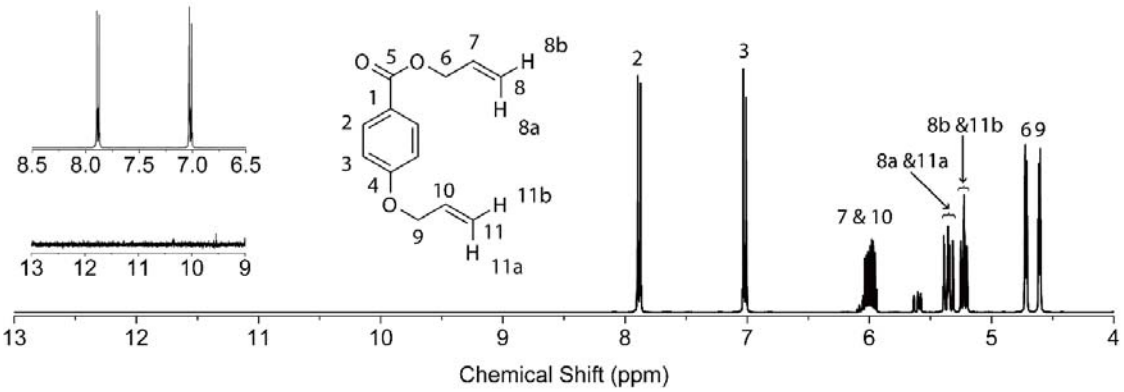

Figure S3c: Chemical structure of and ^{1}H NMR data obtained from allyl (4-allyloxy)benzoate. Data were obtained prior to extraction.

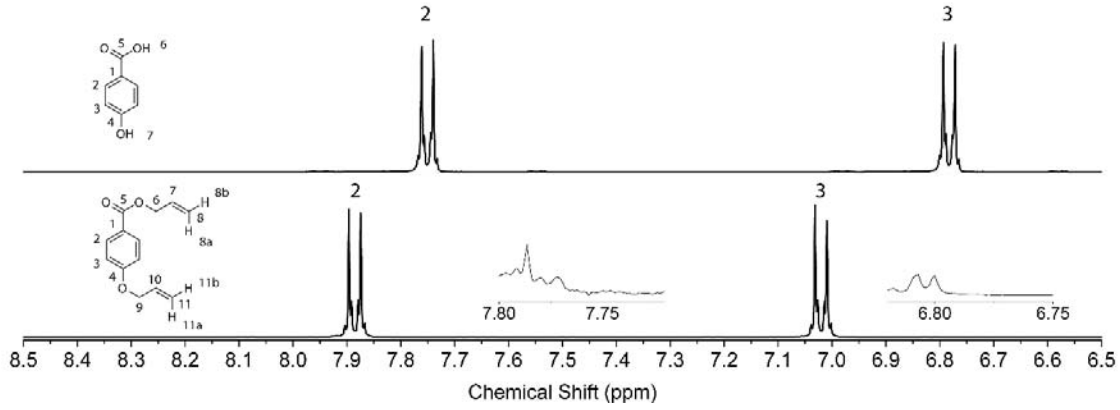

Figure S3d: ^{1}H NMR data obtained from (top) 4-hydroxybenzoic acid and (bottom) allyl (4-allyloxy)benzoate. The spectrum of allyl (4-allyloxy)benzoate was obtained prior to extraction for the purposes of determining the reaction conversion.

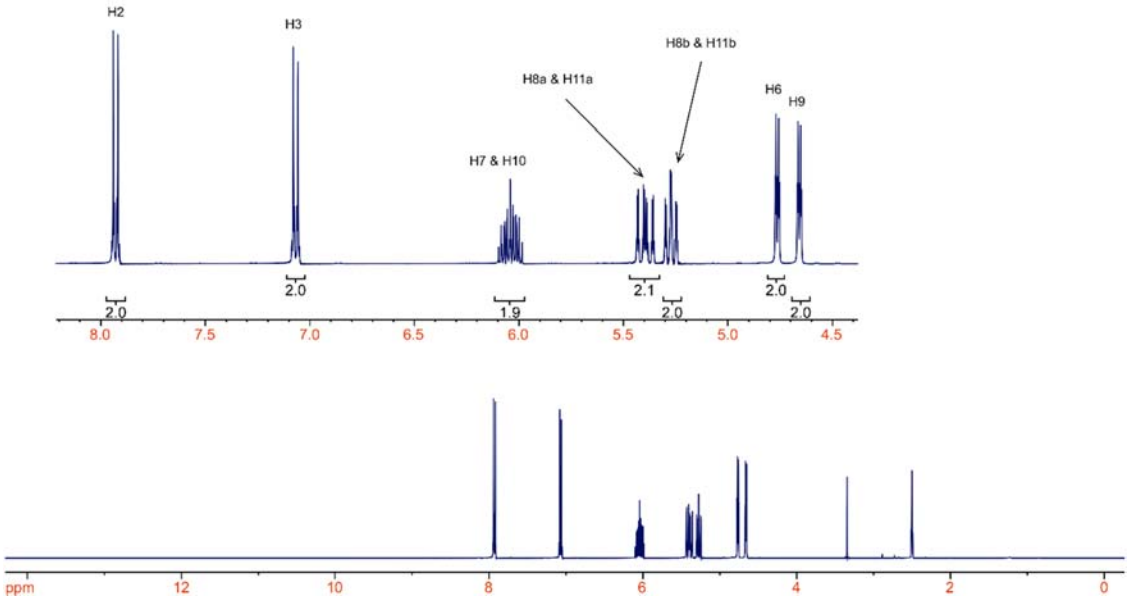

Figure S3e: ^{1}H NMR data obtained from allyl (4-allyloxy)benzoate.

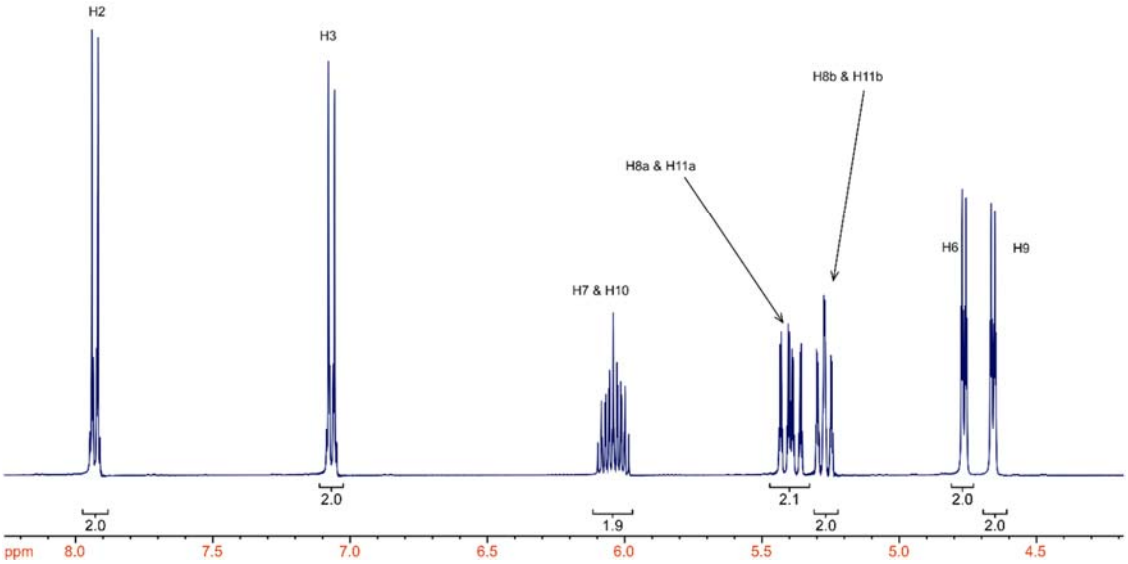

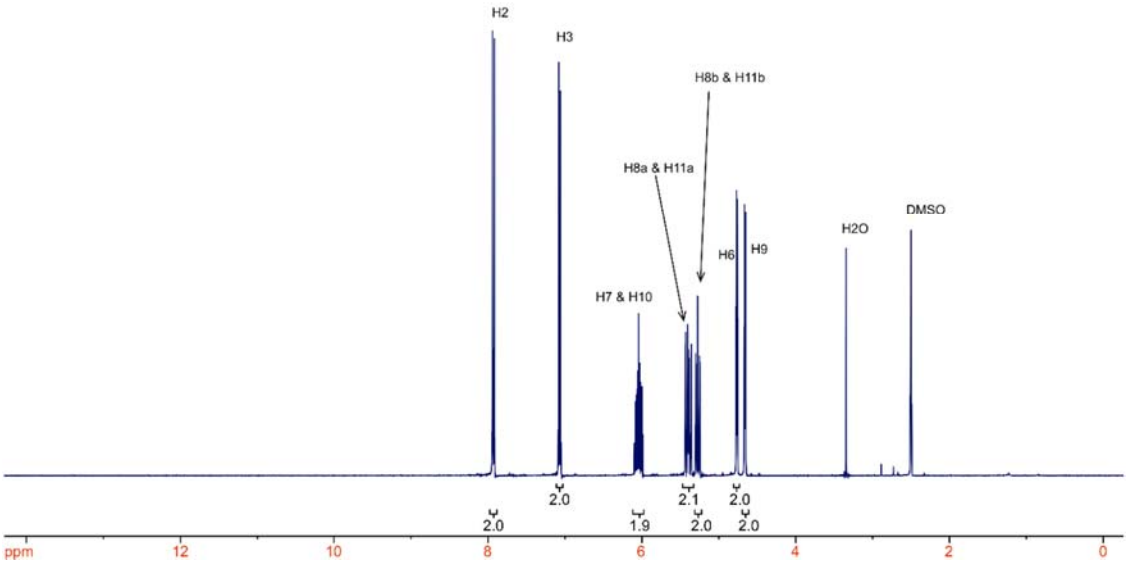

Figure S3f: ^{1}H NMR data obtained from allyl (4-allyloxy)benzoate (closer view).

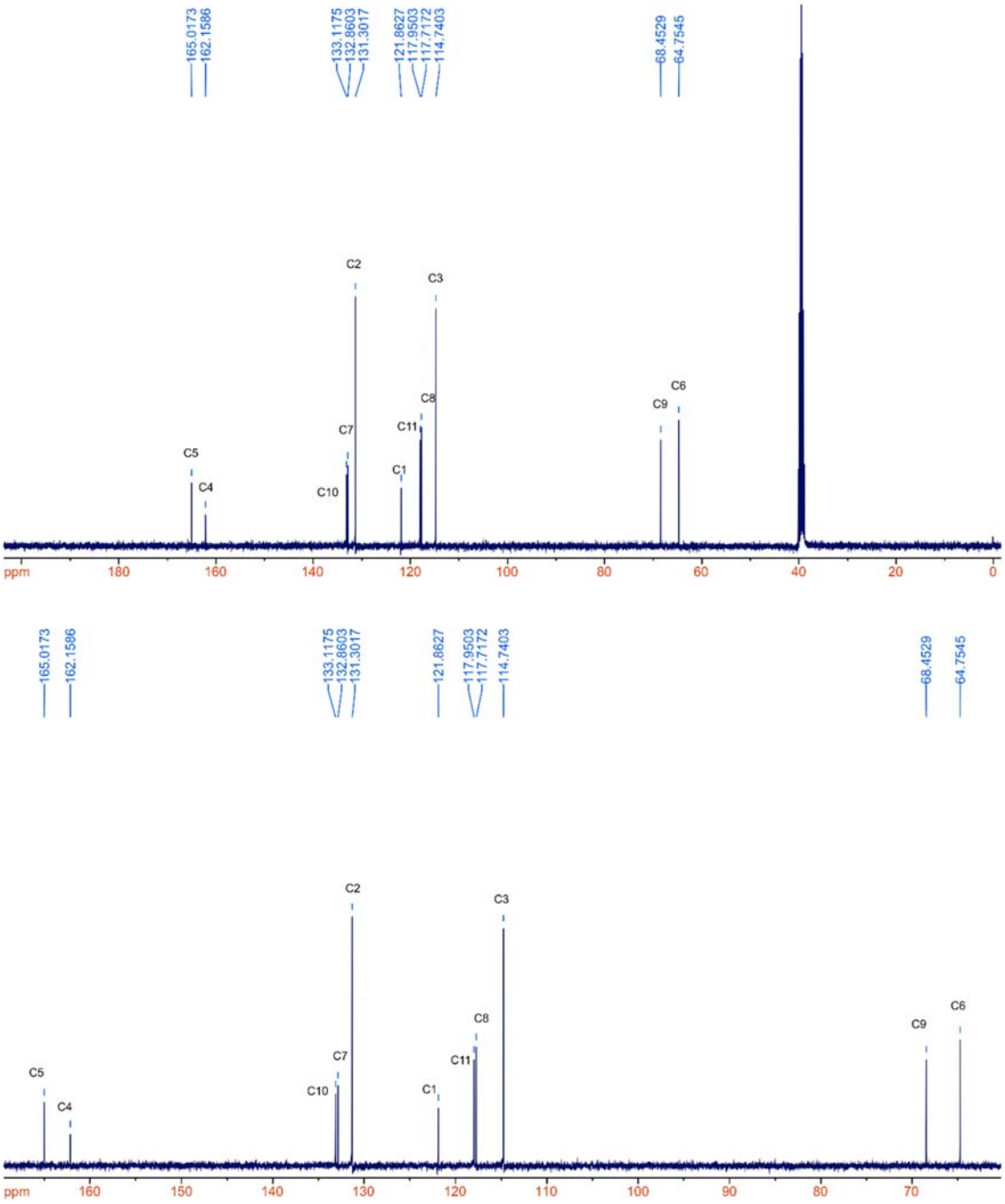

Figure S3g: ^{13}C NMR data obtained from allyl (4-allyloxy)benzoate.

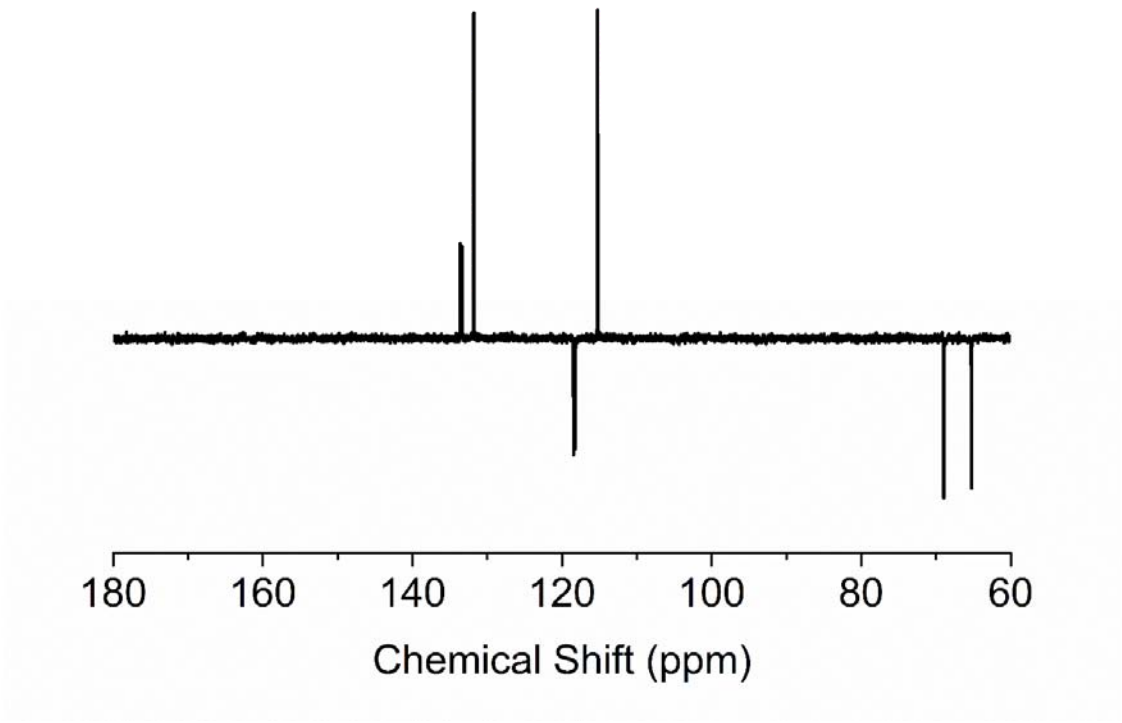

Figure S3h: DEPT 135 data obtained from allyl (4-allyloxy)benzoate.

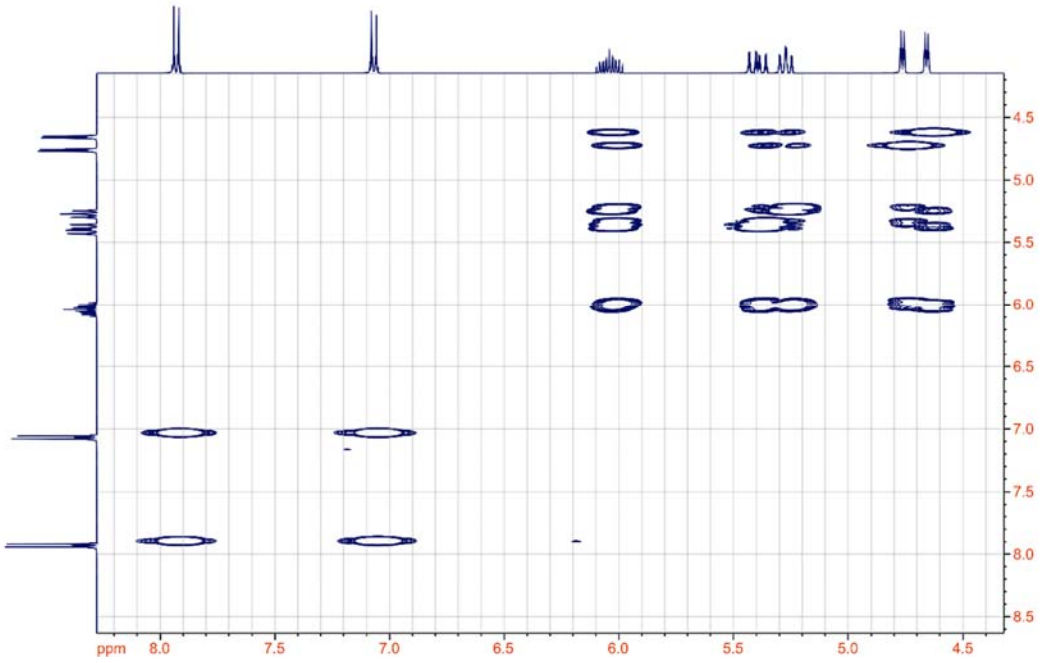

Figure S3i: COSY data obtained from allyl (4-allyloxy)benzoate.

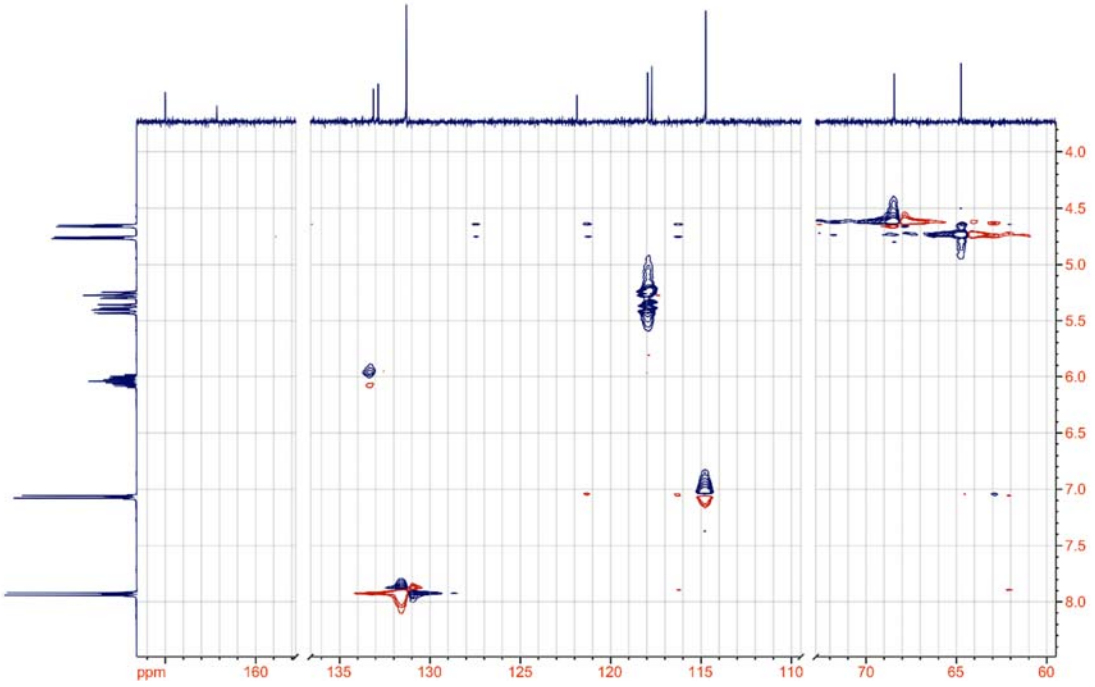

Figure S3j: HSQC data obtained from allyl (4-allyloxy)benzoate.

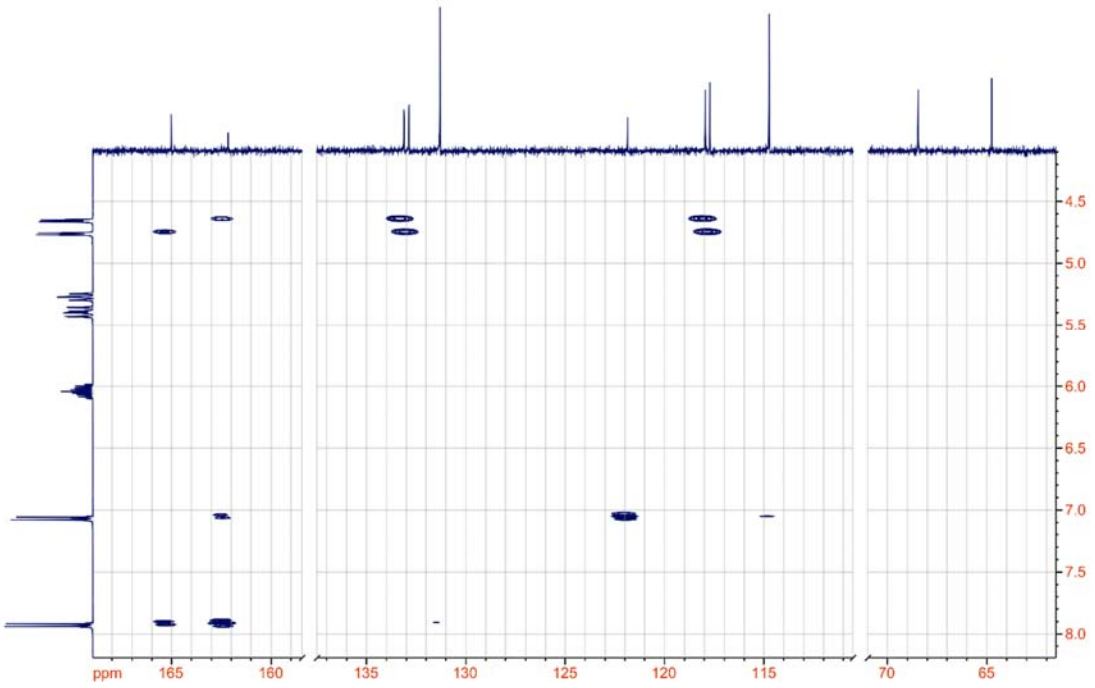

Figure S3k: HMBC data obtained from allyl (4-allyloxy)benzoate.

Section 4: NMR Characterization of Ally 2,5-bis(allyloxy)benzoate

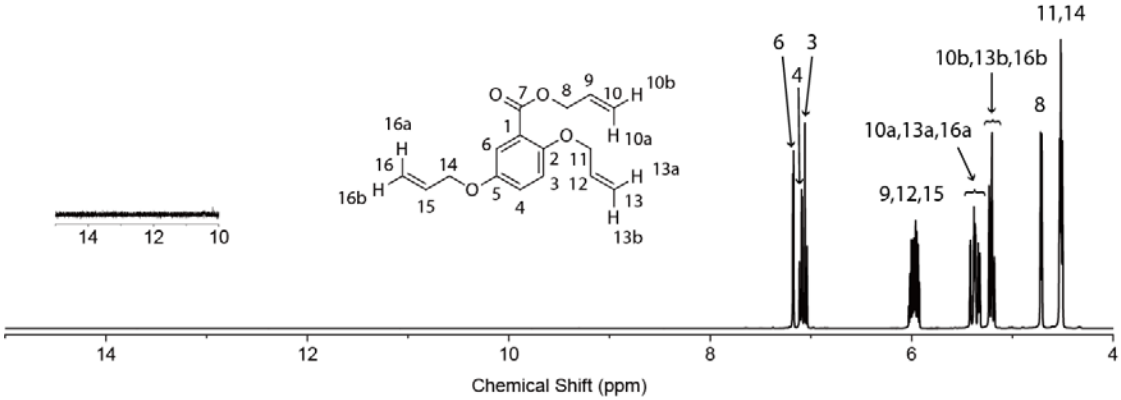

Figure S4a: Chemical structure of and ^{1}H NMR data obtained from allyl 2,5-bis(allyloxy)benzoate. Data were obtained from final purified product.

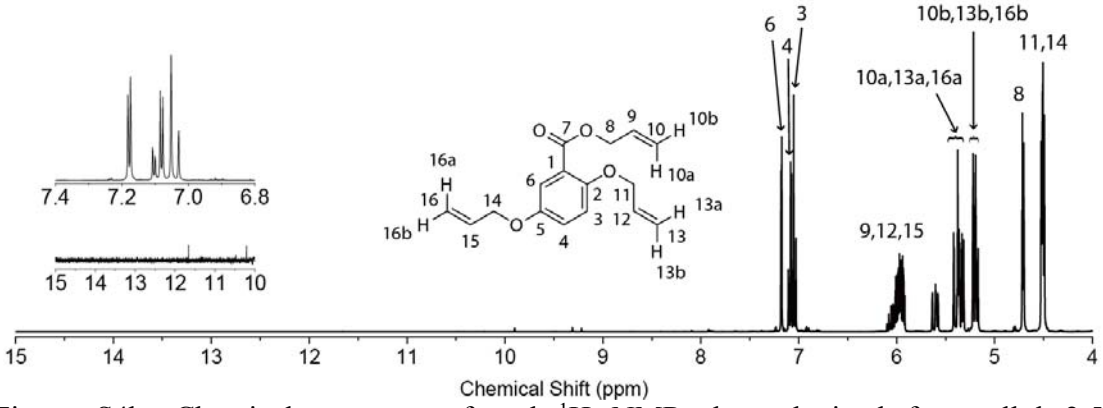

Figure S4b: Chemical structure of and ^{1}H NMR data obtained from allyl 2,5-bis(allyloxy)benzoate. Data were obtained prior to extraction.

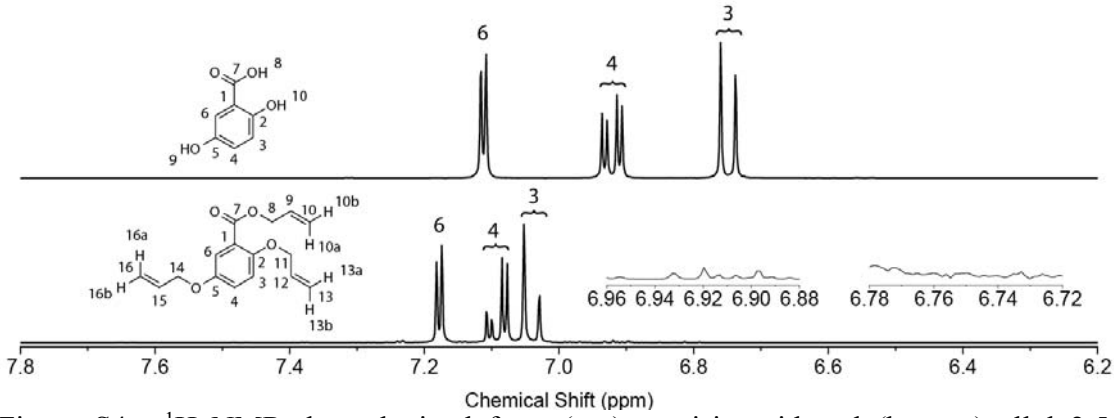

Figure S4c: ^{1}H NMR data obtained from (top) gentisic acid and (bottom) allyl 2,5-bis(allyloxy)benzoate. The spectrum of allyl 2,5-bis(allyloxy)benzoate was obtained prior to extraction for determining the reaction conversion.

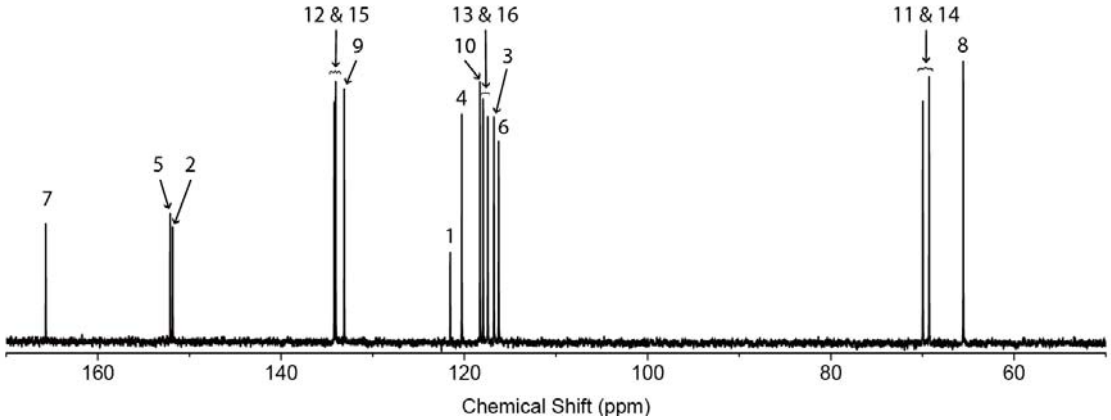

Figure S4d: ^{13}C NMR data obtained from allyl 2,5-bis(allyloxy)benzoate.

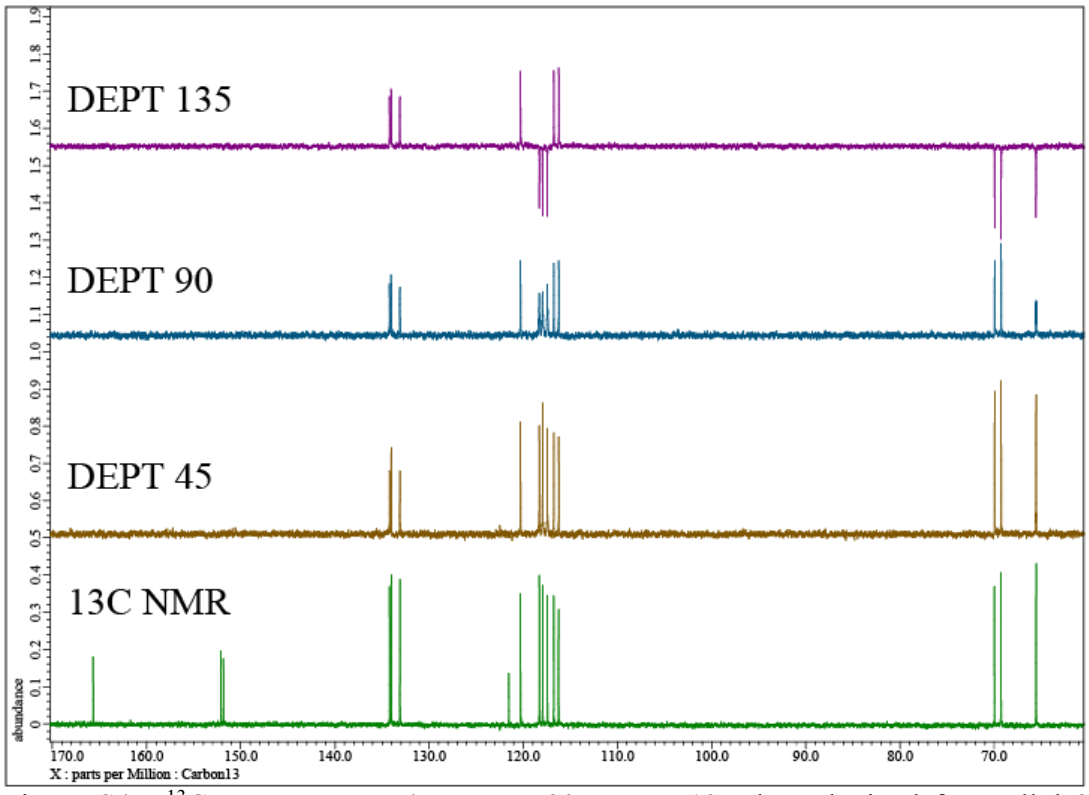

Figure S4e: ^{13}C NMR, DEPT 45, DEPT 90, DEPT 135 data obtained from allyl 2,5-bis(allyloxy)benzoate.

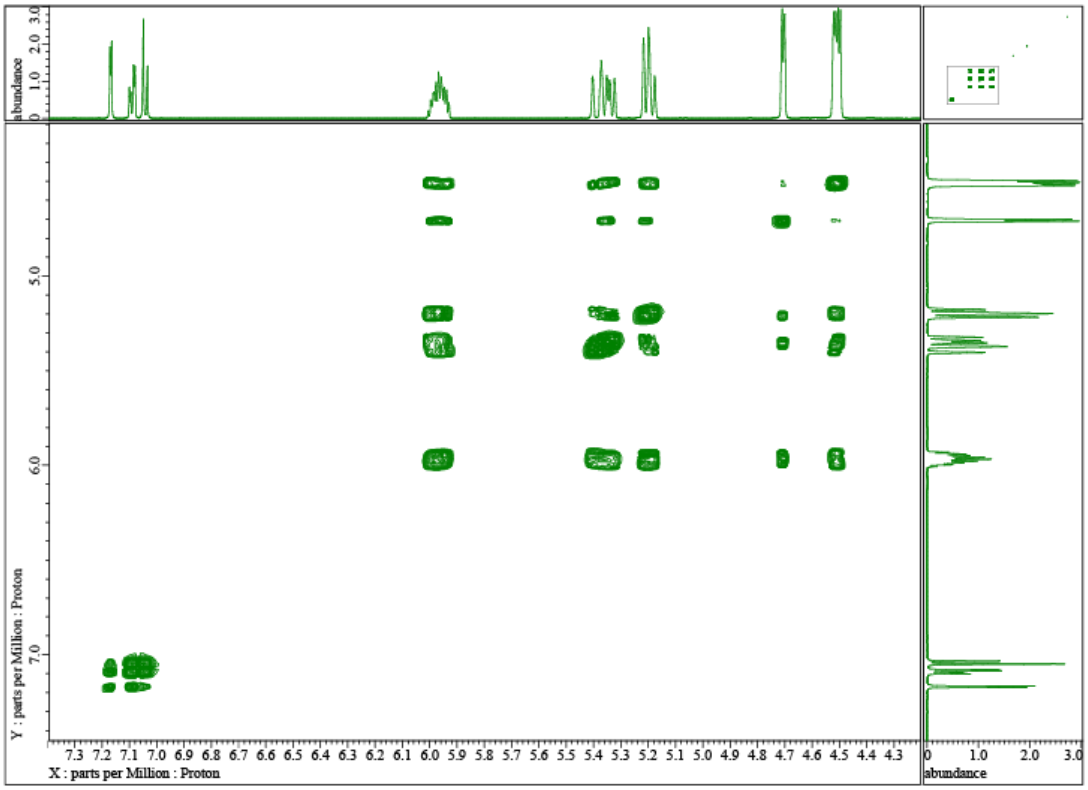

Figure S4f: COSY data obtained from allyl 2,5-bis(allyloxy)benzoate

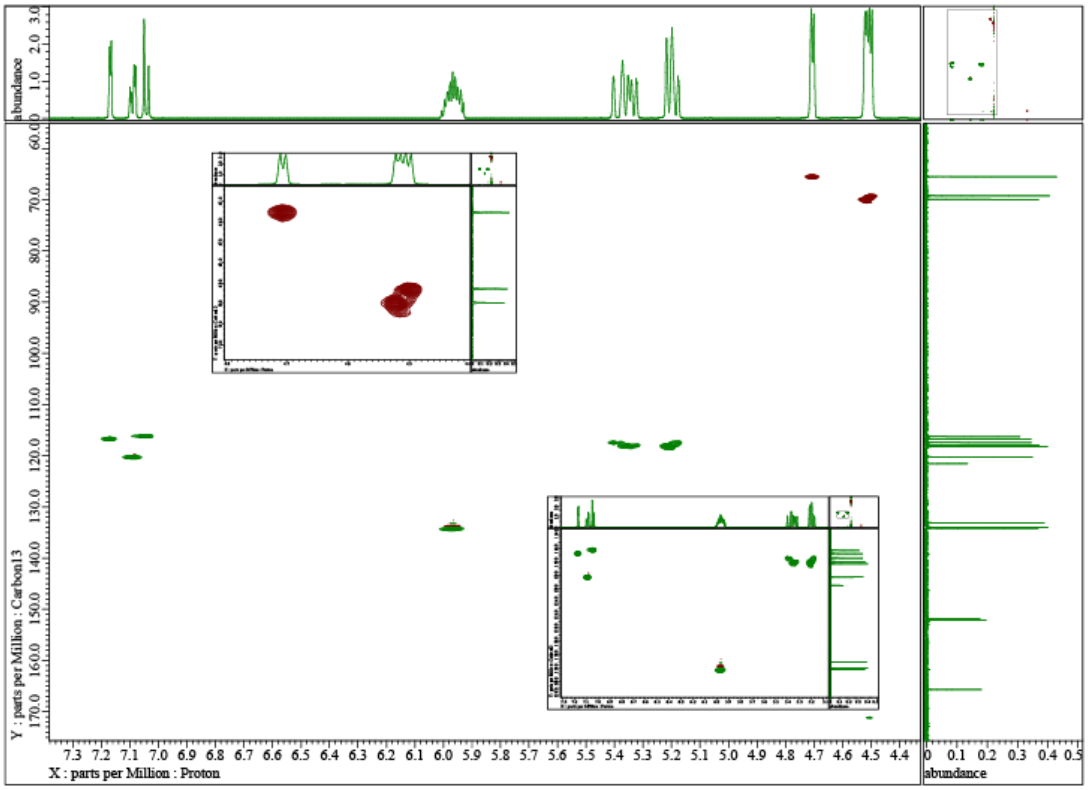

Figure S4g: HSQC data obtained from allyl 2,5-bis(allyloxy)benzoate

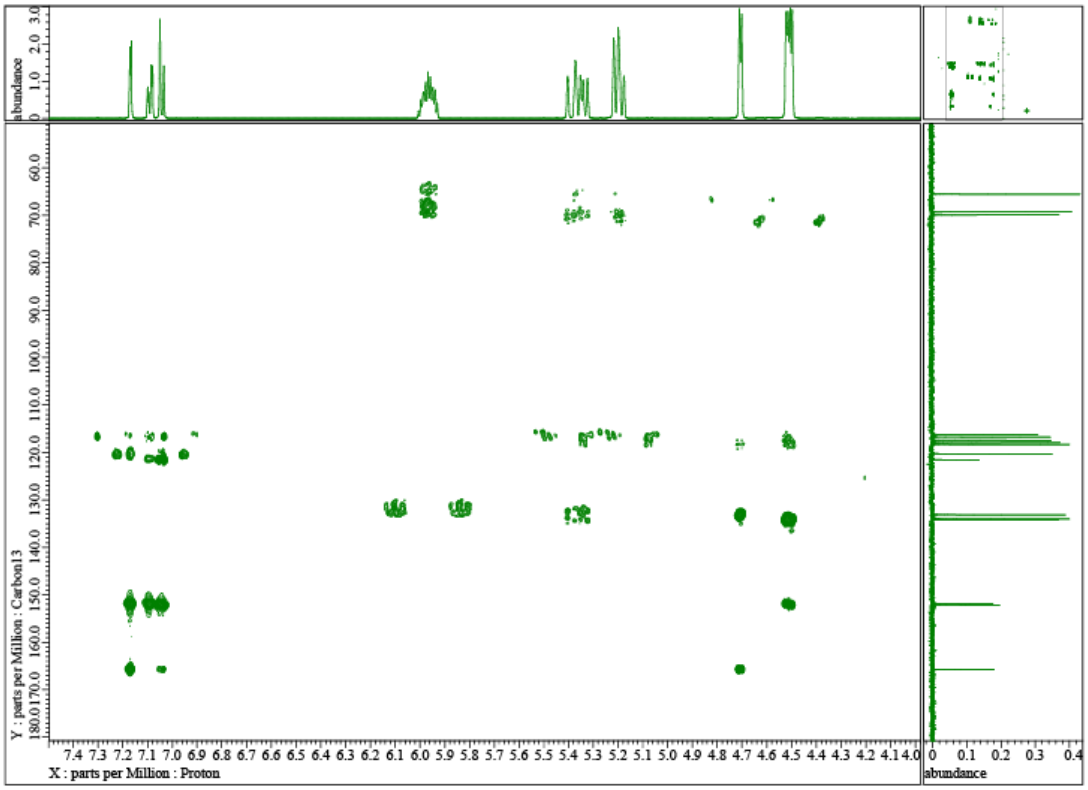

Figure S4h: HMBC data obtained from allyl 2,5-bis(allyloxy)benzoate

Section 5: NMR Characterization of Allyl 3,4,5-tris(allyloxy)benzoate

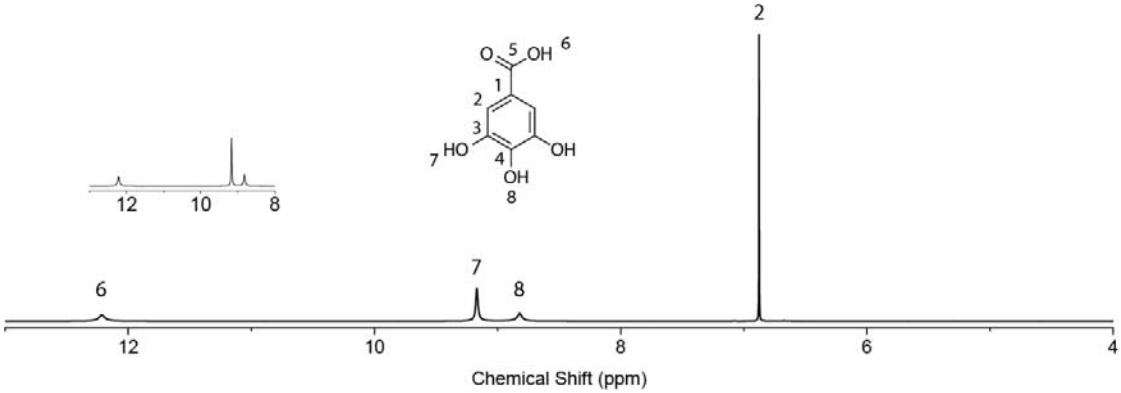

Figure S5a: Chemical structure of and ^{1}H NMR data obtained from gallic acid.

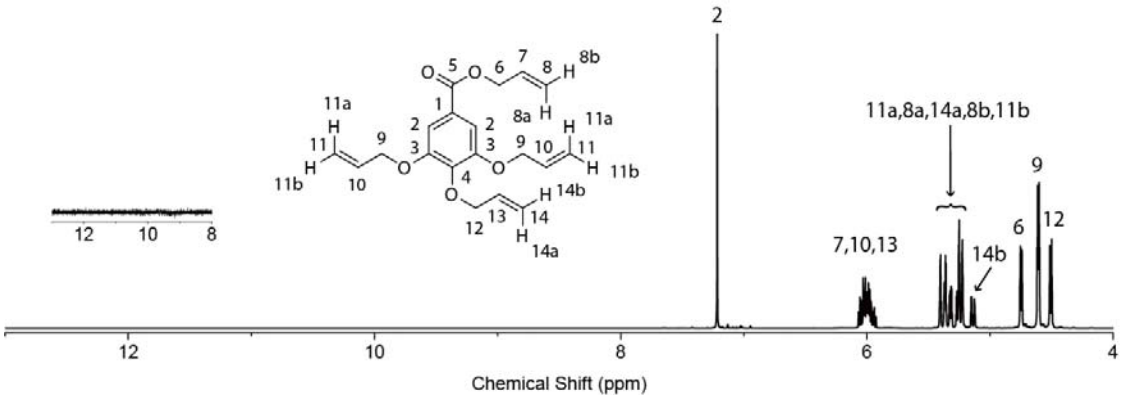

Figure S5b: Chemical structure of and ^{1}H NMR data obtained from allyl 3,4,5-tris(allyloxy)benzoate. Data were obtained from final purified product.).

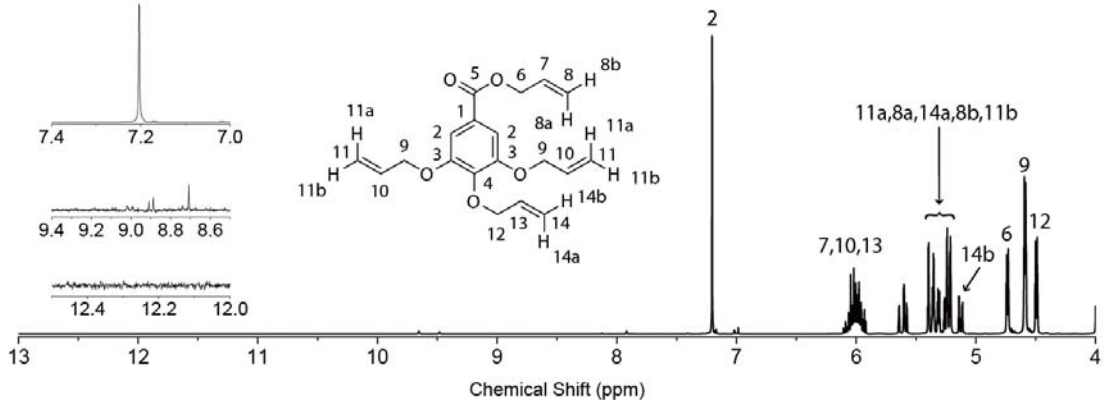

Figure S5c: Chemical structure of and 1H NMR data obtained from allyl 3,4,5-tris(allyloxy)benzoate. Data were obtained prior to extraction.

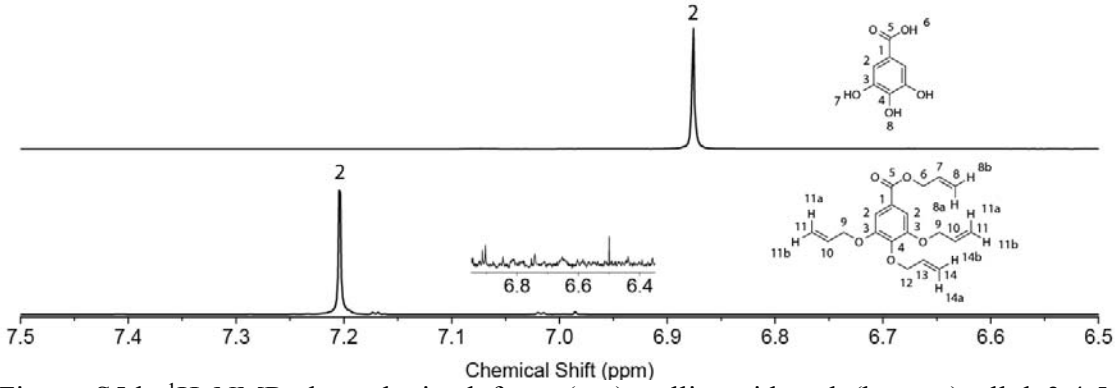

Figure S5d: ^{1}H NMR data obtained from (top) gallic acid and (bottom) allyl 3,4,5-tris(allyloxy)benzoate. The spectrum of allyl 3,4,5-tris(allyloxy)benzoate was obtained prior to extraction for determining the reaction conversion.

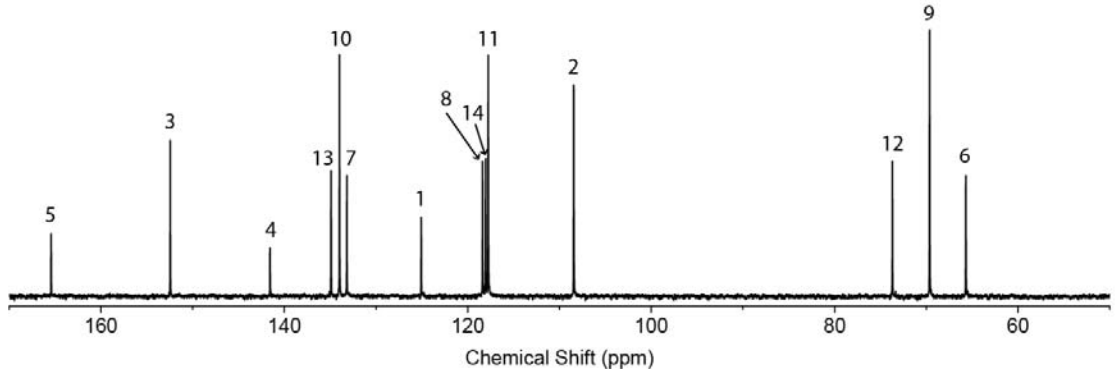

Figure S5e: ^{13}C NMR data obtained from allyl 3,4,5-tris(allyloxy)benzoate.

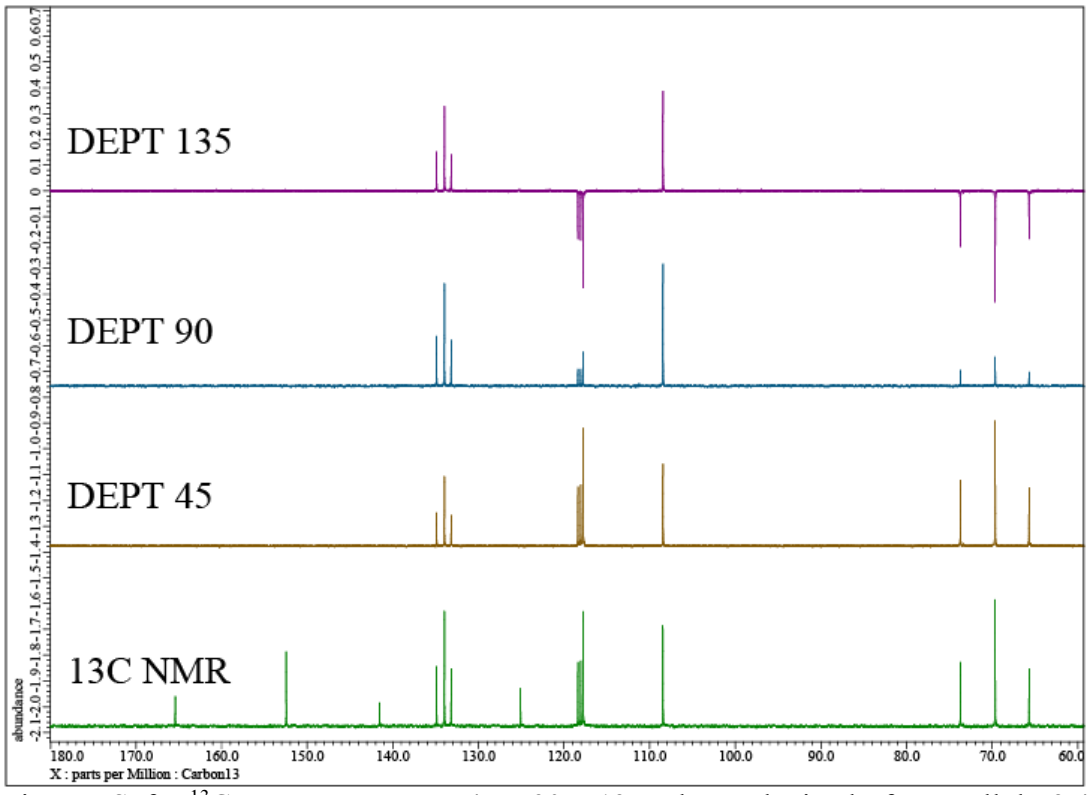

Figure S5f: ^{13}C NMR, DEPT 45, 90, 135 data obtained from allyl 3,4,5-tris(allyloxy)benzoate

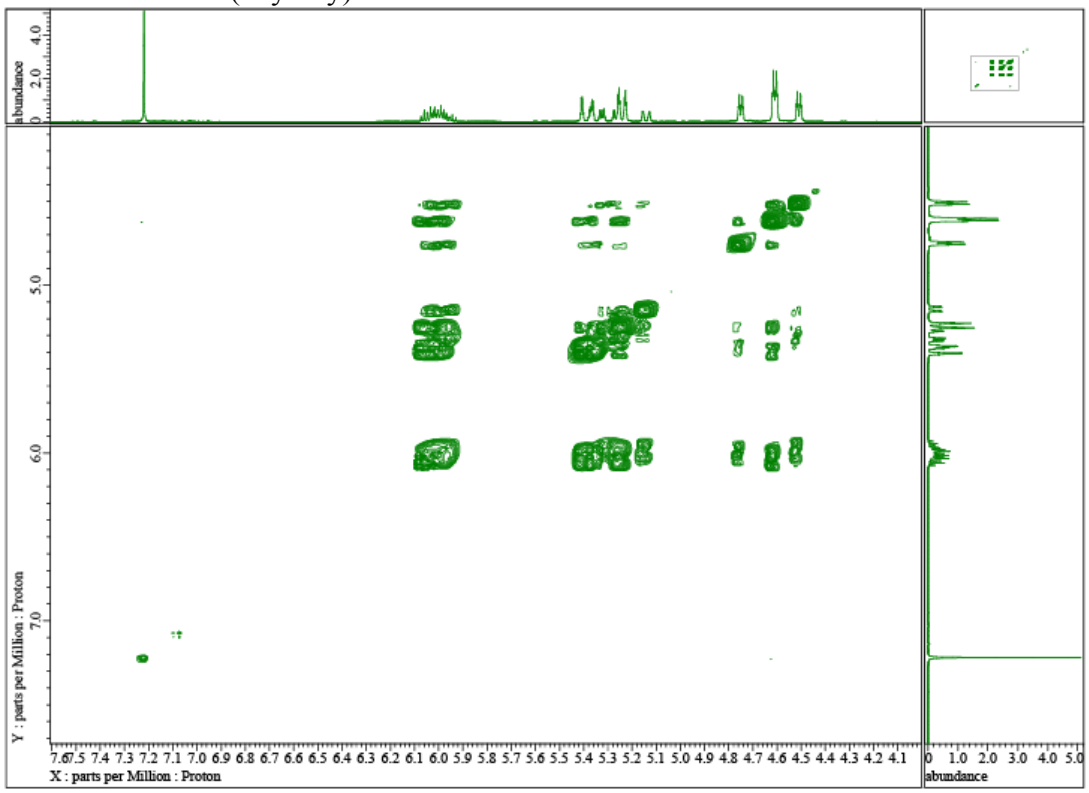

Figure S5g: COSY data obtained from allyl 3,4,5-tris(allyloxy)benzoate

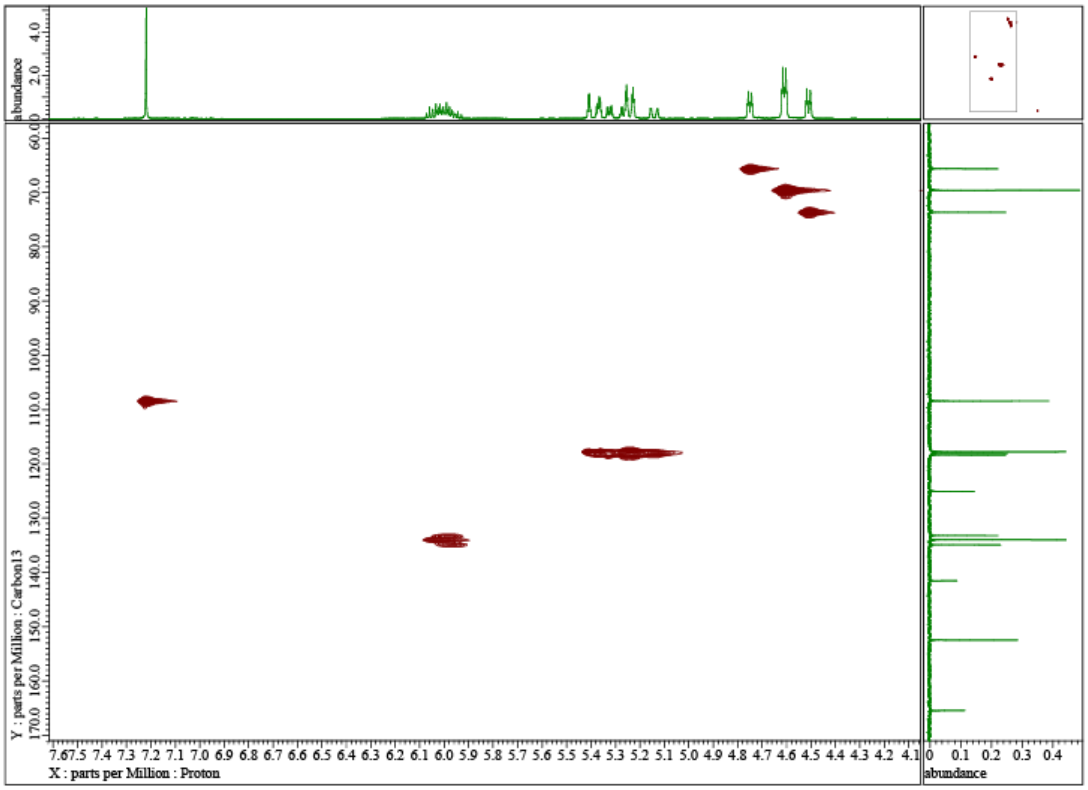

Figure S5h: HSQC data obtained from allyl 3,4,5-tris(allyloxy)benzoate

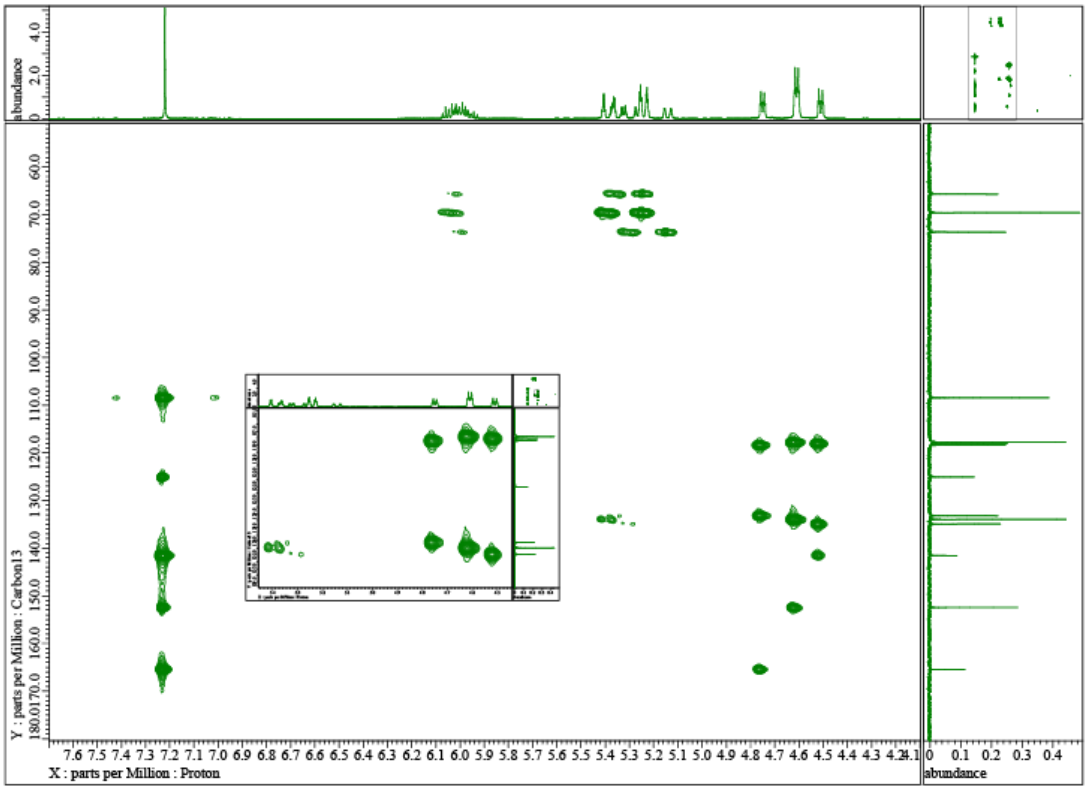

Figure S5i: HMBC data obtained from allyl 3,4,5-tris(allyloxy)benzoate

Section 6: NMR Characterization of 3-Hydroxybenzoic Acid

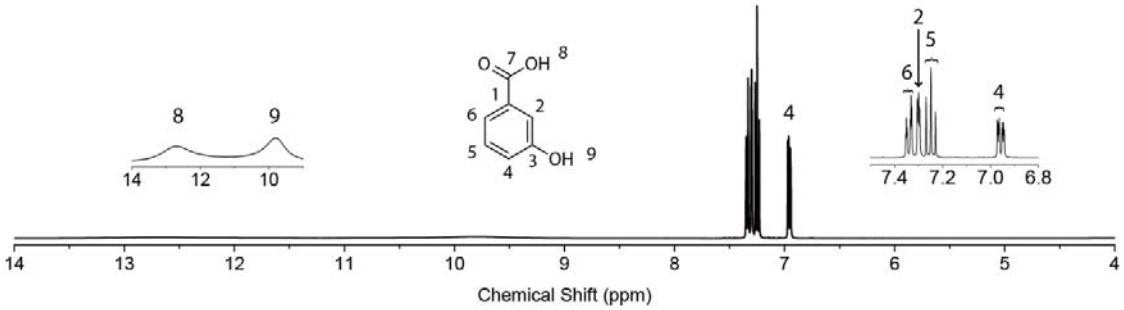

Figure S6a: Chemical structure of and ^{1}H NMR data obtained from 3-hydroxybenzoic acid (referred to as "3HBA" in main text).

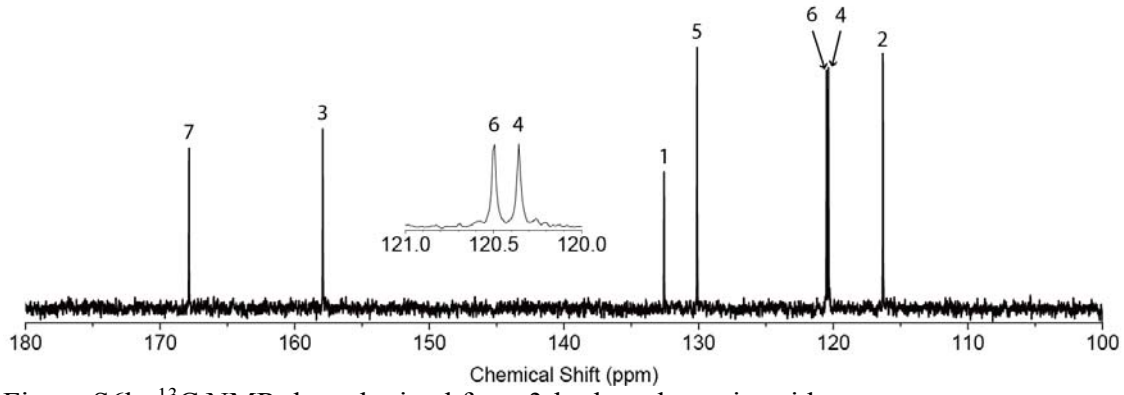

Figure S6b: ^{13}C NMR data obtained from 3-hydroxybenzoic acid.

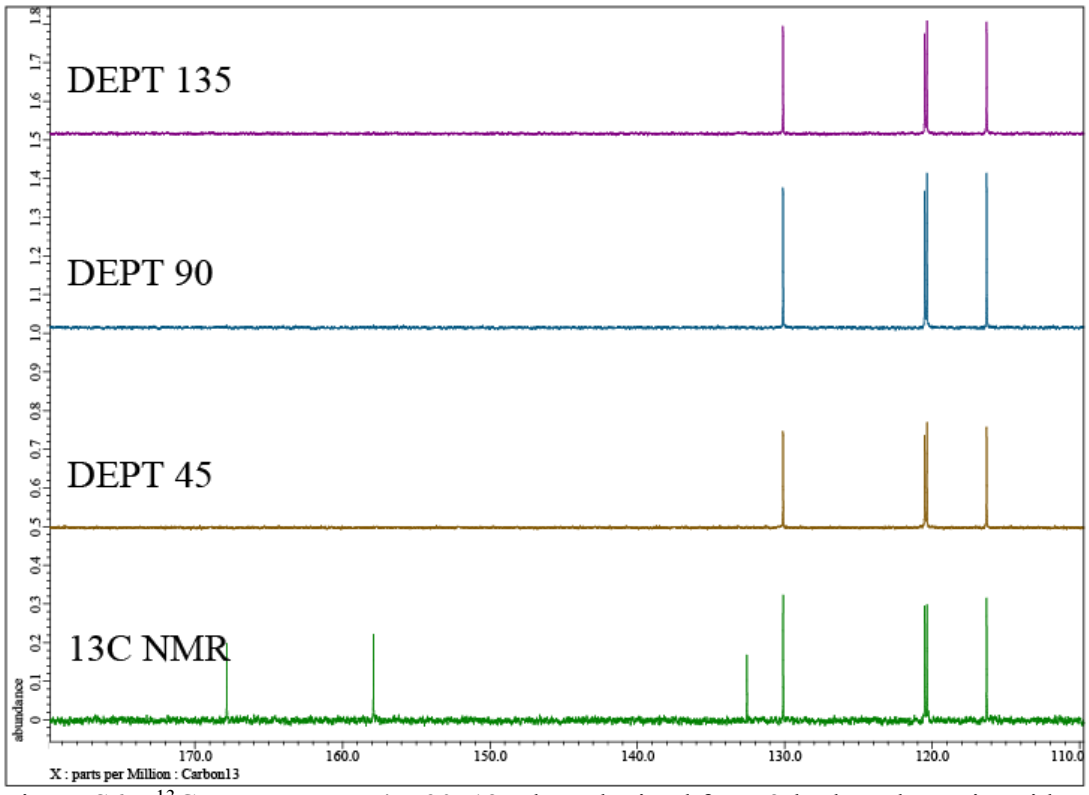

Figure S6c: ^{13}C NMR, DEPT 45, 90, 135 data obtained from 3-hydroxybenzoic acid

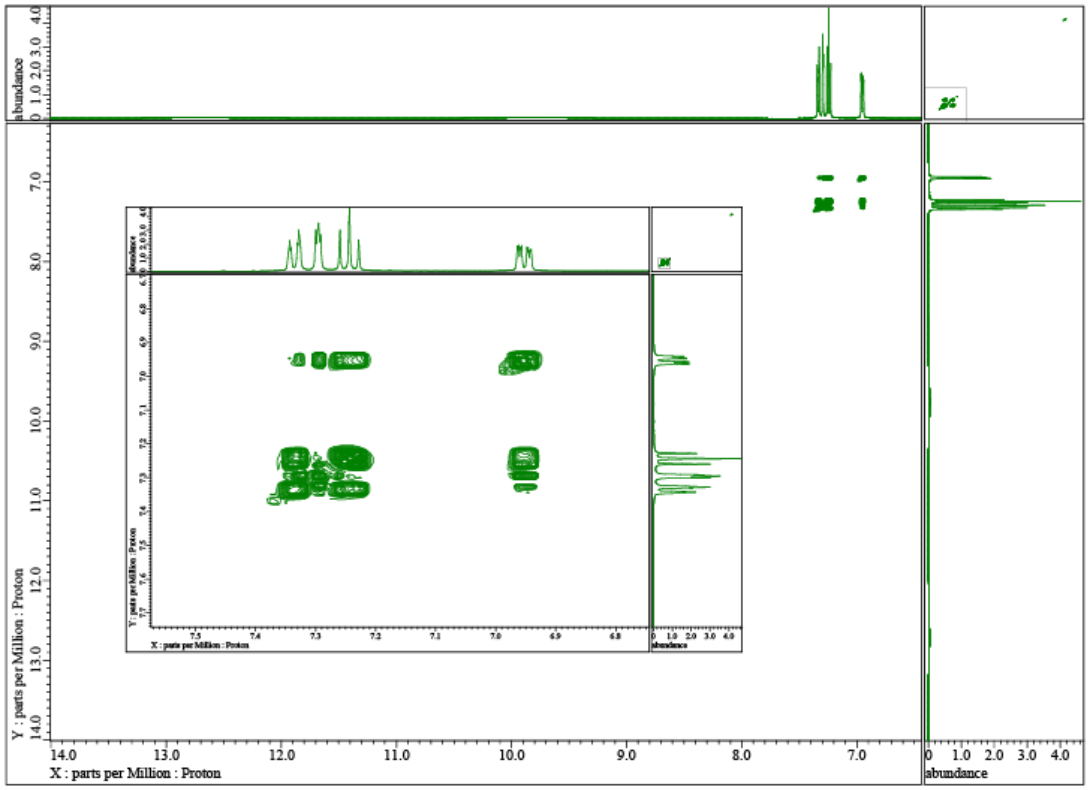

Figure S6d: COSY data obtained from 3-hydroxybenzoic acid

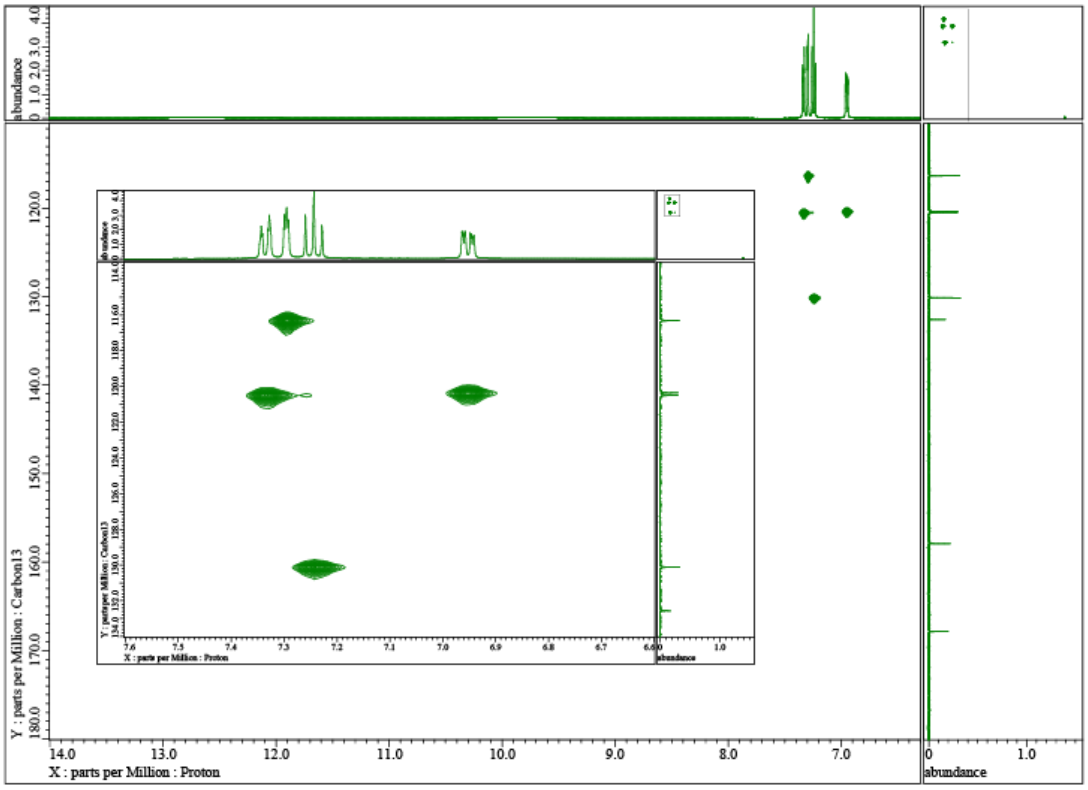

Figure S6e: HSQC data obtained from 3-hydroxybenzoic acid

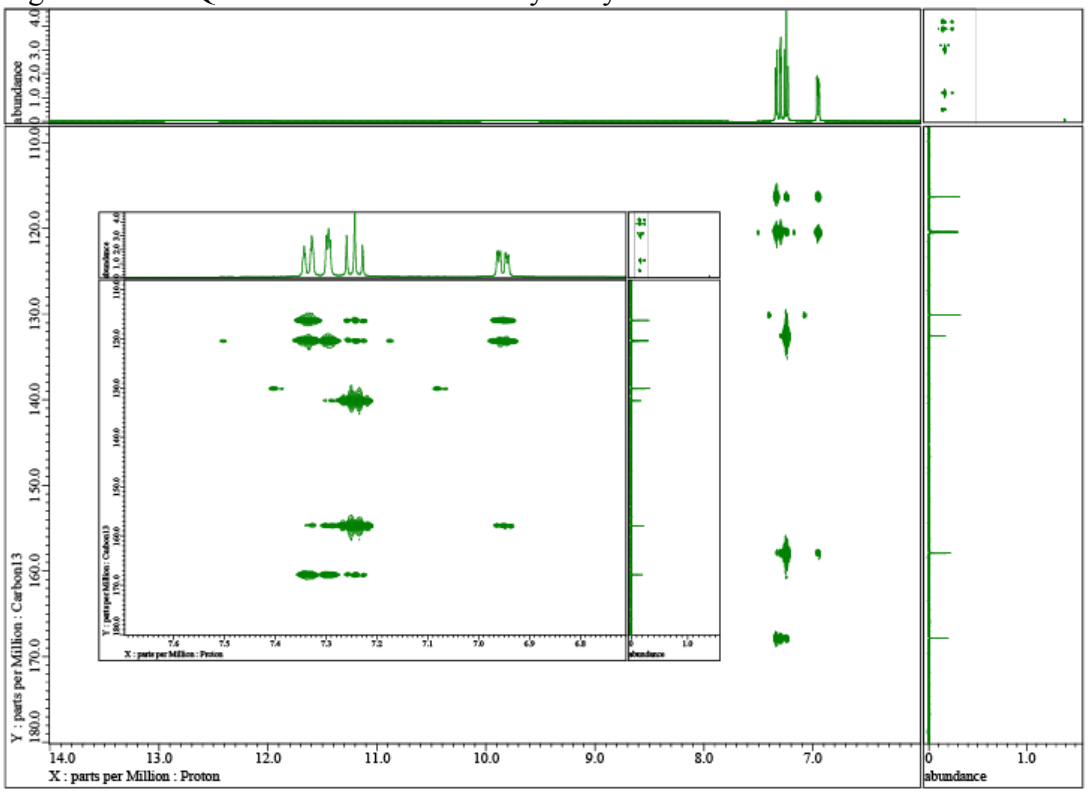

Figure S6f: HMBC data obtained from 3-hydroxybenzoic acid

Section 7: NMR Characterization of Gentisic Acid

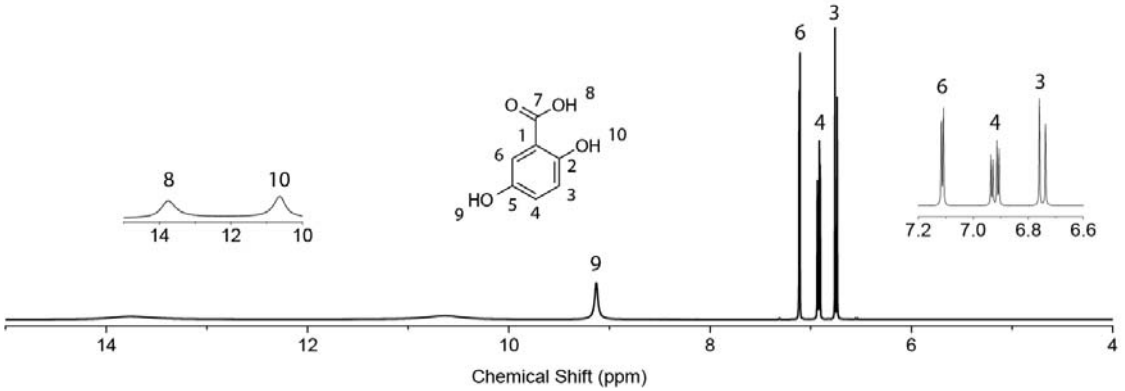

Figure S7a: Chemical structure of and ^{1}H NMR data obtained from gentisic acid (referred to as "GenA" in main text).

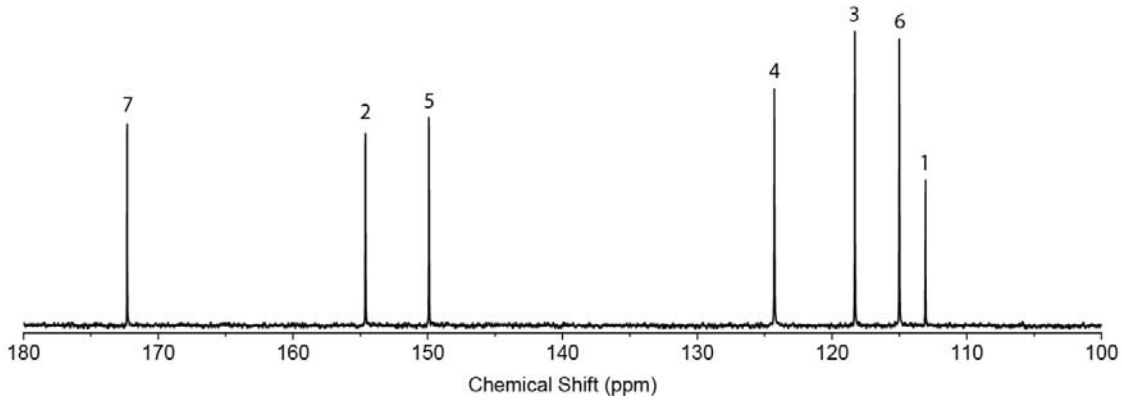

Figure S7b: ^{13}C NMR data obtained from gentisic acid.

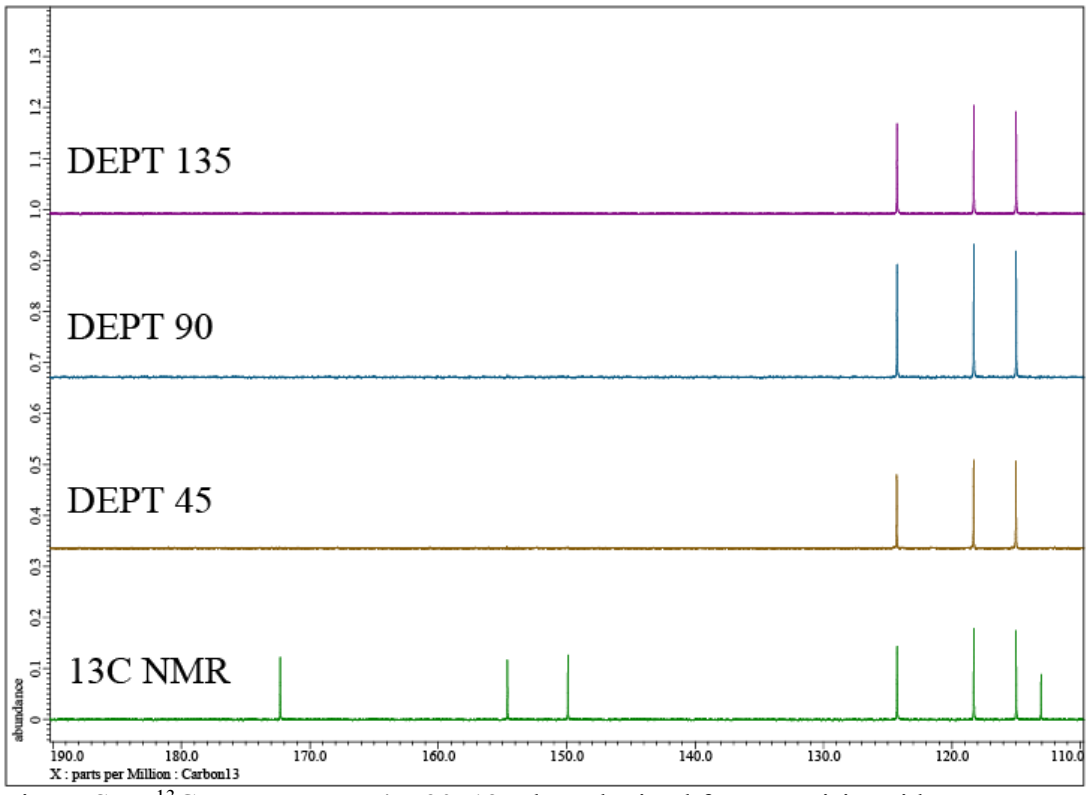

Figure S7c: ^{13}C NMR, DEPT 45, 90, 135 data obtained from gentisic acid

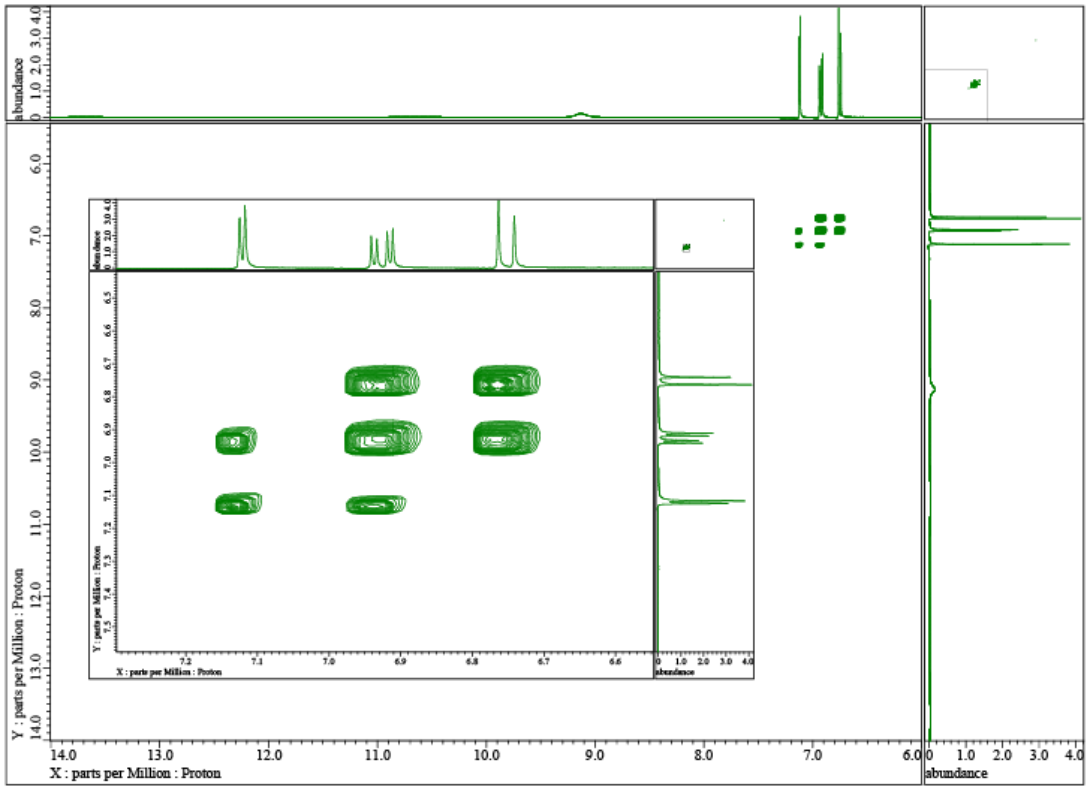

Figure S7d: COSY data obtained from gentisic acid

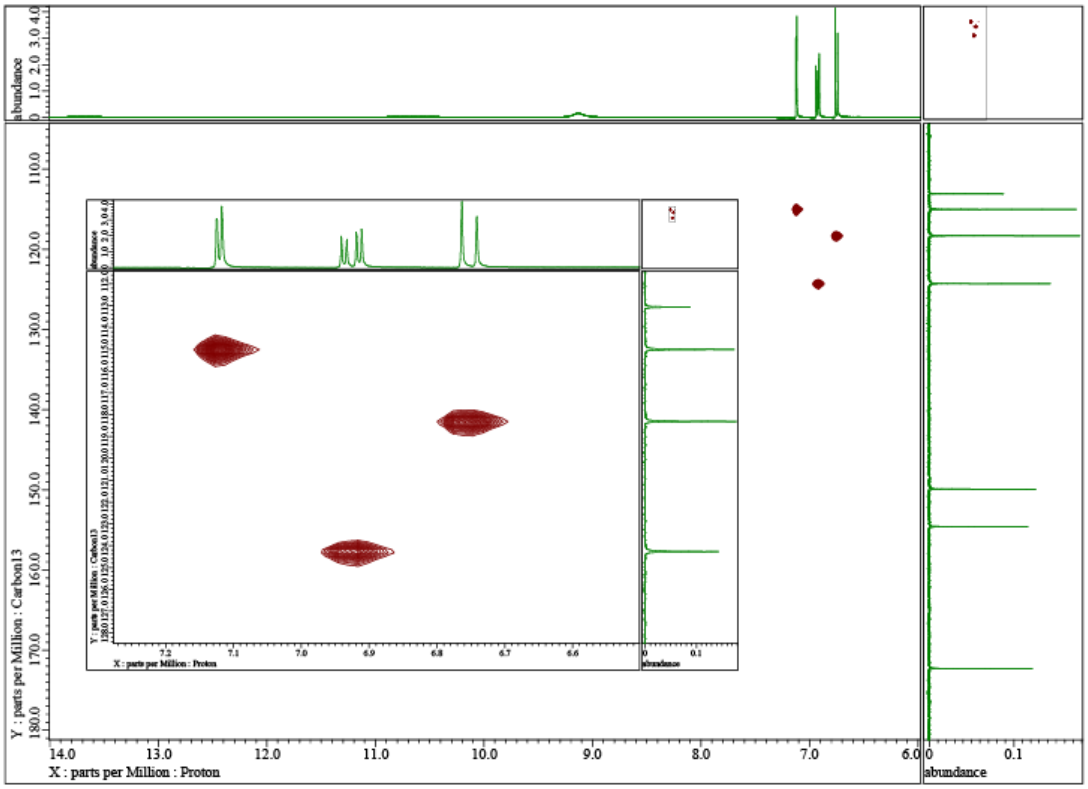

Figure S7e: HSQC data obtained from gentisic acid

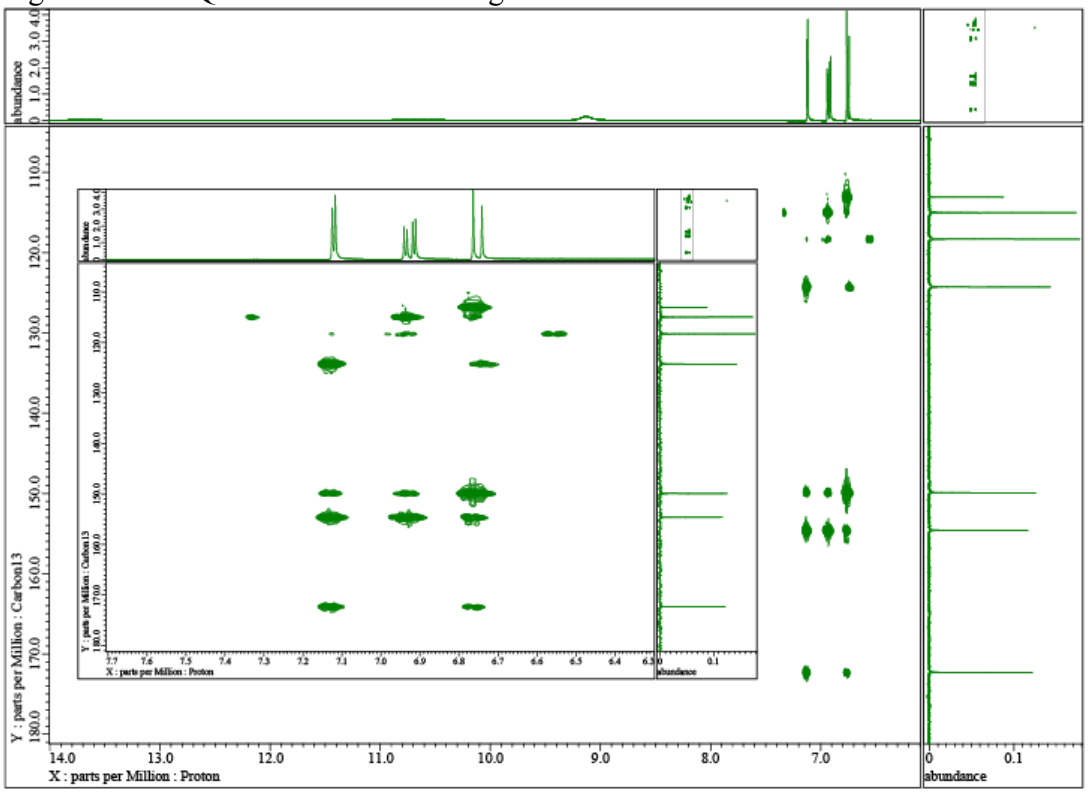

Figure S7f: HMBC data obtained from gentisic acid

Appendix B. Glass Transition of Phenolic Acid-based Thiol-Ene network

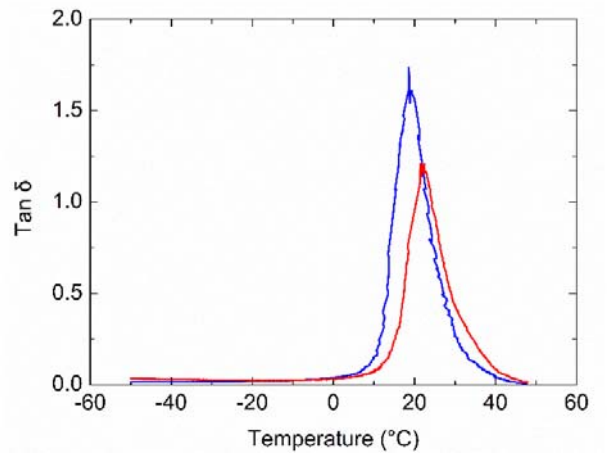

Figure S8: Tan δ (E"/E'), measured through DMA, as a function of temperature of thiol-ene networks derived from SA (blue curve) and 4HBA (red curve)..

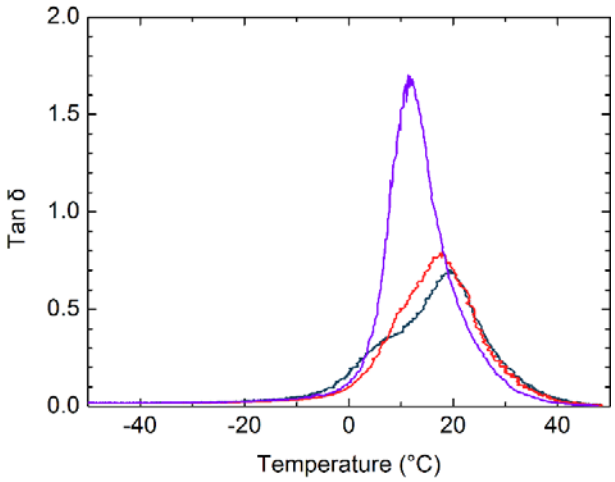

Figure S9: Tan δ (E"/E'), measured through DMA, as a function of temperature of thiol-ene networks derived from allylated 3-HBA (purple curve), GenA (blue curve) and GalA (red curve).

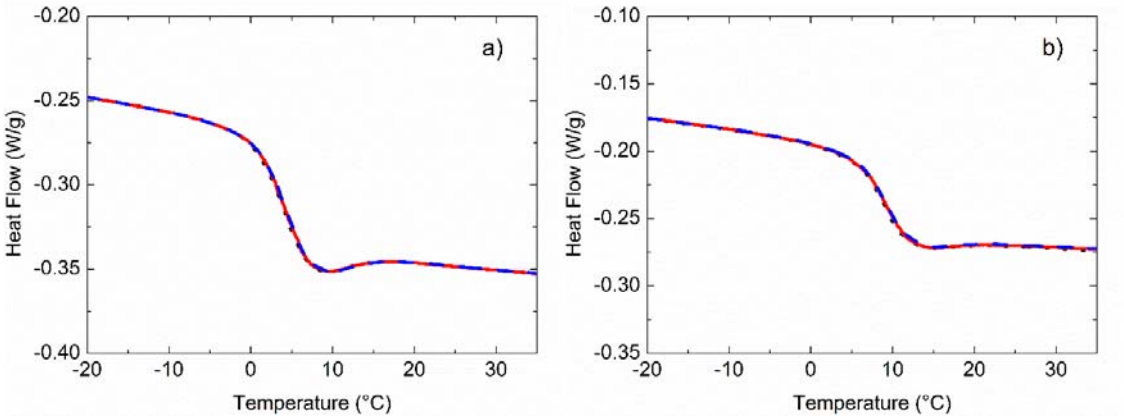

Figure S10: DSC heat flow as a function of temperature for thiol-ene networks derived from (a) allylated SA and (b) allylated 4HBA. Samples were exposed to UV for 15 min and were cured at 150 °C for 10 min.

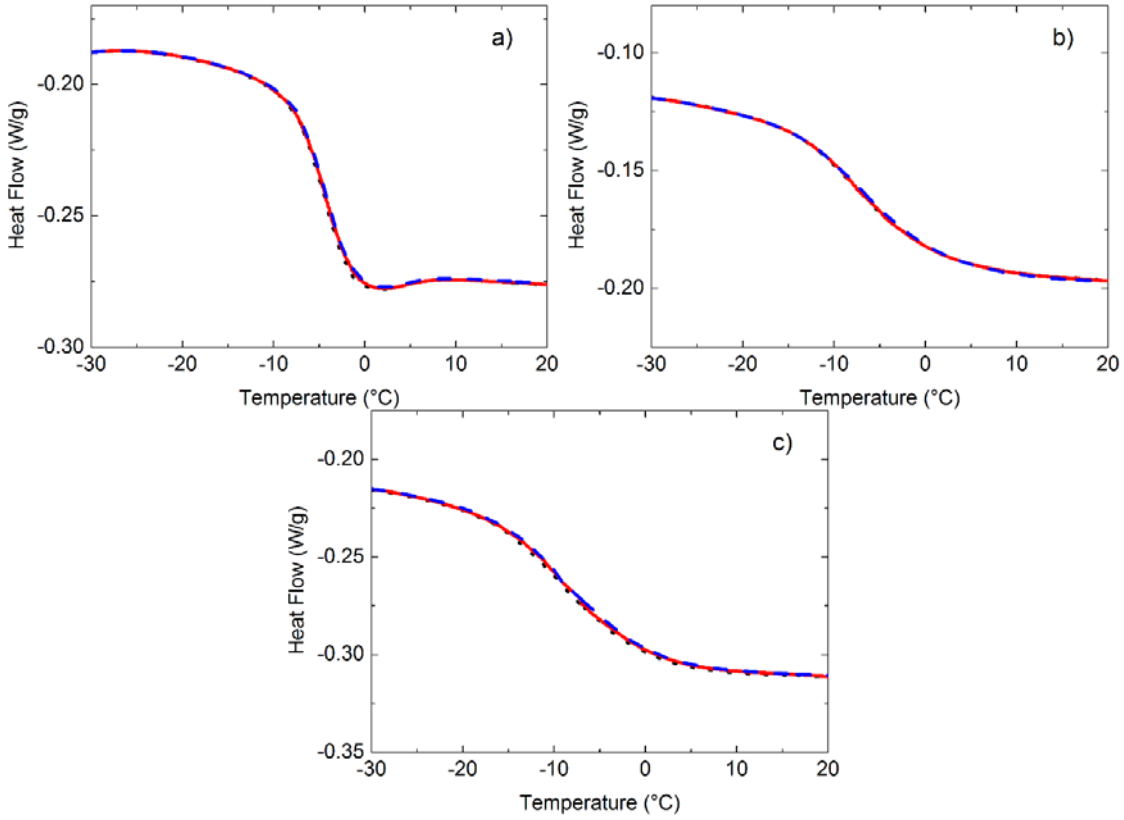

Figure S11: DSC heat flow as a function of temperature for thiol-ene networks derived from (a) allylated 3HBA, (b) allylated GenA and (c) allylated GalA.

Appendix C. Conversion of Phenolic Acid-based Thiol-Ene network

Conversion was quantified through measurement of the maximum intensity of the absorbance peak associated with S-H stretching (2570 cm^{-1}). Quantifying the conversion from this FTIR data has significant uncertainty, due to the small size of this peak (note the high absorbance of other peaks that were not relevant to the thiol-ene reaction, due to the large sample thickness required for this measurement). The error on measurements described in the table below represent multiple measurements obtained on independently prepared specimens.

Table S1: Conversion of aSA Network

Measurements on multiple specimens:

Reaction Condition	Conversion
15 min UV	93% ± 0.4%
15 min UV + 10 min 150 °C	97% ± 0.1%

Measurement on a single specimen to probe influence of UV curing time:

Reaction Condition	Conversion
15 min UV	90%
30 min UV	90%

Table S2: Conversion of a3HBA Network

Measurements on multiple specimens:

Reaction Condition	Conversion
15 min UV	80% ± 4%
15 min UV + 10 min 150 °C	88% ± 3%

Measurement on a single specimen to probe influence of UV curing time:

Reaction Condition	Conversion
15 min UV	82%
30 min UV	83%

Table S3: Conversion of a4HBA Network

Measurements on multiple specimens:

Reaction Condition	Conversion
15 min UV	82% ± 1%
15 min UV + 10 min 150 °C	88% ± 2%

Measurement on a single specimen to probe influence of UV curing time:

Reaction Condition	Conversion
15 min UV	86%
30 min UV	86%

Table S4: Conversion of aGenA Network

Measurements on multiple specimens:

Reaction Condition	Conversion
15 min UV	76% ± 1%
15 min UV + 20 min 150 °C	88% ± 2%

Measurement on a single specimen to probe influence of UV curing time:

Reaction Condition	Conversion
15 min UV	78%
30 min UV	80%

Table S5: Conversion of aGalA Network

Measurements on multiple specimens:

Reaction Condition	Conversion
15 min UV	71% ± 2%
15 min UV + 20 min 150 °C	83% ± 2%

Measurement on a single specimen to probe influence of UV curing time:

Reaction Condition	Conversion
15 min UV	67%
30 min UV	71%

Table S6: Summary of Final Conversions for Curing Protocol Used in Manuscript

Allylated Phenolic Acid	Reaction Condition	Conversion
aSA	15 min UV + 10 min 150 °C	97% ± 0.1%
a3HBA	15 min UV + 10 min 150 °C	88% ± 3%
a4HBA	15 min UV + 10 min 150 °C	88% ± 2%
aGenA	15 min UV + 20 min 150 °C	88% ± 2%
aGalA	15 min UV + 20 min 150 °C	83% ± 2%

Appendix D. Crosslink Density of Thiol-ene Networks Derived from Phenolic acid

Table S7: Crosslink Density of SA Networks Determined through DMA

Batch #	Specimen #	E'_r in rubbery plateau (MPa) at 30 °C	υ_c (x 10^{-3}mol/cm^3)
1[a]	1	7.11	0.94
2	1	8.83	1.17
	2	8.73	1.15
	3	8.65	1.14
Average of batch 2		8.74 ± 0.09	1.16 ± 0.01
3	1	9.55	1.26
	2	9.24	1.22
	3	8.55	1.13
Average of batch 3		9.11 ± 0.51	1.21 ± 0.07
4	1	8.76	1.16
	2	9.24	1.22
	3	8.63	1.14
Average of batch 4		8.88 ± 0.32	1.17 ± 0.04
Average		8.46 ± 0.91	1.12 ± 0.12

Table S8: Crosslink Density of 3HBA Networks Determined through DMA

Batch #	Specimen #	E'_r in rubbery plateau (MPa) at 30 °C	υ_c (x 10^{-3}mol/cm^3)
1	1	7.16	0.95
	2	7.68	1.02
	3	8.61	1.14
Average of batch 1		7.82 ± 0.73	1.03 ± 0.10
2	1	8.80	1.16
	2	8.11	1.07
	3	8.03	1.06
Average of batch 2		8.31 ± 0.42	1.10 ± 0.06
3	1	7.47	0.99
	2	7.66	1.01
	3	7.70	1.02
Average of batch 3		7.61 ± 0.12	1.01 ± 0.02
Average		7.91 ± 0.73	1.05 ± 0.10

Table S9: Crosslink Density of 4HBA Networks Determined through DMA

Batch #	Specimen #	E'_r in rubbery plateau (MPa) at 30 °C	υ_c (x 10^{-3}mol/cm^3)
1[a]	1	11.6	1.53
2	1	9.87	1.31
	2	10.3	1.36
	3	11.1	1.47
Average of batch 2		10.4 ± 0.6	1.38 ± 0.09
3	1	10.4	1.37
	2	10.4	1.37
	3	11.4	1.51
Average of batch 3		10.7 ± 0.6	1.42 ± 0.08
4	1	9.09	1.20
	2	9.63	1.27
	3	9.51	1.26
Average of batch 4		9.41 ± 0.28	1.24 ± 0.04
Average		10.5 ± 0.9	1.39 ± 0.12

Table S10: Crosslink Density of GenA Networks Determined through DMA

Batch #	Specimen #	E'_r in rubbery plateau (MPa) at 30 °C	υ_c (x 10^{-3}mol/cm^3)
1	1	12.2	1.61
2	1	11.9	1.57
	2	11.7	1.55
	3	11.6	1.54
Average of batch 2		11.7 ± 0.1	1.55 ± 0.02
3	1	10.6	1.40
	2	10.7	1.42
	3	10.6	1.40
Average of batch 3		10.6 ± 0.1	1.40 ± 0.01
4	1	10.3	1.36
	2	10.4	1.37
	3	10.6	1.40
Average of batch 4		10.4 ± 0.1	1.37 ± 0.02
Average		11.2 ± 0.9	1.49 ± 0.12

Table S11: Crosslink Density of GalA Networks Determined through DMA

Batch #	Specimen #	E'_r in rubbery plateau (MPa) at 30 °C	υ_c (x 10^{-3}mol/cm^3)
1	1	13.3	1.75
2	2-1	10.8	1.43
	2-2	11.3	1.50
	2-3	12.0	1.59
Average of batch 2		11.4 ± 0.6	1.51 ± 0.08
3	3-1	10.3	1.36
	3-2	10.2	1.34
	3-3	9.7	1.28
Average of batch 3		10.0 ± 0.3	1.33 ± 0.04
4	4-1	9.9	1.31
	4-2	10.6	1.41
	4-3	10.7	1.42
Average of batch 4		10.4 ± 0.5	1.38 ± 0.06
Average		11.3 ± 1.4	1.49 ± 0.19

Appendix E. Tensile Data of Thiol-ene Elastomer

Table S12: Tensile Properties of Thiol-Ene Networks Derived from Allylated Phenolic Acids

Phenolic acid	Tensile strength (MPa)	% elongation at break	Modulus (MPa)	Toughness (MPa)
SA	2.7 ± 0.3	25.0 ± 2.2	10.8 ± 0.4	0.36 ± 0.06
3HBA	1.8 ± 0.1	20.4 ± 2.1	8.6 ± 0.5	0.20 ± 0.03
4HBA	3.7 ± 0.3	29.6 ± 2.4	12.4 ± 0.3	0.57 ± 0.09
GenA	2.7 ± 0.5	18.1 ± 3.9	14.6 ± 0.6	0.32 ± 0.13
GalA	2.1 ± 0.4	15.4 ± 3.1	13.0 ± 0.5	0.17 ± 0.06

[a] Samples were prepared following the protocol in *Table 2.3*.

Table S13: Parameters Extracted from the Fit of the Mooney-Rivlin Equation to the Tensile Data

Phenolic acid	Strain Range	C_1	C_2
SA	All	2.20 ± 0.21	-0.07 ± 0.32
3HBA	All	1.66 ± 0.17	0.12 ± 0.18
4HBA	$\varepsilon < 0.202 \pm 0.008$	2.82 ± 0.25	-0.35 ± 0.34
4HBA	$\varepsilon > 0.202 \pm 0.008$	4.10 ± 0.16	-1.88 ± 0.18
GenA[a]	$\varepsilon < 0.144 \pm 0.017$	2.60 ± 0.35	0.29 ± 0.49
GenA[a]	$\varepsilon > 0.144 \pm 0.017$	3.90 ± 0.21	-1.23 ± 0.35
GalA[b]	$\varepsilon < 0.153$	2.13 ± 0.85	0.43 ± 0.91
GalA[b]	$\varepsilon > 0.153$	3.45	-1.14

[a]Three of the five tested specimens showed a deviation from the ideal elastomer model. The strain value at which the data deviated from the model differed from specimen to specimen (deviation occurred at $\varepsilon = 0.144 \pm 0.017$). The Mooney-Rivlin model was fit to the data both above and below this critical strain value.
[b]One of the five tested specimens showed a deviation from the ideal elastomer model. The data deviated from the model $\varepsilon = 0.153$. The Mooney-Rivlin model was fit to the data both above and below this critical strain value.

Appendix F. TGA Data of ESO Epoxy Resins

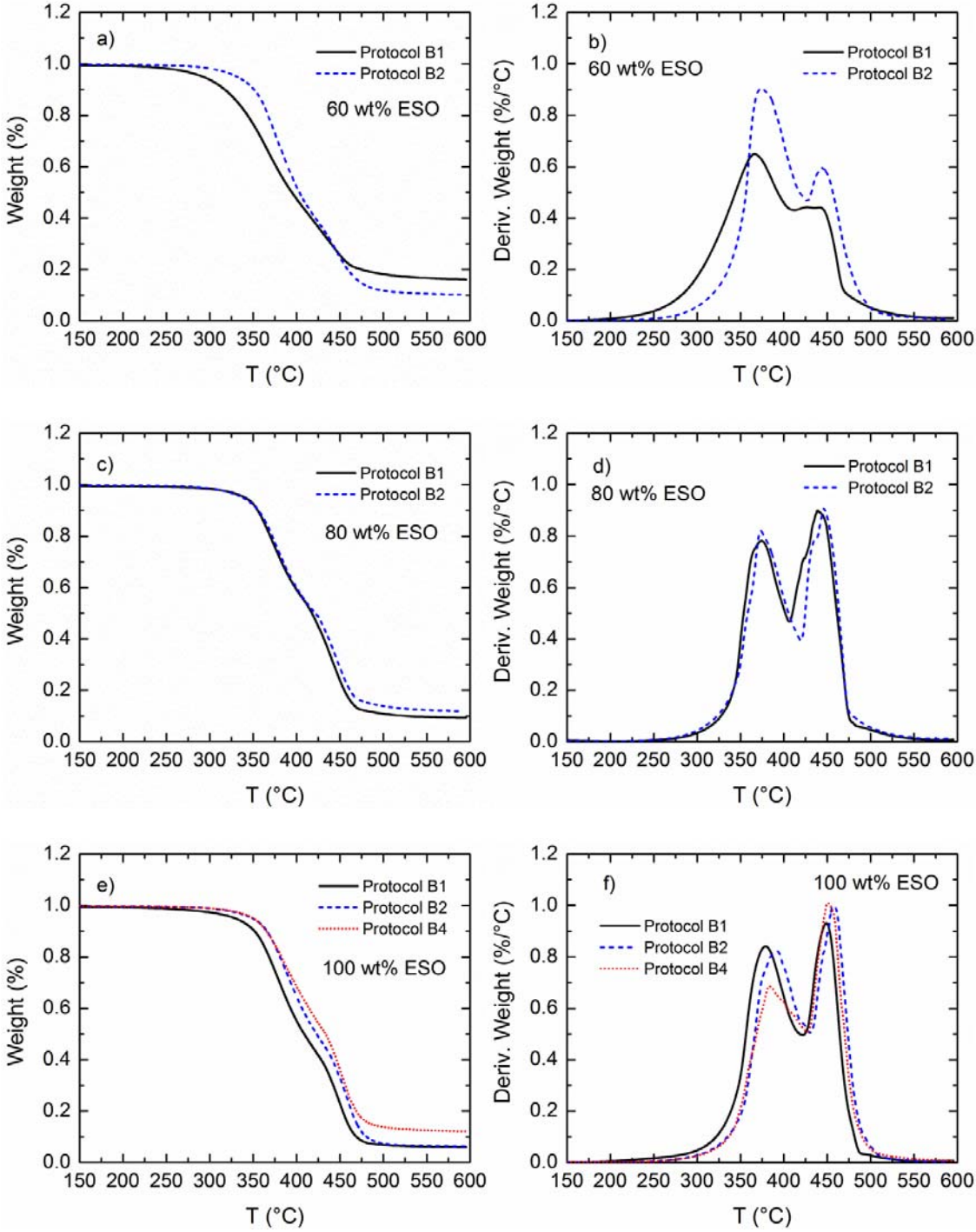

Figure S12: TGA data for polymers prepared with various curing protocols (described in the Table 1 of the main text), containing 60 (a, b), 80 (c, d), and 100 (e, f) wt% ESO.

Appendix G. Hydrolytic Degradation Data of ESO Epoxy Resins

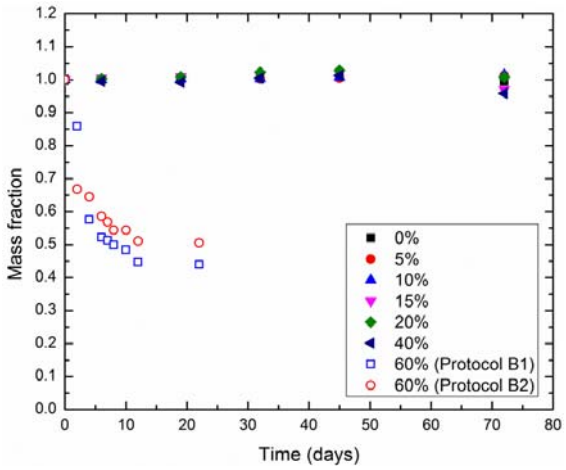

Figure S13: Fraction of mass remaining as a function of time in a 3 wt% NaOH solution at 80 °C. The wt% ESO is indicated for each curve (relative to the total DGEBA + ESO content in the polymer).

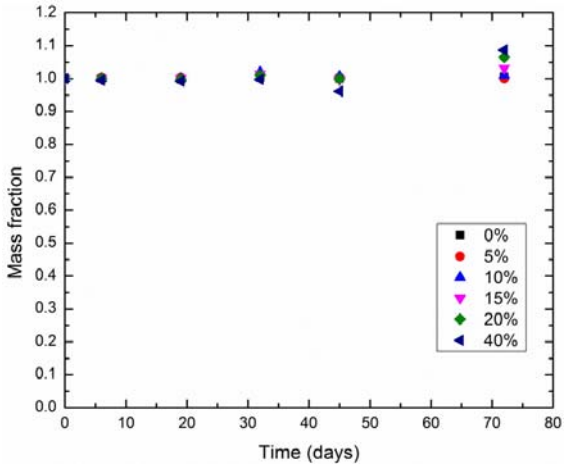

Figure S14: Fraction of mass remaining as a function of time in a 10 wt% NaOH solution at 80 °C. The wt% ESO is indicated for each curve (relative to the total DGEBA + ESO content in the polymer).